Unravelling the effects of melt depletion and secondary infiltration on mantle re-os isotopes beneath the french Massif Central

Journal Item

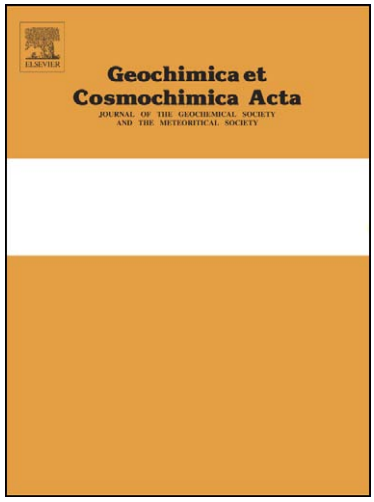

Unravelling the effects of melt depletion and secondary infiltration on mantle re-os isotopes beneath the french massif central

J. Harvey, A. Gannoun, K.W. Burton, P. Schiano, N.W. Rogers, O. Alard

PII: S0016-7037(09)00609-7
DOI: 10.1016/j.gca.2009.09.031
Reference: GCA 6469

To appear in: *Geochimica et Cosmochimica Acta*

Received Date: 6 April 2009
Accepted Date: 21 September 2009

Please cite this article as: Harvey, J., Gannoun, A., Burton, K.W., Schiano, P., Rogers, N.W., Alard, O., Unravelling the effects of melt depletion and secondary infiltration on mantle re-os isotopes beneath the french massif central, *Geochimica et Cosmochimica Acta* (2009), doi: 10.1016/j.gca.2009.09.031

UNRAVELLING THE EFFECTS OF MELT DEPLETION AND SECONDARY INFILTRATION ON MANTLE RE-OS ISOTOPES BENEATH THE FRENCH MASSIF CENTRAL.

J. Harvey [a*], A. Gannoun [a,b], K.W. Burton [a,c], P. Schiano [b], N.W. Rogers [a], O. Alard [a,d].

[a] Department of Earth and Environmental Sciences, The Open University, Walton Hall, Milton Keynes, MK7 6AA, UK.

[b] Laboratoire 'Magmas et Volcans', Université Blaise Pascal, 5 Rue Kessler, 63000 Clermont-Ferrand, France.

[c] Department of Earth Sciences, University of Oxford, Parks Road, Oxford, OX1 3PR, UK

[d] Géosciences Montpellier, UMR 5243 – CC60, Université Montpellier 2, Place E. Bataillon, 34095 Montpellier cedex 5, France.

[*] Corresponding author: email j.harvey@open.ac.uk; Tel: +44 (0)1908 332629

ABSTRACT

Spinel lherzolite xenoliths from Mont Briançon, French Massif Central, retain evidence for multiple episodes of melt depletion and melt / fluid infiltration (metasomatism). Evidence for primary melt depletion is still preserved in the co-variation of bulk-rock major elements (MgO 38.7–46.1 weight %; CaO 0.9–3.6 weight %), and many samples yield unradiogenic bulk-rock Os isotope ratios ($^{187}Os/^{188}Os$ = 0.11541-0.12626). However, many individual xenoliths contain interstitial glasses and melt inclusions that are not in equilibrium with the major primary minerals. Incompatible trace element mass balance calculations demonstrate that metasomatic components comprise a significant proportion of the bulk-rock budget for these elements in some rocks, ranging to as much as 25% of Nd and 40% of Sr Critically, for Re-Os geochronology, melt / fluid infiltration is accompanied by the mobilisation of sulfide. Consequently, bulk-rock isotope measurements, whether using lithophile (e.g. Rb-Sr, Sm-Nd) or siderophile (Re-Os) based isotope systems, may only yield a perturbed and / or homogenised average of these multiple events.

Osmium mass balance calculations demonstrate that bulk-rock Os in peridotite is dominated by contributions from 2 populations of sulfide grain: (i) interstitial, metasomatic sulfide with low [Os] and radiogenic $^{187}Os/^{188}Os$, and (ii) primary sulfides with high [Os] and unradiogenic $^{187}Os/^{188}Os$, which have been preserved within host silicate grains and shielded from interaction with transient melts and fluid. The latter can account for > 97% of bulk rock Os and preserve geochronological information of the melt from which they originally precipitated as an immiscible liquid. The Re-depletion model ages of individual primary sulfide grains preserve

evidence for melt depletion beneath the Massif Central from at least 1.8 Gyr ago despite the more recent metasomatic event(s).

1. INTRODUCTION

Ultramafic xenoliths brought to the surface as accidental inclusions in alkali basalts and kimberlites provide some of the best direct evidence of the composition of the sub-continental lithospheric mantle (SCLM). This is because, unlike orogenic peridotite massifs, xenoliths experience rapid transport to the surface and, where interaction with the host lava is minimal, the composition of the mantle source is largely retained.

Systematic co-variations of major and compatible trace elements in peridotite xenoliths have been used to demonstrate the effects of melt extraction on the composition of fertile mantle (Ross et al., 1954; Kuno and Aoki, 1970; Frey and Green, 1974; Jagoutz et al., 1979) and to estimate the composition of undepleted, i.e. primitive mantle (e.g. Frey and Prinz, 1978; Meisel et al., 1996, 2001). However, incompatible trace element compositions of upper mantle samples are frequently decoupled from the more coherent major element trends. This feature is commonly attributed to re-fertilization processes. Several potential agents of this re-fertilization, or metasomatism, have been suggested, including CO_2-rich fluids (Andersen et al., 1984; O'Reilly and Griffin, 1988), siliceous melts and related fluids (Roden et al., 1984; Menzies et al., 1987; Schiano and Clocchiatti, 1994; Schiano and Bourdon, 1999), carbonated hyper-alkaline melts (Meen et al., 1989), kimberlite-like melts (e.g. Menzies and Wass, 1983), and carbonatitic melts (Yaxley et al., 1991; Dautria et al., 1992; Ionov et al., 1993, Rudnick et al., 1993; O'Reilly and Griffin, 1988; Griffin et

al., 1996). Much of the SCLM has experienced a multi-stage history of melt depletion and enrichment in lithophile elements since segregation from the homogenising effects of the convecting mantle (Galer and O'Nions 1988; McKenzie and Bickle, 1988; Zindler and Jagoutz, 1988; Pearson et al., 1995a; Pearson 1999), yet all of the conventional geochronometers rely upon silicate-hosted lithophile elements (Rb-Sr, Sm-Nd, U-Th-Pb, Lu-Hf). Critically, perturbation of a primary lithology through interaction with secondary, lithophile element-rich melts and / or fluids results in the perturbation of geochronological information relating to the primary melt depletion event(s).

In contrast, the high temperature behaviour of the siderophile elements Re and Os potentially offers a means to "see through" recent metasomatic events and provide geochronological information relating to prior melt depletion. This is because Os behaves compatibly during melting and is preferentially retained in the mantle, whereas Re is moderately incompatible and enters the melt (e.g. Pegram and Allègre, 1992; Hauri and Hart, 1997). Thus, melt depletion generates a low Re/Os ratio in the residue which, with time, through the decay of ^{187}Re (parent) to ^{187}Os (daughter), evolves to unradiogenic ^{187}Os/^{188}Os ratios compared to those of the contemporaneous undepleted mantle (e.g. Meisel et al., 2001). The high Os concentration of the residual mantle effectively buffers against the effects of secondary processes as the Os elemental abundance in silicate metasomatic melts and fluids should be low. Several recent studies have shown that, in many cases, the Os isotope ratio of lithospheric mantle peridotite indicates evolution in a low Re environment following ancient partial melting events i.e. 3.4 Ga in cratonic SCLM (Pearson et al., 1995b; Burton et al., 2000; Griffin et al., 2004) and > 2 Ga in abyssal peridotites (Alard et al., 2005; Harvey et al., 2006; Liu et al., 2008).

Exceptionally high sulfide/silicate partition coefficients derived experimentally ($K_D^{sulfide/silicate}$ ~ 10^4-10^5 of Bezman et al., 1994; Fleet et al., 1991, 1996) and in natural samples ($K_D^{sulfide/silicate}$ 4.8 x 10^4, Roy-Barman et al., 1998), coupled with the low affinity of Os for silicate minerals (e.g. Righter et al., 2004; Brenan et al., 2005), suggest that volumetrically insignificant sulfide will dominate bulk-rock Os budgets. This is consistent with studies of natural samples (e.g. Hart and Ravizza, 1996; Burton et al., 1999; Alard et al., 2002; Alard et al., 2005; Harvey et al., 2006). However, at least two discrete populations of mantle sulfide have been identified; one residual after melt depletion and a second, interstitial population attributed to redistribution or precipitation by a metasomatising melt or fluid (Alard et al., 2002). This implies that the bulk-rock Re and Os budget will be controlled by the relative contributions from each of these two sulfide populations. Moreover, as interstitial sulfide may be mobile during metasomatism, re-distribution of Re and / or Os has the potential to obscure primary geochemical and isotope signatures in a similar way to that of the lithophile-based isotope systems.

This study presents major and trace element abundances for bulk-rock and mantle minerals along with Re-Os isotope and elemental data for bulk-rocks, silicate minerals, and individual sulfide grains from a suite of spinel lherzolite and spinel harzburgite xenoliths from the Mont Briançon scoria cone, Devès volcanic province, French Massif Central. Variations between the major elements indicate that the sample suite has experienced differing degrees of melt depletion while bulk-rock and mineral trace element measurements reveal that many samples have also experienced extensive cryptic metasomatism. Moreover, analysis of trails of melt inclusions preserved within silicate minerals and along grain boundaries suggests that sulfide has also been added or re-distributed during metasomatism. Despite a significant

metasomatic overprint on many of the Mont Briançon xenoliths, the Re-Os isotopic measurements of sulfide grains included within silicate minerals demonstrate that some melt depletion occurred at least 1.8 Gyr ago, and that in many xenoliths the recent addition of metasomatic sulfide has had little overall effect on the bulk-rock Re-Os isotope systematics.

2. GEOLOGICAL SETTING AND SAMPLE PETROLOGY

The French Massif Central volcanic province is the largest volcanic area in Europe (Figure 1) and forms part of a much larger igneous province that extends as far east as Poland. Despite the regional thickening imposed during the Variscan orogeny, the Massif Central is characterised by particularly thin crust and a lithospheric thickness as low as 60 km (Hirn, 1980). Elevated heat flow in the region is comparable to other tectono-magmatically active regions (Lucazeau and Bayer, 1982; Granet et al., 1995) and the presence of a transient 20–30 mW m^{-2} anomaly is considered to be plume-related temperature augmentation (200-250°C) at a depth of 60-70 km (Coisy and Nicolas, 1978; Nicolas et al., 1987; Sobolev et al., 1996), which may indicate a hot mantle body extending to depths of at least 270 km (Granet et al., 1995; Sobolev et al 1996). A lithospheric boundary at 45° 30' N, which separates northern and southern lithospheric domains, has been suggested based upon several lines of evidence; textural and bulk-rock trace element data (Lenoir et al., 2000); seismic anisotropy (Babuska et al., 2002); clinopyroxene trace elements, Sr and Nd isotope analyses (Downes et al., 2003); Pb and Lu-Hf isotope analyses of clinopyroxene grains from spinel-facies xenoliths (Wittig et al., 2006, 2007). These mantle domains not only possess distinct mantle topographies at the lithosphere / asthenosphere boundary, but also delimit the distribution of the dominant styles of metasomatism in peridotite xenoliths of the Massif Central.

The volcanic activity in the south-eastern Massif Central is characterised by Tertiary to Recent basaltic plateaux, strombolian scoria cones and alkalic plugs. The samples from this study are all spinel peridotite xenoliths from the Mont Briançon scoria cone in the Devès area, located in the southern lithospheric domain. This region was last volcanically active during the Pliocene (c. 1-4 Ma). The 17 samples from this study, like previous studies of Mont Briançon xenoliths (Lorand and Alard, 2001; Meisel et al., 2001), have predominantly protogranular textures (Coisy and Nicholas, 1978; Brown et al., 1980). Grains are separated by curvilinear boundaries and, while strain-free neoblasts are mostly absent, a degree of polygonisation to a coarse sub-structure is apparent in some samples. Two samples (MBr13 and MBr19) are characterized by both protogranular and porphyroclastic textures, while a single sample (MBr24) has a porphyroclastic texture. This suggests that most samples display a high degree of textural equilibrium.

Large (> 1 kg) xenoliths were preferentially selected so that host basalt could be trimmed and the possible effects of host infiltration minimized while still retaining sufficient material (> 500 g) to represent a heterogeneous sample at the bulk-rock scale. The samples for this study were also selected so as to represent a wide range of clinopyroxene modal abundance, estimated visually in the field and subsequently calculated using a least squares regression method (Tarantola and Valette, 1982). Chrome-diopside modal abundance ranges from 3.3 to 17.2 (± 1.6) %. No discrete metasomatic phases (e.g. phlogopite, amphibole, apatite) were detected during this study, or any prior study of this locality.

The temperatures at which these xenoliths last equilibrated range from 887°C to 1055°C (this study, online supplementary material; Coisy and Nicolas, 1978; Brown et al., 1980; Lorand and Alard, 2001; Sobolev et al., 1996). These calculations

199 are based upon clinopyroxene-orthopyroxene equilibria (Wells, 1977; Brey and
200 Kohler, 1990). Assuming a geothermal gradient of 13.5 °C $kbar^{-1}$ (Lucazeau and
201 Bayer, 1982) or 4.2 °C km^{-1} (Granet et al., 1995), this suggests that they last
202 equilibrated at depths of 55 – 65 km, i.e. near to the local lithosphere / asthenosphere
203 boundary (Hirn, 1980). Entrainment depths are supported by minimum trapping
204 pressures of CO_2-rich inclusions preserved in silicate grains within the xenoliths of
205 1.3 GPa (Schiano and Clocchiatti, 1994).
206
207
208
209
210
211
212
213
214
215
216
217
218
219
220
221

3. ANALYTICAL METHODS

Samples were cut and washed to remove host basalt, surface alteration and contamination, and following repeated rinsing in ultra-pure water, were dried and then powdered in an agate mortar. Bulk-rock major elements were measured using a ARL 8420+ dual goniometer wavelength dispersive XRF spectrometer. Major element and Ni data quality was assessed using two rock standards (WS-E and OUG-94). Reproducibility is within 2% of the recommended values (online supplementary material). Bulk-rock trace elements were measured on an Agilent 7500a ICP-MS. Error on LREE measurements ranges from < 1 % for high concentration samples to > 20 % for the lowest concentration sample (MBr1). Errors on Sr measurements are all < 3 %. Errors on Yb measurements are below 7 % with the exception of the low concentration sample MBr16 (11 %). Reproducibility of 3 peridotite reference materials (PCC-1, UB-N and JP-1) can be found in the online supplementary material. Mineral trace elements were obtained by LA ICP-MS using a New Wave Nd:YAG 213 nm laser. Error on clinopyroxene REE measurements ranges from 7 to 18 %, with the exception of MBr4 where the 2 σ error is up to an order of magnitude higher. Errors on Sr measurements range between 7 to 8 % (2 σ). The long-term reproducibility of NIST 612 reference material is presented in the online supplementary material. Mineral and sulfide major elements were determined using a Cameca SX100 electron microprobe at The Open University. Reproducibility of major elements (Mg, Fe, Si, Ca, Al, Ni) of an in-house silicate secondary standard

ranges from 1 to 9 % (2 σ), and for Mn 28 % (2 σ). For minor elements (present at < 0.015 weight %; Cl, Na, K, P, S, Ti, Cr) this increases to < 230%. Repeat analyses of an in-house pentlandite standard yields errors on major elements (S, Fe, Ni) of 2, 5 and 6 % (2 σ) respectively, with minor elements (Co, Cu) errors (2 σ) of 22 % and 70 % respectively. Minerals used for electron microprobe calibration and details of the long term reproducibility of in-house standards are presented in the online supplementary material. Sulfur abundances were measured using a Leco CNS 2000 at The Open University. The uncertainty on the measurements (2 σ) is ± 12 %. Trapping pressures of CO_2 inclusions and major element compositions of silicate melt inclusions were determined at the Laboratoire des Magmas et Volcans, University of Blaise Pascal, Clermont Ferrand, France; the latter using a Cameca SX100 electron microprobe.

For the Re-Os chemistry ~ 0.5 g of sample was dissolved by low temperature acid attack (LTAA) as in previous studies (e.g. Birck et al., 1997). To accurately determine Os isotope ratios and abundances of Re and Os a spike solution, enriched in ^{185}Re and ^{190}Os, was added immediately before the addition of 2 ml of Teflon-distilled (TD) 9M HBr and 2 ml of commercial grade 29M HF to prevent the combination of sample and spike forming a button-like clot which prevents effective sample / spike equilibration. Samples were digested in an oven at 140 ^{o}C for not less than 72 hours (cf. Meisel et al., 2003). The samples were removed from the oven on a daily basis, shaken vigorously, and placed in an ultrasonic bath for at least 30 minutes each day, before being returned to the oven. At the end of the digestion the sample was examined and if complete dissolution had not occurred, a further quantity of 29M HF was added, and the digestion procedure repeated. The reference material UB-N, a serpentinized peridotite, was digested several times (n = 3) to assess the efficacy of

the LTAA dissolution method for bulk-rock peridotite. Meisel et al., (2003) suggested that LTAA is not an efficient means for peridotite dissolution, often leaving resistant phases undissolved and leading to poor reproducibility of Os concentrations and Os isotope ratios. However, the digestions of UB-N, duplicate digestions of MBr bulk-rock samples (MBr9 and MBr16) by LTAA, and duplicates of an in-house peridotite standard from Kilbourne Hole, dissolved by both LTAA and Carius tubes (Shirey and Walker, 1995), performed during this study suggest that digestions in small vessels (7 mL) yield reproducible results. Osmium concentrations obtained during this study are higher than those derived by LTAA by Meisel et al., (2003) and approach the preferred Os concentration of 3.85 ppb for UB-N. Moreover, the Os isotope ratios are indistinguishable from those derived by high temperature asher (HTA) by Meisel et al., (2003). The results of several dissolutions of UB-N by LTAA and Carius tube, and a comparison with the HTA digestions of Meisel et al., (2003) are presented in the online supplementary material.

After digestion, Osmium was purified using liquid Br_2, CrO_3 in HNO_3 and HNO_3, and recovered in the Br_2, leaving Re in the supernatant fraction. The Os was subsequently recovered from the Br_2 in HBr, micro-distilled for 3 hours at 90 °C and dried. Rhenium was extracted by reducing the CrO_3-rich supernatant with a 1:1 ethanol: ultrapure H_2O solution which was then dried. The residue was redissolved in 2M TD HNO_3 and Re was recovered in isoamylol, cleaned in a wash of 2M TD HNO_3 and finally extracted in ultrapure H_2O (Birck et al., 1997). The total procedural blank for bulk-rock Os during this study was 0.29 ± 0.26 pg, $^{187}Os/^{188}Os$ = 0.2003 ± 0.0639, and for bulk-rock Re 3.13 ± 2.37 pg. The short-term reproducibility of the blank was ± 10 % or better, but the absolute values varied between each batch of prepared reagents. Re-Os chemistry for individual hand-picked sulfide grains was achieved

using a modified microdistillation technique that closely follows previously reported procedures (Pearson et al., 1998). The total procedural blanks for Os in individual sulfides were 0.10 ± 0.06 pg, $^{187}Os/^{188}Os$ = 0.36 ± 0.50, and for Re 3.14 ± 0.61 pg. Both Re and Os samples were analysed on platinum filaments using negative thermal ionisation mass spectrometry (N-TIMS) (Volkening et al., 1991; Creaser et al., 1991) using a Thermo Scientific Triton. Long term reproducibility of a Johnson Matthey standard solution (14 pg – 8 ng; n=85) is generally within 0.1 % of the recommended values for $^{187}Os/^{188}Os$. Details of the analysis of the standard solution is presented in the online supplementary material.

4. RESULTS

4.1. Bulk-rock analyses

Mineral modal abundances, calculated using a least squares linear regression (Tarantola and Valette, 1982), demonstrate that, with the exception of MBr16, all of the samples studied are spinel lherzolites. MBr16, with clinopyroxene modal abundance of 3.3 (± 1.5) % is the only spinel harzburgite (mineral modal abundances are presented in the online supplementary material). Selected bulk-rock major element abundances are presented Table 1 (full major element analyses are presented in the online supplementary material). Co-variations between MgO/SiO_2 and Al_2O_3/SiO_2 (Figure 2) coupled with positive co-variations between bulk rock CaO weight % and Al_2O_3 weight %, bulk-rock Mg# (Mg# = $(MgO/40.32)/\{(MgO/40.32)+[(Fe_2O_{3(Total)}/79.8)\times 0.9]\}$) of 88-91 and the given range of clinopyroxene modal abundance indicates that these xenoliths are compositionally similar to other Massif Central xenoliths (Downes and Dupuy, 1987; Lenoir et al., 2000; Zangana et al., 1999; Figure 2), non-cratonic xenoliths worldwide (e.g. Nixon and Boyd, 1973; Sobolev, 1974; Boyd and Nixon, 1978; Frey and Prinz, 1978; Frey and Green, 1974; Gurney and Hart, 1980; Irving, 1980; Stosch and Seck, 1980; Roden et al., 1988; Kopylova et al., 1999) and massif peridotites (Boudier and Nicolas, 1977; Bodinier, 1988; Menzies and Allen, 1974; Frey et al., 1991; Dickey, 1970; Frey et al., 1985; Hartmann and Wedephol, 1993; Carswell, 1968; Bodinier and Godard, (2004)

and references therein), but typically less refractory than cratonic xenoliths (e.g. Nixon and Boyd, 1973; Sobolev, 1974; Boyd and Nixon, 1978; Gurney and Hart, 1980; Kopylova et al., 1999) and depleted abyssal peridotites (e.g. Alard et al., 2005; Harvey et al., 2006; Liu et al., 2008). Bulk-rock major element compositions therefore suggests that most of these xenoliths may be related by varying, yet moderate, degrees of melt depletion (< c. 18 %) prior to being brought to the surface in the host basalt.

Unlike bulk-rock massif peridotites such as Lherz, which extend to 5 weight % Al_2O_3 (e.g. Le Roux et al., 2007) no Mont Briançon bulk-rock lherzolites have more than 3.4 weight % Al_2O_3. Bulk-rock co-variations of Cr_2O_3, Al_2O_3 and MgO of Mont Briançon xenoliths all co-vary strongly. This contrasts with similar bivariate plots for re-fertilized massif peridotites which commonly lie on two distinct trends (e.g. Le Roux et al., 2007). Many of the Mont Briançon xenoliths lie within a similar range of bulk-rock Al_2O_3 weight % ($1.6 < Al_2O_3 < 3.5$ weight %) to Tok cratonic peridotites (Ionov et al., 2006) ascribed as having melt depletion signatures, and only one sample (MBr16) can be described as particularly refractory ($Al_2O_3 < 1.3\%$; Ionov et al., 2006) and therefore particularly susceptible to subsequent metasomatism (McDonough and Frey, 1989). Bulk-rock Al_2O_3 abundances calculated from the product of mineral modes and the Al_2O_3 weight % of the constituent minerals indicate that a significant proportion of the bulk-rock Al_2O_3 cannot be accounted for by the silicate minerals and spinel. Taking into account the uncertainties in the modal abundance calculations a grain boundary phase accounts for at least 8 % of the bulk-rock Al_2O_3 of MBr13 and as much as 33 % of MBr28.

With the exception of MBr13, which have elements of both protogranular and porphyroclastic textures and a relatively high olivine modal abundance for its Mg#, the Mont Briançon xenolith suite demonstrates a broad positive co-variation between

372 olivine modal abundance and bulk-rock Mg#. This contrasts with many tectonically
373 emplaced peridotite suites whose longer transit to the surface has led to more
374 complicated bulk-rock and mineralogical systematics, e.g. ophiolite peridotite from
375 the Ligurian Alps (Rampone et al., 2005; Rampone and Borghini, 2008). Bulk-rock
376 abundances of moderately incompatible elements, e.g. Yb, Sc and V all show strongly
377 co-varying trends.

378 Co-variations between bulk-rock major element indices of melt depletion and
379 incompatible trace element abundances are notably absent, and many xenoliths have
380 moderate to strong enrichments in incompatible elements. Three different
381 incompatible trace element fingerprints are evident (Figure 4). The first group of
382 xenoliths (n = 7) is depleted in light rare earth elements (LREE), i.e. Ce/Yb ratios
383 normalized to primitive mantle after Palme and O'Neil, (2004) ($[Ce/Yb]_N$) range from
384 0.2 to 0.6. REE fractionation is accompanied by a moderate relative enrichment in Zr,
385 Nb and sometimes Ti, and moderate relative enrichments of Sr. In contrast, a second
386 group of samples (n = 7) possess $(Ce/Yb)_N \leq 2$. In the absence of metasomatic
387 accessory phases (e.g. phlogopite, amphibole, apatite) this is indicative of cryptic
388 LREE enrichment. A single sample (MBr6) is characterised by a flat, yet depleted,
389 MREE – HREE pattern, however $(Ce/Yb)_N$ is highly enriched (4) and is accompanied
390 by a large Sr enrichment. With the exception of MBr6, which is anomalous, the first
391 two groups strongly resemble the incompatible trace element patterns for southern
392 domain FMC xenoliths of Lenoir et al., (2000). Like the other 7 xenoliths with
393 elevated $(Ce/Yb)_N$ ratios, the trace element composition of MBr6 cannot be attributed
394 to melt depletion alone and must be due to subsequent interaction with a metasomatic
395 agent or agents.

396

4.2. Mineral compositions

4.2.1. Silicates and spinel

Electron microprobe analyses of the constituent phases of 18 xenoliths (online supplementary material) reveal that olivine Mg# ranges from 0.88-0.91 and co-varies with Ni content. Mineral major element compositions are, in most samples, similar to spinel-facies peridotite xenoliths from non-cratonic settings worldwide (e.g. Frey and Green, 1974; Ionov et al., 1993; Frey and Prinz, 1978; Wilshire and Shervais, 1975; Stosch and Seck, 1980). For example, olivine MgO ranges from 46.85 (± 0.18) to 49.70 (± 0.85) weight %; clinopyroxene CaO and Na_2O range from 19.35 (± 0.31) to 20.77 (± 0.15) and 1.29 (± 0.04) to 1.92 (± 0.06) weight % respectively; orthopyroxene Al_2O_3 ranges from 2.76 (± 0.20) to 4.74 (± 0.39) weight %; spinel Cr_2O_3 and Al_2O_3 range from 8.75 (± 0.21) to 23.79 (± 0.98) and 42.71 (± 0.85) to 57.97 (± 0.39) weight % respectively. Bulk-rock TiO_2 strongly co-varies with clinopyroxene TiO_2 abundance; a continuum between the most and least refractory peridotites being evident. Three xenoliths (MBr3, 13 and 24) are exceptional in that they have higher Al_2O_3 in orthopyroxene for a given co-existing spinel Cr# (Cr# = ([Cr_2O_3/151.99]/{[Cr_2O_3/151.99]+[Al_2O_3/101.96]})). MBr24 is the only sample with a porphyroclastic texture and MBr13 is one of only two examples transitional between protogranular and porphyroclastic, suggesting that mineral composition may be related to xenolith texture (cf. Brown et al., 1980; Zangana et al., 1999).

Trace element compositions of the constituent major phases of MBr2, MBr3, MBr6 and MBr8 were obtained by laser ablation ICP-MS (online supplementary material). These samples were selected as being representative of the three contrasting bulk-rock trace element profiles described in section 4.1. Chrome-diopside

incompatible trace element patterns closely match those of the corresponding bulk-rock. Clinopyroxene $(Ce/Yb)_N$ range from 0.27 to 1.35. The lowest values, $(Ce/Yb)_N$ = 0.27 and 0.34, are derived from MBr1 and MBr8 respectively; two of the xenoliths whose bulk-rock $(Ce/Yb)_N$ is indicative of melt depletion. Clinopyroxene from MBr2 and MBr3 have $(Ce/Yb)_N$ of 0.60 and 1.35 respectively, whereas MBr6, the sample with the most elevated bulk-rock $(Ce/Yb)_N$ has a clinopyroxene $(Ce/Yb)_N$ of 1.09. This suggests that, in many xenoliths, the majority of the bulk-rock trace element inventory can be accounted for by clinopyroxene. However, the Ce/Yb ratio of MBr6 clinopyroxene is much lower than its corresponding bulk-rock which suggests that there is a significant LREE component not accounted for by clinopyroxene. Relative depletions in clinopyroxene HFSE and Ti are most pronounced in MBr6, less so in MBr3, MBr2 and MBr8. These depletions are complemented by enrichments in co-existing orthopyroxene, an antithetic relationship common in peridotite (e.g. Rampone et al., 1991; Rivallenti et al., 1996).

The incompatible trace element budget of several other Mont Briançon xenoliths cannot wholly be accounted for by their constituent minerals. While the majority of MREE and HREE are contained in the major peridotite minerals, deficiencies in the mass balances become more pronounced in the LREE and, with the exception of U and Th, increase with growing incompatibility.

4.2.2. Melt inclusions

Trails of melt inclusions trapped within fractures in silicate minerals are common in Mont Briançon xenoliths (Schiano and Clocchiatti, 1994) and often cross-cut individual silicate grains before terminating at grain boundaries lined with

447 interstitial glass. Individual melt inclusions rarely exceed 10 μm in diameter, and
448 comprise silicate glass with rare daughter phases located at the inclusion walls. At
449 least one fluid bubble is preserved within each melt inclusion. Experiments on a
450 cryometric stage and laser-Raman analyses reveal that these fluids are almost pure
451 CO_2 and became trapped within their host phase at pressures of at least 1.3 GPa, i.e. a
452 depth of at least 40 km (Schiano and Clocchiatti, 1994). Therefore, when the fracture
453 hosting the melt inclusions annealed, the trapped melt, which now encloses the fluid
454 inclusions, was CO_2 saturated. Discrete CO_2 inclusions not associated with silicate
455 glass and trapped at shallower depths are also common. The CO_2 saturated silicate
456 melt inclusions are also associated with minute sulfide blebs (≤ 10 μm diameter)
457 within the silicate / CO_2 inclusion trails. In rare examples all three co-genetic phases,
458 i.e. silicate glass, CO_2 fluid and sulfide, are present within a single inclusion and the
459 immiscible nature of the co-genetic silicate and sulfide phases is clear (Figure 4).

460 A total of 54 glassy inclusions in 6 Mont Briançon xenoliths were analysed for
461 major element abundance, along with S and Cl concentrations (supplementary online
462 material). The majority (n = 35) are hosted in olivine grains. The remainder are
463 included in clinopyroxene (n = 15) or orthopyroxene (n = 4). Inclusions were not re-
464 homogenised prior to analysis as only inclusions with no daughter minerals were
465 analysed. High $Na_2O + K_2O$ (≤ 7.8 weight %), S abundances (320-2960 ppm) and
466 Al_2O_3 and SiO_2 (≤ 24.4 and 61.9 weight %, respectively), are consistent with previous
467 measurements of re-homogenised Mont Briançon melt inclusions, and similar to
468 inclusions from both oceanic and continental intra-plate settings (Schiano with
469 Clocchiatti, 1994).

470

471 *4.2.3. Sulfide grains*

Major element analyses (S, Fe, Ni, Cu, Co – online supplementary material) were made on 62 discrete sulfide blebs using a Cameca SX100 electron microprobe. The sulfides can be divided into 5 distinct groups based upon textural constraints, i.e. interstitial or wholly enclosed within a silicate grain, degree of weathering, and proximity to interstitial glass and corroded spinel. The degree of alteration of each sulfide was assessed qualitatively under reflected light and quantitatively on the electron microprobe by assessing measured S/O ratios.

Unweathered included, often rounded, sulfide grains (Group A, Figure 5a) have the most uniform compositions (Figure 6), and are characterized by high Ni/Fe (0.19 – 1.18) and high S/O ratios (14.21 – 166.93). Although the S/O ratio suggests that even these "unweathered" sulfides have, in some instances, experience some alteration, this group of sulfide are the closest to a pentlandite mineralogy as previously observed in other non-cratonic peridotite xenoliths (e.g. Dromgoole and Pasteris, 1987). Often, these seemingly isolated sulfides are associated with trails of micron-scale sulfide blebs which commonly terminate at grain boundaries (Figure 5b). Weathered included sulfides (Group B), by contrast, have lower Ni/Fe and S/O ratios (0.03 – 0.50 and 0.003 – 1.06, respectively) and deviate from a simple pentlandite-like composition. The weathered sulfides in general no longer possess conventional sulfide compositions because of the formation of iron oxy-hydroxides, and perturbed metal : sulfur ratios. Interstitial grains are often less rounded, more ragged and even elongate in shape (Figure 5c with 5d), and occasionally infill cracks in deformed silicate grains (Figure 5d). The Ni/Fe ratios of weathered interstitial sulfides (Group C, Figure 5e) range from 0.03 – 0.57 and S/O ratios 0.003 – 3.01, i.e. a field that wholly encompasses that of weathered included sulfides. Unweathered

interstitial grains (Group D, Figure 5d) form two separate compositional groups in Ni/Fe vs. S/O space. Half of the grains are compositionally indistinguishable from weathered interstitial grains, whereas the remainder have compositions similar to the unweathered included grains with the highest Ni/Fe ratios (~1).

The final group of sulfides (Group E, Figure 5f) are predominantly rounded, although much smaller than included sulfides, are generally unweathered in appearance, and exclusively associated with interstitial glass and corroded spinels. Compositionally, these sulfides are very similar to unweathered interstitial grains and exhibit a similar bimodal distribution in Ni/Fe vs. S/O compositional space.

4.3. Re-Os concentration and isotope ratios

4.3.1. Bulk-rock analyses

Sixteen xenoliths were analysed for Re and Os elemental abundance and isotope ratios (Table 2). Osmium concentrations (0.83 – 2.19 ppb) are similar to other non-cratonic peridotite xenoliths worldwide (e.g. Meisel et al., 2001) but lower than those obtained from orogenic massifs (e.g. Reisberg and Lorand, 1995), cratonic peridotite xenoliths (≤ 9.2 ppb, Pearson et al., 1995a, 1995b; Chesley et al., 1999; Gao et al., 2002; Irving et al., 2003; Wu et al., 2003; Yuan et al., 2007), the average upper mantle concentration of 3.1 (± 0.3) ppb (Morgan, 1986) and the calculated primitive upper mantle (PUM) value of 3.9 (± 0.5) ppb (Becker et al., 2006). Rhenium concentrations range from 0.063 to 0.634 ppb and show a bimodal distribution. Six samples have Re concentrations that are similar to or less than the concentration inferred for fertile mantle, i.e. 0.260 ppb (Morgan, 1986), and significantly below that

522 estimated for PUM (0.35 ± 0.06; Becker et al., 2006) while the remainder have Re
523 concentrations far in excess of fertile mantle. Consequently, more than half of the
524 xenoliths analysed have suprachondritic Re/Os ratios (> 0.406, Shirey and Walker,
525 1998).

526 Bulk-rock $^{187}Os/^{188}Os$ ratios range from 0.11541 (± 0.00021) to 0.12897 (±
527 0.00032) i.e. below the maximum present day estimate of the primitive upper mantle
528 (PUM $^{187}Os/^{188}Os \leq 0.1292$, Meisel et al., 2001), and all but one (MBr1) below the
529 present day mean chondrite value i.e. $^{187}Os/^{188}Os < 0.127$ (Shirey with Walker, 1998).
530 Bulk-rock $^{187}Re/^{188}Os$ ratios range from 0.112 to 3.436, possess a wide range of
531 $^{187}Re/^{188}Os$ values for a given Os isotope ratio, show no clear correlation with
532 $^{187}Os/^{188}Os$, and therefore yield no meaningful isochron age information (Figure 7a).
533 The scatter between $^{187}Re/^{188}Os$ and $^{187}Os/^{188}Os$ is, in general, much higher in
534 xenolith suites than massif peridotites (Reisberg and Lorand, 1995) but is particularly
535 high amongst the xenoliths from Mont Briançon. Scatter is usually attributed to Re
536 mobility, as this element, unlike Os, may be mobile under a wide range of conditions
537 (e.g. Reisberg and Lorand, 1995; Meisel et al., 2001; Sun et al., 2003). The use of a
538 suitable immobile proxy for bulk-rock $^{187}Re/^{188}Os$ has sometimes yielded more
539 coherent correlations with $^{187}Os/^{188}Os$ in instances where Re abundance may have
540 been disturbed. In a suite of peridotites related by a single stage of melt depletion
541 from a homogenous starting composition, one should find a linear correlation between
542 the index of melt depletion (e.g., Al_2O_3) and $^{187}Os/^{188}Os$ (e.g. Rudnick and Walker,
543 2009). While proxies such as Al_2O_3 (Reisberg and Lorand 1995), [S], (Burnham et al.,
544 1998) and [Yb], (Reisberg et al., 2005) may reduce scatter on disturbed isochron-type
545 plots no significant improvement is obtained using any of these proxies in this study
546 (Figure 7b, 7c and 7d respectively).

547

548 *4.3.2. Mineral separates*

549

550 Optically pure mineral separates of olivine, orthopyroxene and clinopyroxene
551 from MBr2, 3, 6, 8 and 20 yield Os concentrations (Table 3) of 3.7 - 29.3 ppt in
552 olivine, 8.0 - 91.6 ppt in orthopyroxene (the value of 815 ppt for MBr3 is probably
553 derived from an unseen sulfide included within one or more of the grains, cf. Burton
554 et al., 1999), and 28.2 - 185.1 ppt in clinopyroxene. While Os concentrations in spinel
555 range from 11.7 ppt to 450.8 ppt, the opacity of this mineral makes it difficult to
556 assess whether this is due to spinel-hosted Os, sulfide contamination or a combination
557 of the two. Notwithstanding the possibility of sulfide contamination, mean Os
558 abundance increases thus: olivine < orthopyroxene < clinopyroxene < spinel, with
559 absolute values similar to those measured by Hart and Ravizza, (1996) and Burton et
560 al., (1999). The measured Os concentrations do not therefore simply reflect the effects
561 of variable degrees of sulfide incorporation. Rhenium concentrations of the same
562 silicate phases (Table 3) are 21.8 – 94.3 ppt in olivine, 35.3 – 239 ppt in
563 orthopyroxene and 61.2 - 421 ppt in clinopyroxene. Rhenium concentrations in spinel
564 are higher than in the silicate phases (80.2 - 924 ppt), but like Os, the origin of Re in
565 spinel is not unequivocal. Therefore, mean Re concentrations increase thus: olivine <
566 orthopyroxene < clinopyroxene < spinel.

567 Mineral $^{187}Os/^{188}Os$ ratios (Table 3) range from 0.120 to 0.136 for olivine,
568 0.121 to 0.142 for orthopyroxene, 0.120 to 0.203 in clinopyroxene and 0.128 and
569 0.291 in spinel (Figure 8). As previously reported (Burton et al., 1999) mineral Os
570 isotope ratios are consistently higher than their corresponding bulk-rock. The
571 $^{187}Re/^{188}Os$ ratios of the mineral phases range from 2.05 to 78.5 for olivine, 0.58 to

125 for orthopyroxene and 5.7 to 187 for clinopyroxene, while spinel $^{187}Re/^{188}Os$ ranges from 4.53 to 181. Mean $^{187}Re/^{188}Os$ ratios for all of the separated phases are much greater than present day chondrite, i.e. $^{187}Re/^{188}Os = 0.406$ (Shirey and Walker, 1998), however there is no individual sample that appears systematically enriched in Re across all of its constituent phases. Moreover, no particular phase across the wide compositional range of xenoliths selected appears to be either particularly susceptible to, or immune from, Re enrichment. Silicates show little variability in $^{187}Os/^{188}Os$ ratio for a wide range of $^{187}Re/^{188}Os$ and closely resemble the Os isotope composition of the bulk-rock, although each sample has at least one phase significantly more radiogenic than the rest.

4.3.3. Individual sulfide grains

In addition to the optically pure mineral separates, 14 individual sulfide grains were recovered from the crushate of MBr3 (n = 3), MBr6 (n = 4), MBr8 (n = 3), and MBr20 (n = 4). Both Re and Os concentrations vary widely (0.01 – 412 ppm, and 0.047 – 40.84 ppm respectively), and a wide range of Os isotope ratios was also obtained, ranging from $^{187}Os/^{188}Os = 0.115$ to 0.171 (Figure 9) (Table 3). Many of the sulfides (n=9) have subchondritic Os isotope ratios (0.115 – 0.126) that yield T_{RD} model ages of up to 1.78 Ga (Figure 10), that is, similar to the oldest T_{RD} obtained from bulk-rock Os isotope analyses (1.71 Ga).

5. DISCUSSION

Melt depletion and subsequent secondary melt and / or fluid infiltration, either as individual or multiple events, are thought to be the main processes responsible for the present-day composition of peridotite xenoliths. Depletion of SCLM by removal of a basaltic melt results in systematic trends in bulk-rock major and trace element composition, modal mineralogy and, crucially for dating melt depletion events in the SCLM, the systematic fractionation of parent-daughter elements that comprise the traditional radiogenic isotope systems. However, metasomatism systematically obscures the elemental and isotopic fingerprints of ancient melt depletion, overprinting or completely erasing evidence for earlier events. Early studies suggested that the Re-Os isotope system is robust against the effects of metasomatism (e.g. Carlson and Irving, 1994; Pearson et al., 1995a) as bulk-rock Re and Os abundance and isotope ratios are controlled almost entirely by volumetrically insignificant sulfide (e.g. Hart and Ravizza, 1996; Burton et al., 1999; Alard et al., 2002; Harvey et al., 2006). However, interaction with sulfur-saturated metasomatic melts or fluids can result in the precipitation of secondary sulfides which in turn make bulk-rock Re-Os isotope analyses simply the weighted mean of the two generations of sulfide, yielding complex geochronological information. Despite the interaction with metasomatic agents, geochemical evidence of early melt depletion may still be preserved in sulfide grains trapped within host silicates and thus protected from interaction with metasomatic melts or fluids. By systematically dis-assembling individual xenoliths

and examining their constituent components it is still possible to extract information regarding the relative timing of melt depletion and subsequent, secondary processes.

5.1. Petrological and major element evidence for melt depletion and subsequent metasomatism

5.1.1. Melt depletion

The SCLM underlying the Massif Central is considered to have experienced multiple melt depletion events; (i) subduction related volcanism prior to the Variscan orogeny (Pin and Marini, 1993; Alexandrov et al., 2000; Lardeaux et al., 2001; Wittig et al., 2007), (ii) at 257 Myr ago (Femenias et al., 2004), and (iii) voluminous Pliocene volcanism (c.1 – 4 Ma). Strong co-variations between traditional indices of melt depletion (e.g. CaO weight %, Al_2O_3 weight % and MgO weight %) suggest that evidence for partial melting is, at least in part, preserved. While clinopyroxene modal abundances (3.3 ± 1.5 to 17.2 ± 1.6 modal %) are consistent with variable degrees of melt depletion, the ranges of modal abundance of all the major silicate phases are not consistent with melting experiments of synthetic peridotites, natural lherzolites or pyrolites (Baker and Stolper, 1994; Baker et al., 1995). Repeated extraction of smaller proportions of melt, i.e. incremental batch melting (Robinson et al. 1998), produces ranges of mineral modal abundance consistent with the multiple episodes of melt depletion known to have occurred in the southern French Massif Central.

Many peridotites are re-fertilized after an earlier period of melt depletion, and the precipitation of secondary clinopyroxene is an almost ubiquitous process. Abyssal peridotite (Seyler et al., 2007) and orogenic massifs such as Lherz (Le Roux et al.,

2007) and Totalp (van Acken et al., 2008) all preserve evidence for such re-fertilization events. However, evidence is scant for the addition of secondary clinopyroxene in the Mont Briançon suite. Firstly, the range of clinopyroxene modal abundance at Mont Briançon is consistent with melt depletion; re-fertilization such as that observed at Lherz (Le Roux, 2007) would have the potential for extending the compositional range of moderately melt depleted lherzolites into that of pyroxenites, i.e. if re-fertilization had occurred, there is no reason why it should stop at c. 17 modal % clinopyroxene. Moreover, there is no textural evidence for re-fertilization. All of the Mont Briançon peridotites possess protogranular to porphyroclastic textures; and no evidence of mechanical mixing of peridotite and pyroxenite at the centimetre scale (cf. Le Roux, 2007; van Acken et al., 2008) is evident. The chemical composition of the Mont Briançon clinopyroxenes, discussed below, also suggests that they are part of an equilibrium melt depleted residue and that evidence for a secondary origin for some or all of the clinopyroxene is scant.

Strong correlations between bulk-rock TiO_2 and clinopyroxene TiO_2 abundances suggests that the more fertile MBr lherzolites are linked to the less fertile lherzolites and harzburgite by melt depletion. These bulk-rock characteristics contrast with arched patterns seen in re-fertilized massif peridotites (Bodinier and Godard, 2004, and references therein). Moreover, no evidence for wholesale olivine precipitation or pyroxene dissolution is evident from an examination of the xenoliths in hand specimen and thin section or from calculated modal abundances. Apart from MBr13, with elements of both protogranular and porphyroclastic textures and has a relatively high olivine modal abundance for its Mg#, the co-variation between olivine modal abundance and bulk-rock Mg# is consistent with melt depletion. There is no petrological and very little major element evidence for significant degrees of melt /

671 rock interaction, i.e. the formation of melt channels such as those described by e.g.
672 Kelemen et al., (1992) Rampone et al (2005) Rampone and Borghini (2008) and
673 Buchl et al., (2002) can be discounted. The broad inverse co-variation of
674 clinopyroxene modal abundance with olivine Mg# also suggests that Mont Briançon
675 clinopyroxene is primary.

676 Bulk-rock Al_2O_3 abundances of 0.8 – 1.0 weight % are consistent with a
677 peridotite residue containing 3-5 modal % clinopyroxene (Canil, 2004), the result of
678 partial melting at significantly less than F = 0.20 which is consistent with the most
679 depleted Mont Briançon peridotites. In addition, evidence for the likely depth of at
680 least some of the melt extraction and the redox conditions within the mantle at that
681 depth can be obtained from the systematic behaviour of moderately incompatible
682 elements. Bulk-rock [Yb] vs Al_2O_3 suggests that the Mont Briançon xenoliths lost at
683 least some of their melt at < 3.0 GPa. The behaviour of V during mantle melting is
684 sensitive to fO_2 and variations of this element in peridotite can provide a paleoredox
685 indicator (Canil and Fedortchouk, 2000). Bulk-rock [V] vs. Al_2O_3 suggests an fO_2 of
686 between NNO-2 and NNO (NNO = nickel-nickel-oxide) at 1.5 GPa (Canil, 2004).
687 This is consistent with melt loss in a mantle environment more oxidizing than that of
688 abyssal peridotites and similar to peridotites whose melt depletion signature has been
689 attributed to subduction related melting, typically at fO_2 of NNO-3 to NNO (Canil,
690 2002). However, bulk-rock [V] vs. [Yb] is a better discriminator between the effects
691 of pressure and fO_2 (Canil, 2004) and places the Mont Briançon peridotite suite closer
692 to an fO_2 of NNO at 1.5 GPa than bulk-rock [V] vs. Al_2O_3 weight %.

693 Only one xenolith (MBr16) can be described as particularly refractory.
694 Siberian cratonic peridotites from Tok (Ionov et al., 2006) and Udachnaya (Boyd et
695 al., 1997) with < 1.6 weight % Al_2O_3 retain evidence for melt extraction in excess of

20 %, and show the greatest degree of metasomatism. Cratonic xenoliths (e.g. Ionov et al., 2006) with intermediate bulk-rock Al_2O_3 abundances ($1.6 < Al_2O_3 < 3.5$ weight %) preserve the best melt depletion fingerprint. This range encompasses all but 3 samples from this study (MBr1, 6, 19).

5.1.2. Metasomatism

Given the prior melt depletion history of the Massif Central region, it is unlikely that local segments of the SCLM escaped melt depletion entirely. However, several samples (n = 7) have bulk-rock Al_2O_3 and CaO abundances that approach primitive upper mantle values (Hart and Zindler, 1986; Jagoutz et al., 1979; Palme and Nickel, 1985; McDonough, 1990; McDonough and Sun, 1995), which could suggest that these xenoliths have been re-fertilized through the addition of metasomatic pyroxene. In addition, because of the similar incompatibility of Na and Al in clinopyroxene, which dominates bulk-rock Na and Al budgets, the bulk-rock abundances of these elements should co-vary systematically if only partial melting had influenced their composition. Mont Briançon clinopyroxenes have a wide range of Na_2O abundance for a given Al_2O_3 weight % which is difficult to reconcile solely with melt depletion. Metasomatic clinopyroxene addition would have little discernable effect on bulk-rock composition unless, as discussed above, the degree of re-fertilization was such that > c.17 modal % clinopyroxene resulted. A scenario could be envisaged where all of the clinopyroxene in the Mont Briançon suite is secondary, but there is no evidence for all of the xenoliths being previously depleted to the point of clinopyroxene exhaustion, followed by the subsequent addition of varying amounts of secondary clinopyroxene.

No discrete metasomatic phases (e.g. apatite, phlogopite, amphibole) have been observed at this locality (Rosenbaum et al., 1997; Alard et al., 2002; this study). Petrographic evidence for metasomatism is however provided by the presence of trails of melt inclusions preserved in annealed fractures and texturally linked to interstitial glass. Highly silicic, alkali-enriched melts found as inclusions or as interstitial melts have been observed in anhydrous peridotite xenoliths worldwide (e.g. Frey and Green, 1974; Stosch and Seck, 1980, Schiano and Clocchiatti, 1994; Yaxley et al., 1999) and have been variously attributed to decompression melting of pre-existing metasomatic phases, the migration of volatile-rich melts, deeply sourced mantle fluids, and small volume partial melts from a peridotite source. Experimentally, highly silicic, alkali-rich melts can be generated by very low degrees of melting of a primitive mantle-like precursor at pressures around 1 GPa (Baker and Stolper, 1994; Baker et al., 1995; Hirschmann et al., 1998, Schiano et al., 1998). However, based upon their major-element compositions that differ drastically from upper mantle lithologies, their systematic association with CO_2-fluid inclusions and the presence of multi-phase, multiply volatile-saturated inclusion assemblages, it has also been proposed that they could act as metasomatic agents of the upper mantle. Similarly, P-rich grain boundary phases (Rosenbaum et al., 1997) cannot be attributed to basaltic melt.

Moreover, the discrepancy between bulk-rock Al_2O_3 weight % and that calculated from the sum of the main silicate minerals and spinel cannot be ignored. A significant reservoir of Al_2O_3 can only be accounted for by a grain boundary phase. Figure 4 illustrates that melt inclusions that terminate in areas of interstitial and intergranular glass are clearly the product of a secondary, metasomatic process. Irrespective of their mode of generation, discussed further in section 5.4 below, they comprise 20 – 24 weight % Al_2O_3 (online supplementary material). Combined with

746 the contribution from the interstitial glasses they therefore contribute a significant
747 proportion of bulk-rock Al_2O_3. Unlike other metasomatized European spinel
748 lherzolites brought to the surface during Cenozoic volcanism, e.g. Ackerman et al.,
749 (2009), large melt / rock ratios are not responsible for metasomatism of Mont
750 Briançon peridotites. In addition to the elevation of bulk-rock Al_2O_3, 5 samples, with
751 either porphyroclastic textures or textures transitional towards porphyroclastic (MBr1,
752 2, 13, 15 and 24), have elevated bulk-rock FeO (> 8.5 weight %) which cannot be
753 attributed to shallow (1-2 GPa) polybaric melting (Walter, 2003; Herzberg, 2004).
754 Ionov and Hofmann, (2007) attribute elevated FeO (> 8.5 weight %) to post-melting
755 interaction of melt depleted peridotite with percolating Fe-rich melt. However, the
756 majority of Mont Briançon peridotites have lower bulk-rock FeO (< 8.5 weight %)
757 with bulk-rock Al_2O_3 that ranges from 0.8 to 2.2 weight %, consistent with melt
758 depletion conditions outlined above. Other possible indicators of re-fertilization in
759 peridotites are discussed by van Acken et al., (2008) and Walter, (2003) and
760 references therein, particularly the generation of linear trends between bulk-rock
761 Na_2O, MgO and Al_2O_3. In instances where up to 10 % basaltic melt has infiltrated the
762 peridotite, e.g. at Lherz (Le Roux et al., 2007, 2008) or in other massif peridotites
763 (Bodinier and Godard, 2004) this re-fertilization is obvious and consistent with
764 precipitation of clinopyroxene from melts during porous melt flow and melt–rock
765 reaction (Müntener et al., 2004) but has not occurred at Mont Briançon where there
766 are no such co-variations and an absence of textural evidence.
767

768 **5.2. Trace element evidence for melt depletion and subsequent metasomatism**
769

770 Trace element analyses of Mont Briançon bulk-rocks and corresponding
771 clinopyroxenes demonstrate decreasing LREE/HREE consistent with melt depletion
772 (Figure 3a). Ophiolitic clinopyroxenes also commonly preserve depleted LREE
773 profiles (Rampone et al., 2005: Rampone and Borghini, 2008), although in these
774 peridotites the incompatible trace element patterns are ascribed to the precipitation of
775 secondary clinopyroxenes from impregnating melts derived from depleted melt
776 fractions. However, in addition to LREE depletion, ophiolite clinopyroxenes often
777 possess convex-upwards REE patterns or high HREE/MREE which suggests
778 equilibration with evolved silicate melts at high melt-rock ratios, for which no
779 evidence is preserved at Mont Briançon. But, partial melting cannot account for the
780 trace element abundances of the majority of this xenolith suite (Figures 3b and 3c).
781 Globally, LREE enrichment is a ubiquitous feature of harzburgites and depleted
782 lherzolites (McDonough and Frey, 1989). Interaction with a transitory metasomatising
783 melt or fluid has the greatest effect on the most depleted peridotites due to their lower
784 bulk distribution coefficients. Three samples from this study (MBr6, 13, and 19),
785 characterised by high Ce/Yb ratios for a given Ce concentration, are indicative of such
786 an enrichment process. The low Yb concentrations, coupled with low modal
787 clinopyroxene in two of the three samples also suggests that they experienced a high
788 degree of prior melt depletion.

789 MBr13 and MBr19, the samples with transitional porphyroclastic textures,
790 also have higher Ce/Yb ratios than the remainder of the suite. While MBr13 has a
791 higher clinopyroxene content (14.3 modal %), its anomalously low Mg# (bulk-rock =
792 0.863; clinopyroxene = 0.868) is clearly not attributable to melt depletion (Pearson et
793 al., 2003 and references therein). It is conceivable that this xenolith has experienced
794 some re-fertilization through the addition of clinopyroxene and that its bulk-rock

795 characteristics have been substantially modified through interaction with a
796 metasomatic melt or fluid, although major element and petrographic evidence is
797 lacking. Elsewhere in the southern Massif Central the effects of metasomatism are
798 also generally restricted to the most refractory peridotites (Downes and Dupuy, 1987;
799 Xu et al., 1998), and to deformed facies (Downes, 1990). A feedback relationship
800 between percolation and deformation that concentrates metasomatic fluids in
801 lithospheric shear zones has been postulated as the tectonic mechanism controlling
802 melt / fluid mobility (Downes, 1990). In both brittle (Wilshire and Kirby, 1989) and
803 ductile stress regimes (Downes, 1990), LREE enrichment accompanies the
804 deformation of peridotite which could account for the enriched characteristics of the
805 most deformed samples from the Mont Briançon suite (cf. Zangana et al., 1997).
806 Moreover, the xenoliths with little or no LREE enrichment have lower equilibration
807 temperatures (887 ^{o}C – 964 ^{o}C) than the xenoliths with the most enriched composition
808 (962 ^{o}C – 1019 ^{o}C) (Wells, 1977). Griffin et al. (2004) suggested that metasomatized
809 cratonic peridotite xenoliths are more likely to have equilibrated at greater depths in
810 the lithosphere and are therefore more susceptible to interaction with asthenospheric
811 melts at the base of the non-cratonic lithosphere. Mont Briançon xenoliths
812 demonstrate a similar relationship between depth of final equilibration and the degree
813 of metasomatism, suggesting that enrichment is ubiquitous at or near the base of the
814 lithosphere, consistent with the hypotheses of previous studies (Eggler, 1987; Zindler
815 and Jagoutz, 1988; McKenzie 1989, Chesley et al., 1999; Ackerman et al., 2009).
816 However, one of the most depleted samples studied here (MBr6, 5.1 modal %
817 clinopyroxene) possesses the highest bulk-rock and clinopyroxene Ce/Yb ratios, and
818 yet has one of the lowest equilibration temperatures of the entire suite (903^{o}C),
819 implying that either not all enrichment occurs at the base of the lithosphere, or

820 additional processes have modified the composition of this xenolith, e.g. fluid flow
821 through shear zones (Downes, 1990).

822 It is possible to account for the bulk-rock budget of peridotite xenoliths from
823 the summed contribution of their major constituent phases (e.g. Eggins et al., 1998).
824 Occasionally samples with trace element budgets entirely attributable to the major
825 upper mantle phases can be found in the same locality as xenoliths that require an
826 additional trace element reservoir in order to effect a mass balance (e.g. Condie et al.,
827 2004). More commonly, it is not possible to account for bulk-rock incompatible trace
828 element abundances simply from their concentrations in the major silicate phases. The
829 majority of Mont Briançon xenoliths contain melt inclusions, but there is no
830 unequivocal relationship between the presence or absence of inclusions and trace
831 element evidence of metasomatism. While the effect of the volumetrically
832 insignificant melt inclusions on bulk-rock trace element abundances is most likely
833 small, their presence is indicative of a larger reservoir of incompatible trace elements
834 derived from interstitial metasomatic melt nearby in the SCLM. Figure 11 illustrates
835 the composition of the melt needed to balance the incompatible trace element budget
836 of MBr9. The most incompatible REEs and fluid mobile elements, such as Rb and Ba,
837 are the most deficient. The magnitude of the deficiency co-varies inversely with the
838 partition coefficient of the elements in mantle silicates. Previous work (Bedini and
839 Bodinier, 1999) demonstrated the presence of a LREE and Ba-rich pervasive
840 interstitial component, with fluid inclusions and a reaction layer around spinel grains
841 accounting for the deficit in Rb and HFSE. Wittig et al., (2009) have also
842 demonstrated that a significant proportion of bulk-rock U and Th can be accounted for
843 by grain boundary components. Furthermore, Yaxley and Kamenetsky, (1999)
844 demonstrated that interstitial melts derived from decompression breakdown of

metasomatic amphibole provide silicic, alkali-enriched melts that are highly enriched in LREE, Nb, Ta and Ba, the most deficient elements at Mont Briançon. While this mechanism is a possible source for the Mont Briançon glasses it (i) fails to account for the large reservoir of "missing" Rb, (ii) requires a pre-existing metasomatic event to generate amphibole, for which no evidence is present and (iii) produces different textural relations between the major silicate phases and the glass to those actually observed. Small percentage melting of wet, fertile mantle produces a similar melt composition, but is also enriched in Rb (Chazot et al., 1996). Fluid fluxing during Variscan subduction of oceanic lithosphere beneath the Massif Central could provide the mechanism for deep, wet partial melting of the lithospheric mantle and a small contribution to the melt from volatiles fluxed from oceanic sediment could also account for the high P content of some intergranular glasses at Mont Briançon (Rosenbaum et al., 1997).

5.3. The origins of Re and Os elemental abundances and isotope ratios

Mont Briançon xenoliths, like all non-cratonic xenoliths, are characterized by significantly less Os than other peridotites. Mont Briançon xenoliths contain < 30 ppm sulfur (this study; Lorand and Alard, 2001), an order of magnitude lower than fertile mantle ([S] = 300 ppm; McDonough, 2004) and only 25% of that of depleted mantle ([S] = 119 ppm; Salters and Stracke, 2004). Supergene weathering, evident in the low S/O ratios of many sulfide grains in this study, may account for some sulfide loss (e.g. Lorand et al., 2003) although it is unclear whether Os would also be mobilised during weathering of sulfide grains. While interstitial sulfide grains may be vulnerable to the effects of surface processes, sulfide grains preserved within the

interior of silicate grains should not be affected. Since these primary grains characteristically have much higher Os concentrations than interstitial sulfides, supergene weathering seems unlikely to be entirely responsible for the low bulk-rock Os concentrations.

The Re concentrations of half of the Mont Briançon xenoliths are consistent with varying degrees of melt depletion (< 260 ppt), but the remainder are enriched by as much as 235%. Moreover, the absence of a correlation between Re/Os and major element indices of melt depletion suggests that Re has become mobile after melt depletion, and / or the bulk-rock budget of otherwise immobile proxies of melt depletion have been disturbed. Alternatively, in addition to Re mobility, the Os budget may have also been perturbed, either by the addition of radiogenic Os, or through Re addition and subsequent ingrowth of ^{187}Os.

With one exception (MBr1) the bulk-rock sub-chondritic Os isotope ratios are broadly consistent with melt depletion ($^{187}Os/^{188}Os_{chondrite}$ = 0.127, Shirey and Walker, 1998). Bulk-rock Mont Briançon $^{187}Os/^{188}Os$ ranges from 0.11737 to 12897, similar to other melt depleted peridotite xenoliths associated with European Cenozoic volcanism (e.g. Schmidt and Snow, 2002; Witt-Eickschen and Kramm, 1998; Witt-Eickschen et al., 2003; Ackerman et al., 2009) However, the lack of a coherent correlation between $^{187}Os/^{188}Os$ and bulk-rock Al_2O_3, clinopyroxene Al_2O_3 and clinopyroxene modal abundance suggests that these factors are not simply linked by the prior extraction of basaltic melt. Bulk-rock Re depletion ages ((T_{RD} = 1/λ x ln {[($^{187}Os/^{188}Os_{chon}$ – $^{187}Os/^{188}Os_{sample}$) / $^{187}Re/^{188}Os_{chon}$] +1}), i.e. model ages which assume no change in $^{187}Os/^{188}Os$ after melt depletion, are widely scattered, ranging from 0.11 to 1.71 Ga. While the oldest T_{RD} may represent a minimum possible age for melt depletion, bulk-rock T_{RD}s should be treated with caution, especially where the possibility exists that

895 both Re and Os have experienced open system behaviour since the time of melt
896 depletion.

897 Despite sulfide representing an insignificant modal proportion of peridotite
898 xenoliths (0.001 – 0.006 weight %, e.g. Luguet et al., 2003) Os sulfide / silicate
899 partition coefficients (Os $K_D^{sulfide/silicate}$) are sufficiently high (10^4 – 10^5) that the
900 silicate phases and spinel of several Mont Briançon xenoliths contribute no more than
901 3% of the Os budget (cf. Hart and Ravizza, 1996; Burton et al., 2000). Thus sulfide
902 will dominate bulk-rock Re-Os systematics. Any perturbation of sulfide compositions
903 subsequent to melt depletion will potentially have a significant effect on bulk-rock
904 Re-Os systematics. Figure 12 demonstrates that bulk-rock Os isotope ratios are
905 dominated by "primary" sulfides, i.e. shielded from interaction with metasomatic
906 melts and fluids by their host silicate grain. Hence, the contribution to the bulk-rock
907 $^{187}Os/^{188}Os$ from the metasomatic sulfides will be negligible.

908 While many of the sulfide grains from this study possess sub-chondritic Os
909 isotope ratios, Re and Os concentration data suggest that many sulfides no longer
910 retain their original Re and Os abundances. With the exceptions of MBr3_1 and
911 MBr6_2, all of the sulfides with subchondritic $^{187}Os/^{188}Os$ ratios possess high Re
912 concentrations (e.g. MBr8_3 and MBr20_4, [Re] = 112 ppm and 412 ppm
913 respectively). For these sulfides to retain subchondritic Os isotope ratios, practically
914 all of the Re must have been added to the sulfide shortly before the host xenolith was
915 brought to the surface. Moreover, not all of the sulfide grains with suprachondritic Os
916 isotope ratios have a high Re abundance. MBr3_4 ([Re] = 0.01 ppm) morphologically
917 resembles a primary sulfide, yet retains a $^{187}Os/^{188}Os$ ratio of 0.12983. Such a
918 radiogenic Os isotope ratio is inconsistent with melt depletion alone, yet cannot be
919 accounted for simply by radiogenic ingrowth of Re. Many peridotite xenoliths and

920 orogenic massif peridotites have experienced Re mobility after initial melt depletion
921 (Meisel et al., 2001; Reisberg and Lorand, 1995). Loss of increasing amounts of
922 primary sulfide (e.g. Handler et al., 1999; Reisberg et al., 2005) would increase the
923 influence of metasomatic sulfide on the bulk-rock Os budget, resulting in higher and
924 more variable Os isotope ratios. The lack of co-variance between bulk-rock Os
925 isotope ratio and Re/Os, or any of its proxies supports the notion that, in addition to
926 Re mobility, the Os budget may have been disturbed.

927 Variscan subduction could have resulted in the fluxing of radiogenic marine
928 Os (e.g. Brandon et al., 1996) at the same time that P-rich fluids were also added to
929 the SCLM beneath the Massif Central. Such a fluid could also be expected to be rich
930 in Ba and Rb (Chesley et al., 2004). However, it is difficult to account for bulk-rock
931 $^{187}Os/^{188}Os$ purely from the addition of a metasomatic, radiogenic source of Os that is
932 characterised by such low Os concentrations. While a contribution to the bulk-rock Os
933 concentration of MBr1 from slab-related fluid cannot be eliminated, the modal
934 abundance of metasomatic sulfide necessary to raise the $^{187}Os/^{188}Os$ to sufficiently
935 radiogenic levels is not supported by (i) the sulfur concentration, or (ii) the observed
936 sulfide modal abundance.

937 Sulfides preserved within silicate grains should be resistant to mobilisation or
938 alteration by transient metasomatic melts or fluid. Only interstitial grains would
939 normally be vulnerable to this mechanism. Interstitial sulfide grains typically have
940 high Re/Os ratios and low Os concentrations (Burton et al., 1999; Alard et al., 2002)
941 and the removal of these grains while lowering Re content would have little effect on
942 bulk-rock Os. In order to sufficiently lower bulk-rock Os to approximately half that of
943 the fertile mantle, the high [Os] enclosed sulfide grains, must also, at least in part, be
944 removed. Many silicate grains are cross cut by planes of secondary melt inclusions

where silicate minerals have fractured during the through-flux of a metasomatic melt. Since sulfides possess melting temperature well below the peridotite solidus (Hsieh et al., 1987; Eggler and Lorand, 1993), Cu-Fe-Ni sulfides may be highly mobile at subcontinental lithosphere temperatures (e.g., Chesley et al., 1999; Gaetani and Grove, 1999), but require dissolution or mobilization in a lower viscosity liquid as molten sulfide itself is immobile at low degrees of porosity (Minarik et al., 1996). As a result of the high Os $K_D^{sulfide/silicate}$ and the low modal abundance of sulfide in fertile mantle, relatively few sulfide grains need be affected in order to significantly lower bulk-rock Os abundance. Therefore the mechanism by which the melt inclusions are emplaced may also be capable of mobilising enclosed sulfide grains with high Os concentrations, thus lowering bulk-rock Os content. The trails of micron-scale sulfide blebs linking seemingly enclosed sulfides to grain boundaries (Figure 5a with 5b) also provide compelling evidence that these "enclosed" sulfides may not have the high [Os], low [Re] and unradiogenic $^{187}Os/^{188}Os$ as previously thought (e.g. Alard et al., 2002).

The removal of sulfide cannot, by itself, account for both low Re bulk-rock concentrations in half of the xenoliths and enriched Re concentrations in the remainder. An additional process, capable of enriching bulk-rock peridotite in Re, while not materially increasing Os abundance must be sought. Silicate magmas are characterized by suprachondritic Re/Os ratios (Shirey and Walker, 1998). Experimental evidence also suggests that Re is highly incompatible in silicate minerals (Righter et al., 2004; Walker et al., 1991; Watson et al., 1987) but may (Righter and Hauri, 1998) or may not (Mallman and O'Neil, 2007) be moderately compatible in garnet. Therefore, during melting of a sulfide-free mantle source, Re should be moderately to strongly enriched in the melt, relative to Os, with the extent

970 of enrichment dependent on the effect of residual garnet. Even in the presence of
971 sulfide, Re $K_D^{sulfide/silicate}$ is at least an order of magnitude lower than Os $K_D^{sulfide/silicate}$
972 (Sattari et al., 2002; Fonseca et al., 2006; Roy-Barman et al., 1998). Thus, irrespective
973 of the presence or absence of sulfide, melts generated in the mantle will have higher
974 Re/Os than their source.

975 Metasomatic re-enrichment could be responsible for the Re and Os elemental
976 abundances of those xenoliths with supra-chondritic Re abundances. Melting of fertile
977 peridotite (e.g. Meisel et al., 2001) by 1 % will produce a magma containing > 4 ppb
978 Re. The same melt derived from an enriched peridotite would have an even higher Re
979 concentration. Figure 13 illustrates the effect of mixing residual peridotite with
980 basaltic magmas of varying compositions. Ocean island basalts (Reisberg et al., 1993;
981 Marcantonio et al., 1995), MORB (Schiano et al., 1997; Gannoun et al., 2004, 2007;
982 Escrig et al., 2005) and melt generated from a fertile or enriched mantle precursor
983 (Meisel et al., 2001) all contain an order of magnitude more Re than lithospheric
984 mantle and it is conceivable that mixing between these two reservoirs could produce
985 the elevated Re concentrations measured in some Mont Briançon xenoliths. The
986 composition of the basalt that brought the Mont Briançon xenoliths to the surface is
987 also shown on Figure 13. Although there is unlikely to be a genetic relationship
988 between the peridotite xenoliths and the Mont Briançon host basalt, the addition of a
989 significant volume of host basalt would have a similar compositional effect to the
990 mixing of residual peridotite and a primary magma generated at depth.

991 Raising the Re concentration of a xenolith to twice the mean mantle
992 concentration requires a melt/rock ratio of > 0.5, for which there is no textural
993 evidence. Even the addition of Re generated by the melting of pyroxenite with [Re]
994 of ≤ 3.2 ppb Re (e.g. van Acken et al., 2008) would require a greater melt / rock ratio

995 than can be accounted for with the textural evidence preserved in Mont Briançon
996 peridotites. The addition of 0.0015 – 0.0020 weight % (15 – 20 ppm) of metasomatic
997 sulfide from an infiltrating melt (e.g. Rehkamper et al., 1999) could sufficiently raise
998 bulk-rock Re concentrations and is supported by textural observations, that is, the
999 presence of sulfide-bearing interstitial glasses and melt inclusions. However, the
1000 mechanism responsible for such an addition at Mont Briançon, i.e. precipitation from
1001 a sulfur-saturated melts versus the addition of locally re-mobilized secondary sulfide
1002 is difficult to identify. The effect of a migrating mafic melt will be strongly influenced
1003 by the degree of sulfur saturation in the melt and its interaction with pre-existing
1004 residual mantle sulfide grains (Mavrogenes and O'Neill, 1999; Bockrath et al., 2004;
1005 Brenan et al., 2005). Sulfur undersaturated melts may remove sulfides and HSE,
1006 whereas sulfur saturated melts may precipitate sulfides (Reisberg et al., 2005). While
1007 the compatibility of Re in sulfide is dependent upon fO_2 and fS_2 (Fonseca et al., 2007),
1008 in effect, interstitial sulfide, when exposed to a high temperature melt or fluid behaves
1009 physically incompatibly and the entire high [Re] sulfide is mobilised (Ballhaus et al.,
1010 2006). Furthermore, Re crystal/silicate melt partition coefficients, controlled by fO_2,
1011 vary by 4-5 orders of magnitude (Mallmann et al., 2007), making generalisations
1012 about Re incompatibility during partial melting of peridotite unreliable. In contrast,
1013 high Os sulfide grains, residual after an early melt depletion event and shielded from
1014 subsequent interaction from melts and fluids are retained in the mantle, resulting in Os
1015 being physically compatible in the residue (Ballhaus et al., 2006).

1016 Rhenium-enrichment would also be accompanied by a moderate addition of
1017 Os, despite the high Re/Os ratio of metasomatic sulfides (Alard et al., 2002) and
1018 inconsistent with the low Os concentrations of the Re-enriched xenoliths here. It is,
1019 therefore difficult to account for the Re and Os abundances of the enriched xenoliths

with a simple, single-stage process. Wholesale removal of both primary sulfides (high [Os], low [Re], unradiogenic $^{187}Os/^{188}Os$; Alard et al., 2002) and pre-existing secondary sulfide (low [Os], high [Re] and radiogenic $^{187}Os/^{188}Os$; Alard et al., 2002) would systematically lower bulk-rock Re and Os abundances. This could be achieved by the breakdown of sulfide as proposed by Handler et al., (1999), but the addition of Re to half of the xenoliths must be derived from an additional process. The subsequent, or synchronous, addition of metasomatic sulfides with low Os and high Re abundance and variably radiogenic $^{187}Os/^{188}Os$ to some, but not all of the xenoliths, would not only raise Re abundances to those measured in the Re-enriched xenoliths, but also elevate Os abundances by a moderate amount from their depleted condition after large-scale sulfide removal (Figure 13b). Evidence for a mechanism capable of the removal of at least some primary sulfides can be seen in the trails of melt inclusions across silicate grains. That some primary sulfides survived this removal and re-enrichment process is evident in the relatively high (< 3 ppb) bulk-rock Os abundance, and the presence of individual sulfide grains that possess high Os concentrations with unradiogenic Os isotope ratios. However, their "included" nature is uncertain. Examples of seemingly enclosed sulfides are joined to grain boundaries by trails of micron-scale sulfide blebs. Several other "included" sulfides are situated very close to grain boundaries, i.e. in the third dimension may not be "included" sulfides. The mis-identification of wholly included sulfides could also account for the presence of weathered "included" sulfides that should have been protected from oxidation by the host grain, yet have experienced significant oxidation. This could also partly account for the compositional, if not textural, similarities between interstitial grains with high Ni/Fe ratios and weathered grains that would otherwise have been described as included sulfides. The similarities between these texturally

variable groups of sulfides suggest that their compositions are the result of a common process. Griffin et al., (2004) also observed a similar relationship in cratonic sulfides. Only those Mont Briançon sulfides identified unequivocally as unweathered and entirely enclosed within silicate grains have a discrete and narrowly defined compositional range. Further deformation and / or comminution of host grains would likely result in an even more comprehensive loss of primary sulfides, and thus lower bulk-rock Os abundances and more radiogenic Os isotope ratios.

5.4. The origin and nature of metasomatism beneath the southern FMC.

Several processes have been proposed to account for the geochemical signature of peridotite xenoliths brought to the surface in Cenozoic European basalts, and more specifically those found within the basalts of the southern French Massif Central. For example, evidence for the existence of phosphorous-rich melts has been recorded in mantle xenoliths from the Massif Central (Rosenbaum et al., 1997) and the influence of carbonate-rich melt or supercritical fluids produced at the base of the lithosphere by separation from mafic alkaline magmas also been suggested (Wilson and Downes 1991; Wilson et al. 1995).

Bedini et al., (1997) proposed a model for the chemical evolution of a basaltic melt infiltrating the SCLM underlying the East African rift during ascent and concluded that the lithospheric mantle near the asthenosphere has higher porosity than mantle just below the Moho. This would permit infiltration of asthenospheric melts into the lower portions of the SCLM, although high melt/rock ratios would lead to a partial to complete re-equilibration of host peridotite with the ascending basaltic melts. A similar process has been proposed to explain the stratified trace element

enrichments observed beneath the Bohemian peridotite massif (Ackerman et al., 2009) and is also consistent with the varying degrees of metasomatism and textural variability with depth in other localities within the southern FMC (e.g. Zangana et al., 1997). In addition, this is supported by the relationship between xenolith equilibration temperatures and degree of metasomatic overprinting suggested by this study.

Elsewhere in the European Cenozoic volcanic province, Witt-Eickschen and Kramm, (1998) and Witt-Eickschen et al., (2003) have described strong correlations between Pb-Sr-Nd and trace elements in clinopyroxenes from Eifel anhydrous xenoliths that resemble depleted MORB mantle, while in the West Eiffel region xenoliths metasomatized with an EM-1 – like component have also been reported. The Eifel xenoliths share some similarities with highly deformed southern FMC peridotite xenoliths (Zangana et al., 1997), but no previous studies of protogranular peridotites from the southern FMC have reported EM-1-like metasomatism. However, the Sr and Nd isotope compositions of protogranular and porphyroclastic FMC peridotite xenoliths reported in previous studies (Downes with Dupuy, 1987; Zangana et al., 1997; Touron et al., 2008; Yoshikawa et al., 2009), show a pronounced relationship between textural type and lithophile element isotope systematics. Xenoliths with relatively enriched isotopic compositions, protogranular and protogranular-to-porphyroclastic textures, define an array trending away from depleted MORB mantle towards Bulk Earth values and towards the range of values calculated for the European Asthenospheric Reservoir (EAR).

Several studies (e.g. Zangana et al., 1997; Lenoir et al., 2000; Touron et al., 2008; Yoshikawa et al., 2009) have also suggested that the southern FMC has been enriched by recent infiltration of small degree partial melts or fluids from the asthenospheric mantle, possibly related to the “low velocity component” of Hoernle et

al. (1995) in European Neogene alkaline magmas. One possible reason for this style of enrichment is that focussing of upwelling mantle beneath the younger and thinner southern SCLM domain may have favoured decompression melting in this area, as suggested by seismic tomography modelling (Sobolev et al., 1996; Lenoir et al., 2000). This is consistent with the accumulation of plume-derived melts at asthenosphere / lithosphere topographic highs as recorded by the high-temperature poikiloblastic xenoliths from Boree, Velay (Xu et al., 1998), caused by the bounding effects, and differing sub-SCLM architecture, of the juxtaposed northern and southern FMC as described by Wittig et al., (2007).

Thus, the southern FMC xenoliths preserve evidence for interaction between asthenospheric mantle-derived melts/fluids and depleted lithospheric mantle. This is supported by the U-Th-Pb and Lu-Hf systematics of clinopyroxenes from southern FMC lherzolites, including two samples from Mont Briançon (Wittig, et al., 2007), which demonstrated that southern FMC peridotites have Hf isotope ratios consistent with melt depletion followed by metasomatic overprinting of a mainly silicate melt, calculated by Yoshikawa et al., (2009) to be consistent with an EAR-derived melt. This contrasts with the hydrous/carbonatitic metasomatic agent that overprinted the incompatible trace element abundances of the northern FMC (Wittig et al., 2007). The source of metasomatism, whether classified as metasomatism in the strictest sense, or low degree partial melting, is therefore at or near the base of the lithosphere and not at shallower depths, consistent with the composition and depth of equilibration of the melt inclusions from this study, the previous work of Schiano with Clocchiatti, (1994) and the recent work of Yoshikawa et al., (2009). The timing of at least the most recent metasomatic episode must be at or near to the eruption age of the host basalts because of the implications for ingrowth of radiogenic Os in sulfides to which Re may have

1120 been added. This is consistent with the perturbations of highly siderophile elements in
1121 the Bohemian massif that were probably linked to Tertiary rifting and volcanism (5 –
1122 25 Ma) rather than during the Variscan orogeny (cf. Ackerman et al., 2009).

1123 Critically, the influx of incompatible trace elements makes it difficult to
1124 extract meaningful geochronological information pertaining to melt depletion that
1125 predates later metasomatic and tectonic events using silicate-hosted lithophile isotope
1126 systems. Evidence for melt depletion events extends as far back as 480 Myr ago (Pin
1127 and Marini, 1993) and multiple incidences of melt depletion have been confirmed by
1128 Wittig et al., (2007) using Lu-Hf of clinopyroxenes; by Yoshikawa et al., (2009) using
1129 Nd isotope systematics in clinopyroxene from an unmetasomatized Mont Briançon
1130 xenolith, and at 257 Myr ago by Femenias et al., (2004). However, the longer scale
1131 evolution of the SCLM beneath the southern FMC remains elusive as the overprinting
1132 of subsequent events only serves to obscure the earliest melt depletion. Fortunately,
1133 the recent metasomatizing silicic melt itself does not possess a significant Os budget.
1134 As Figure 12 illustrates, although the metasomatic melt is S-saturated, the absolute
1135 amount of Re and Os added to the Mont Briançon xenoliths will be negligible. While
1136 the silicate metasomatic melt may well contribute to the incompatible lithophile
1137 element budget, perturbation to Re-Os isotope systematics may only be slight, thus
1138 permitting the chronology of earlier melt depletion events to be investigated.

1139

1140 **5.5. "Seeing through" the addition of metasomatic sulfide**

1141

1142 Osmium isotope disequilibrium likely exists in all the Mont Briançon
1143 xenoliths of this study. As with previous work (e.g. Burton et al., 1999), bulk-rock Os
1144 isotope ratios are somewhat lower than those of the constituent silicate phases. In

addition, at Mont Briançon these silicate phases do not yield any useful geochronological information as the Re-Os systematics of these minerals have been perturbed since the first episode of melt depletion. Consequently, any "ages" obtained from the silicate phases have large errors and are indistinguishable from the eruption of host basalt and the entrainment of the xenolith suite (c.1 – 4 Ma). Mont Briançon sulfide Os isotope ratios, while commonly unradiogenic, more often than not are not representative of those of the corresponding bulk-rock. This is not uncommon in cratonic peridotites (e.g. Griffin et al., 2004) or abyssal peridotites (e.g. Harvey et al., 2006) and bulk-rock Os isotope ratios should not therefore be (i) taken as representing any particular individual event and (ii) be indiscriminately used for calculating T_{RD} ages. In addition, Ackerman et al., (2009) noted that for the Bohemian Massif, the range of bulk-rock Os isotope ratios is similar to the distribution of $^{187}Os/^{188}Os$ ratios reported for samples from the modern convecting upper mantle (e.g., Liu et al., 2008). This is also true for the Mont Briançon xenolith suite. Consequently, the bulk-rock Os isotopic variations in this suite may reflect the formation of lithospheric peridotites by variable degrees of partial melting of a mantle precursor whose $^{187}Os/^{188}Os$ was not perfectly uniform at the time of melting, or a mixed age population (Rudnick and Walker, 2009), although this could also be due to sulfide breakdown (e.g. Handler et al., 1999), removal of sulfide by S-undersaturated melts (e.g. Reisberg et al., 2005) or the time integrated addition of radiogenic Os following the addition of Re sometime in the past. This variability in the upper mantle means that Os isotopes are not useful for discriminating among relatively young, e.g., Phanerozoic events. So, bulk-rock T_{RD} ages of young events should be treated with caution.

Individual sulfide blebs that separated as an immiscible fluid during an ancient partial melting event and were subsequently shielded from interaction with later melts

and fluids should provide a better means for dating individual melt depletion events. Primary sulfides associated with melt depletion should be easily distinguished from secondary metasomatic sulfides based upon their major element composition (e.g. Dromgoole and Pasteris, 1987, Luguet et al., 2003), their morphology and relationship with surrounding silicates (e.g. Burton et al., 1999) and their Re and Os abundance and isotope ratios (e.g. Alard et al., 2002). However, it is not possible to subdivide the Mont Briançon sulfide grains into primary and secondary populations according to their major element composition; similarly, they cannot be subdivided on the basis of their Re/Os ratios, their Os isotope ratio or Re-Os abundances. Even the most unradiogenic sulfides (e.g. MBr20_3) have high Re abundances suggesting that long-term evolution in a low Re environment, to preserve an unradiogenic Os isotope ratio, must have been followed by an event which added a significant amount of Re to the sulfide grain. Unradiogenic sulfides from this study appear to have been exposed to a metasomatic agent that has significantly altered the Re/Os ratio. In fact no single sulfide measured here exhibits the chemical characteristics expected of a primary sulfide i.e. high [Os] and low [Re], and an unradiogenic Os isotope ratio. It seems unlikely that the diffusion of Re through a silicate mineral and into the low [Re] enclosed sulfide is responsible for the elevated [Re] in some seemingly primary sulfides. Diffusion would occur over a protracted period, over timescales that would allow significant ingrowth of ^{187}Os. While this could be a reasonable mechanism to account for some of the seemingly enclosed sulfides from this study, such diffusion of Re would be expected to be a universal process and should affect all enclosed sulfides in xenoliths worldwide. What seems more likely from the textural evidence of Figure 4 is that the two populations of sulfide have experienced limited physical mixing when interstitial melts and melt inclusions were added.

Mixing has therefore occurred between originally high [Os], unradiogenic sulfides and a metasomatic sulfides with high Re/Os and low [Os] (cf. interstitial, metasomatic sulfides of Alard et al., 2002). Alternatively, additional Re may have partitioned into a pre-existing sulfide from a transient silicate melt, but it seems unlikely that a previously enclosed sulfide could exchange Re with a large volume of metasomatic melt or fluid and not be removed from its within-grain location. As long as the hybrid sulfide grain is not removed during interaction with the metasomatic agent, the Os isotope ratio will only be materially affected over longer intervals through radiogenic ingrowth of ^{187}Os. Figure 13b illustrates that for a narrow range of Os isotope ratios, the variation in sulfide Re/Os ratios can be accounted for by varying degrees of mixing between pre-existing sulfide and a metasomatic sulfide with a high Re/Os ratio. Even if wholesale Re addition did occur, because the timing was so close to that of the eruption of the host basalt there has been little measurable ingrowth of ^{187}Os. Thus, the characteristic high [Os] and unradiogenic Os isotope ratio of primary sulfides is still evident and dominates the bulk-rock Os isotope ratios.

However, it is interesting that, if the addition of significant proportions of Re to primary sulfides is recent, and that the unradiogenic sulfides preserve primary or near primary Os isotope ratios, that the "ages" derived from sulfide T_{RD} calculations do not cluster to signify a small number of discrete events. Only two sulfides (MBr3_1 with MBr6_2) yield T_{RD} ages that are within error of each other, yet do not correspond with any discrete event previously reported. Similarly, none of the sulfides yield T_{RD} ages that correspond with ages derived by Lu-Hf geochronology for melt depletion during the Variscan orogeny (Wittig, et al., 2006) or subsequent melt melting at 257 Myr ago (Femenias et al., 2004). However, this is not to say that Re-Os geochronology of individual sulfides is not without merit. As previously discussed

with respect to bulk-rock T_{RD}s, sulfide T_{RD}s should not be wielded indiscriminately, especially when attempting to unravel the cumulative effects of several Phanerozoic events. The utility of sulfide Re-Os isotope systematics lies in the ability of the system to preserve evidence for melt depletion that pre-dates Phanerozoic events, i.e. pre-Phanerozoic T_{RD}s have, by definition, survived the effects of all subsequent processes, metasomatic or otherwise. Seven of the nine sulfide T_{RD}s presented in this study preserve evidence for melt depletion events before the Variscan orogeny, and six of those pre-Variscan T_{RD}s yield ages that span the Neo-proterozoic to the early Paleo-proterozoic. This suggests that the SCLM that now resides beneath the southern FMC experienced a complex melt depletion history before its incorporation into continental Europe during the Variscan orogeny, Phanerozoic melt depletion, and the extraction of further melt and subsequent or synchronous metasomatism during the Cenozoic.

Hence, the sulfide T_{RD} age of 1.78 Ga of MBr20_4, although only a minimum age, is likely the best available estimate of the earliest melt depletion events that this portion of the SCLM experienced, although the limited number of sulfides analysed here does not preclude melt depletion that extends still further into the past, making its history of melt depletion similar to that experienced by abyssal peridotites (Harvey et al., 2006; Alard et al., 2005) or off-cratonic SCLM in Europe (e.g. Schmidt and Snow, 2002) and worldwide (Meisel et al., 2001).

6. CONCLUDING REMARKS

In the absence of a coherent bulk-rock Re-Os isochron, alumichron or co-variation between Os isotope ratios and any immobile proxies of Re, geochronological information pertaining to the earliest melt depletion of the SCLM from bulk-rock compositions will often be erroneous, whether determined by silicate hosted lithophile element isotope systems (e.g. Rb-Sr, Sm-Nd, U-Th-Pb) or siderophile Re-Os isotopes. However, perturbation of [Re] and [Os] in Mont Briançon xenoliths likely occurred only a short time before, or contemporaneously with, the entrainment of the xenolith in the host basalt. Therefore, Re-depletion model ages of individual sulfide grains preserve evidence for older melt depletion that extends back to at least 1.8 Ga. Despite multiple episodes of melt depletion, perturbations of trace element budgets, infiltration of a highly silicic melt, the mobilisation of a significant proportion of the xenoliths sulfide budget and possible Re addition to the remainder, at least some Mont Briançon xenoliths preserve sulfide Re-Os isotope systematics which are still capable of seeing through this range of mantle processes.

Moreover, even in xenolith suites that have experienced greater degrees of metasomatism or addition of much larger quantities of metasomatic sulfide, as long as the metasomatism was recent, or near contemporaneous with a known exhumation age, the effects of mixing metasomatic Re-rich sulfide with primary Os-rich sulfide are negligible, or easily corrected for, and minimum melt depletion ages can still be obtained in all but the most tectonised SCLM, where formerly enclosed sulfides subsequently experience open system behaviour.

ACKNOWLEDGEMENTS

We would like to thank John Watson for assistance with the XRF measurements, Andy Tindle for his help with the electron microprobe at The Open University, Jean Luc Devidal for assistance with the electron microprobe at Blaise Pascal University, Fatima Mokadem for help and advice with the ICP MS analyses and Margot Godard for duplicate ICP MS measurements of reference materials. The manuscript benefitted from an early review and discussion with Hilary Downes and was greatly improved by the suggestions made in reviews by David van Acken, Nadine Wittig and Chuan-Zhou Liu. Funding for this research was provided by NERC grant NER/A/S/2001/00538 which has allowed JH to undertake the isotope measurements presented here.

1293 **REFERENCES.**

1294

1295 Ackerman, L., Walker, R.J., Puchtel, I.S., Pitcher, L., Jelnek, E., Strnad, L. (2009)
1296 Effects of melt percolation on highly siderophile elements and Os isotopes in
1297 subcontinental lithospheric mantle: A study of the upper mantle profile beneath
1298 Central Europe. *Geochim. Cosmochim. Acta* **73**, 2400-2414.

1299

1300 Alard, O., Griffin, W.L., Pearson, N.J., Lorand, J.-P., O'Reilly, S.Y. (2002) New
1301 insights into the Re-Os systematics of sub-continental lithospheric mantle from in-
1302 situ analysis of sulfides. *Earth Planet. Sci. Lett.* **203,** 651-663.

1303

1304 Alard, O., Luguet, A., Pearson, N.J., Griffin, W.L., Lorand, J.-P., Gannoun, A.,
1305 Burton, K.W., O'Reilly, S.Y. (2005) In situ Os isotopes in abyssal peridotites
1306 bridge the isotopic gap between MORBs and their source mantle. *Nature* **436,**
1307 1005-1008.

1308

1309 Alexandrov, P., Cheilletz, A., Deloule, E., Cuney, M. (2000) 319 ± 7 Ma
1310 crystallisation age for the blond granite (northwest Limousin, French Massif
1311 Central) obtained by U/Pb ion probe dating of zircons. *C. R. Acad. Sci. Paris,*
1312 *Sciences de la Terre et des planetès* **330**, 617-622.

1313

1314 Andersen, T., O'Reilly, S.Y., Griffin, W.L. (1984) The trapped fluid phase in upper
1315 mantle xenoliths from Victoria: implications for mantle metasomatism. *Contrib.*
1316 *Mineral. Petrol.* **88,** 72-95.

1317

1318 Babuska, V., Plomerova, J., Vecsey, L., Granet, M., Achauer, U. (2002) Seismic
1319 anisotropy of the French Massif Central and predisposition of Cenozoic rifting
1320 and volcanism by Variscan suture hidden in the mantle lithosphere. *Tectonics,* **21**,
1321 11-20.
1322
1323 Baker, M.D. and Stolper, E.M. (1994) Determining the composition of high pressure
1324 melts using diamond aggregates. *Geochim. Cosmochim. Acta* **58,** 2811-2827.
1325
1326 Baker, M.D., Hirschmann, M.M., Ghiorso, M.S., Stolper, E.M. (1995) Composition
1327 of near solidus peridotite melts from experiments and thermodynamic
1328 calculations. *Nature* **375,** 308-311.
1329
1330 Ballhaus, C., Bockrath, C., Wohlgemuth-Uebewasser, C., Laurenz, V., Berndt, J.
1331 (2006) Fractionation of the noble metals by physical processes. *Contrib. Mineral.*
1332 *Petrol.* **152**, 667-684.
1333
1334 Becker, H., Horan, M.F., Walker, R.J., Gao, S., Lorand, J.-P., Rudnick, R.L. (2006)
1335 Highly siderophile element composition of the Earth's primitive upper mantle:
1336 Constraints from new data on peridotite massifs and xenoliths. *Geochim.*
1337 *Cosmochim. Acta* **70**, 4528-4550.
1338
1339 Bedini, R.M., Bodinier, J.-L., Dautria, J.M., Morten, L. (1997) Evolution of LILE-
1340 enriched small melt fractions in the lithospheric mantle: a case study from the
1341 East African Rift, *Earth Planet. Sci. Lett.* **153**, 67-83.
1342

1343 Bedini, R.M. and Bodinier, J.-L. (1999) Distribution of trace elements between the
1344 constituent phases of spinel peridotite xenoliths: ICP-MS evidence from the East
1345 African Rift. *Geochim. Cosmochim. Acta* **63,** 3883-3900.
1346
1347 Bezmen, N.I., Asif, M., Brugmann, G.E., Romanenko, I.M., Naldrett, A.J. (1994)
1348 Distribution of Pd, Rh, Ru, Ir, Os, and Au between sulfide and silicate melts.
1349 *Geochim. Cosmochim. Acta* **58,** 1251-1260.
1350
1351 Birck, J.-L., Roy-Barman, M., Capmas, F. (1997) Re-Os isotopic measurements at the
1352 femtomole level in natural samples. *Geostand. Newslett.* **20**(1), 19-27.
1353
1354 Bockrath, C., Ballhaus, C., Holzheid, A. (2004) Fractionation of the platinum group
1355 elements during mantle melting. *Science* **305**, 1951-1953.
1356
1357 Bodinier, J.-L. (1988) Geochemistry and petrogenesis of the Lanzo peridotite body,
1358 western Alps. *Tectonophys.* **149**, 67-88.
1359
1360 Bodinier, J.-L. and Godard, M. (2004) Orogenic, ophiolitic and abyssal peridotites.
1361 *Treatise in Geochem.* **2** (04), 103-170. Elsevier Publishing, Amsterdam.
1362
1363 Boudier and Nicolas, 1977; Structural controls on partial melting in the Lanzo
1364 peridotite. In: *Magma Genesis; Proceedings of the American Geophysical Union*
1365 *Chapman Conference on Partial Melting in the Earth's Upper Mantle* (ed. H. J.
1366 B. Dick). State Oregon Department of Geology and Mineral Industries, Portland,
1367 USA, **96**, 63–79.

Boyd, F.R. and Nixon, P.H. (1978) Ultramafic nodules from the Kimberley pipes, South Africa. *Geochim. Cosmochim. Acta* **42,** 1367–1382.

Boyd, F.R., Pokhilenko, N.P., Pearson, D.G., Mertzman, S.A., Sobolev, N.V., Finger, L.W. (1997) Composition of the Siberian cratonic mantle: evidence from Udachnaya peridotite xenoliths. *Contrib. Mineral. Petrol.* **128**, 228– 246.

Brandon, A.D., Creaser, R.A., Shirey, S.B., Carlson, R.W. (1996) Osmium recycling in subduction zones. *Science* **272,** 861–864.

Brenan, J.M., McDonough, W.F., Ash, R. (2005) An experimental study of the solubility and partitioning of iridium, osmium and gold between olivine and silicate melt, *Earth Planet. Sci. Lett.* **237**, 855-872.

Brey, G.P. and Kohler, T. (1990) Geothermobarometry in 4 phase spinel lherzolites II: A practical assessment of existing thermobarometers. *J.Petrol*. **31,** 1353-1378.

Brown, G.M., Pinsent, R.H., Coisy, P. (1980) The petrology of spinel peridotite xenoliths from the Massif Central, France. *Am. J. Sci.* **280-A,** 471-498.

Buchl, A., Brügmann, G., Batanova, V.G., Münker, C., Hofmann, A.W. (2002) Melt percolation monitored by Os isotopes and HSE abundances: a case study from the mantle section of the Troodos ophiolite. *Earth. Planet. Sci. Lett.* **204**, 385-402.

1393 Burnham, O.M., Rogers, N.W., Pearson, D.G., van Calsteren, P., Hawkesworth, C.J.
1394 (1998) The petrogenesis of the eastern Pyrrenian peridotites: An integrated study
1395 of their whole-rock geochemistry and Re-Os isotope composition. *Geochim.*
1396 *Cosmochim. Acta* **62,** 2293-2310.
1397
1398 Burton, K.W., Schiano, P., Birck, J.-L., Allegre, C.J. (1999) Osmium isotope
1399 disequilibrium between mantle minerals in a spinel lherzolite. *Earth Planet. Sci.*
1400 *Lett.* **172,** 311-322.
1401
1402 Burton, K.W., Schiano, P., Birck, J.-L., Allegre, C.J., Rehkämper, M., Halliday, A.N.,
1403 Dawson, J.B. (2000) The distribution of rhenium and osmium amongst mantle
1404 minerals and the age of the lithospheric mantle beneath Tanzania. *Earth Planet.*
1405 *Sci. Lett.* **183,** 93-106.
1406
1407 Canil, D. and Fedortchouk, Y. (2000) Clinopyroxene-liquid partitioning for vanadium
1408 and the oxygen fugacity during the formation of cratonc and oceanic mantle
1409 lithosphere. *J. Geophys. Res.* **105**, 26003-26016.
1410
1411 Canil, D. (2002) Vanadium in peridotites, mantle redox and tectonic environments:
1412 Archean to present. *Earth Planet. Sci. Lett.* **195**, 75-90.
1413
1414 Canil, D. (2004) Mildly incompatible elements in peridotites and the origins of mantle
1415 lithosphere. *Lithos* **77**, 375-393.
1416

1417 Carlson, R.W. and Irving, A.J. (1994) Depletion and enrichment history of sub-
1418 continental lithospheric mantle: an Os, Sr, Nd and Pb isotopic study of ultramafic
1419 xenoliths from the north-western Wyoming craton. *Earth Planet. Sci. Lett.* **126,**
1420 457-472.
1421
1422 Carswell, D. A. (1968) Possible primary upper mantle peridotite in Norwegian basal
1423 gneiss. *Lithos* **1**, 322–-355.
1424
1425 Chesley, J. T., Rudnick, R. L., Lee, C.-T. (1999) Re-Os systematics of mantle
1426 xenoliths from the East African Rift: Evidence for longevity of cratonic mantle
1427 and metasomatic Os addition. *Geochim. Cosmochim. Acta* **63,** 1203–1217.
1428
1429 Chesley, J.T., Righter, K., Ruiz, J. (2004) Large scale mantle metasomatism: a Re-Os
1430 perspective. *Earth Planet. Sci. Lett.* **219,** 49-60.
1431
1432 Chazot, G., Menzies, M.A., Harte, B. (1996) Determination of partition coefficients
1433 between apatite, clinopyroxene, amphibole and melt in natural spinel lherzolites
1434 from Yemen: implications for wet melting of the lithospheric mantle. *Geochim.*
1435 *Cosmochim. Acta* **60,** 423–437.
1436
1437 Coisy, P. and Nicolas, A. (1978) Regional structure and geodynamics of the upper
1438 mantle beneath the Massif Central. *Nature* **274,** 429-432.
1439
1440 Condie, K.C., Cox, J., O'Reilly, S.Y., Griffin, W.L., Kerrich, R. (2004) Distribution
1441 of high field strength and rare earth elements in the mantle and lower crustal

1442 xenoliths from the south-western United States: The role of grain boundary
1443 phases, *Geochim. Cosmochim. Acta* **68,** 3919-3942.
1444
1445 Creaser, R.A., Papanastassiou, D.A., Wasserburg, G.J. (1991) Negative thermal ion
1446 mass spectrometry of osmium, rhenium, and iridium. *Geochim. Cosmochim. Acta*
1447 **55,** 397–401.
1448
1449 Dautria, J.M., Dupuy, C., Tahkerist, D., Dorstal, J. (1992) Carbonate metasomatism in
1450 the lithospheric mantle: peridotitic xenoliths from a melilitic district of the Sahara
1451 Basin. *Contrib. Mineral. Petrol.* **111,** 37-52.
1452
1453 Dickey, J. S., (1970) Partial fusion products in alpine-type peridotites: Serrania de
1454 Ronda and other examples. *Spec. Pap. mineralog. Soc. Am.* **3**, 33-49.
1455
1456 Downes, H. and Dupuy, C. (1987) Textural, isotopic, and R.E.E. variations in spinel
1457 peridotite xenoliths, Massif Central, France. *Earth Planet. Sci. Lett.* **82,** 121-135.
1458
1459 Downes, H. (1990) Shear zones in the upper mantle – Relation between geochemical
1460 enrichment and deformation in mantle peridotites. *Geology* **18,** 374-377.
1461
1462 Downes, H., Reichow, M.K., Mason, P.R.D., Beard, A.D., Thirlwall, M.F. (2003)
1463 Mantle domains in the lithosphere beneath the French Massif Central: trace
1464 element and isotopic evidence from mantle clinopyroxenes. *Chem. Geol.* **200**, 71-
1465 87.
1466

1467 Dromgoole, E.L. and Pasteris, J.D. (1987). Interpretation of the sulfide assemblages in
1468 a suite of xenoliths from Kilbourne Hole, New Mexico. *Geol. Soc. Am. Special*
1469 *Paper* **215,** 25-46.
1470
1471 Eggler, D.H. (1987) Solubility of major and trace elements in mantle metasomatic
1472 fluids: experimental constraints. In: *Mantle metasomatism*. (Eds Hawkesworth, C.
1473 J. with Menzies, M. A.) London, Academic Press Inc.
1474
1475 Eggler, D. H. and Lorand, J.-P. (1993) Mantle sulfide oxybarometry. *Geochim.*
1476 *Cosmochim. Acta* **57,** 2213–2222.
1477
1478 Eggins, S.M., Rudnick, R.L., McDonough, W.F. (1998) The composition of peridotite
1479 and their minerals: a laser ablation ICP MS study. *Earth Planet. Sci. Lett.* **154,** 53-
1480 71.
1481
1482 Escrig, S., Schiano, P., Schilling, J.-G., Allegre, C.J. (2005) Rhenium – osmium
1483 isotope systematics in MORB from the southern mid-Atlantic ridge (40° - 50°).
1484 *Earth Planet. Sci. Lett.* **235,** 528-548.
1485
1486 Femenias, O., Coussaert, J., Berger, J.-C., Mercier, C., Demaiffe, D. (2004)
1487 Metasomatism and melting history of a Variscan lithospheric mantle domain:
1488 evidence from the Puy Beaunit xenoliths (French Massif Central). *Contrib.*
1489 *Mineral. Petrol.* **148,** 13-28.
1490

1491 Fleet, M.E., Stone, W.E., Crocket, J.H. (1991) Partitioning of palladium, iridium, and
1492 platinum between sulfide liquid and basalt melt: Effects of melt composition,
1493 concentration and oxygen fugacity. *Geochim. Cosmochim. Acta* **55,** 2545-2554.
1494
1495 Fleet, M.E., Crocket, J.H., Stone, W.E. (1996) Partitioning of platinum group
1496 elements (Os, Ir, Ru, Pt, Pd) and gold between sulfide liquid and basalt melt.
1497 *Geochim. Cosmochim. Acta* **60,** 2397-2412.
1498
1499 Fonseca, R.O.C., Mallmann, G., O'Neill, H. St. C., Campbell, I.H. (2007) How
1500 chalcophile is rhenium? An experimental study of the solubility of Re in sulfide
1501 mattes. *Earth Planet. Sci. Lett.* **260,** 537-548.
1502
1503 Frey, F.A., and Green, D.H. (1974) The mineralogy, geochemistry and origin of
1504 lherzolite inclusions in Victorian basanites. *Geochim. Cosmochim. Acta* **38,** 1023-
1505 1059.
1506
1507 Frey, F.A., and Prinz, M. (1978) Ultramafic inclusions from San Carlos, Arizona:
1508 petrological and geochemical data bearing on their petrogenesis. *Earth Planet. Sci.*
1509 *Lett.* **38,** 129-176.
1510
1511 Frey, F.A., Suen, C.J., Stockman, H.W. (1985) The Ronda high temperature
1512 peridotite: geochemistry and petrogenesis. *Geochim. Cosmochim. Acta* **49**, 2469-
1513 2491.
1514

1515 Frey, F.A., Shimizu, N., Leinbach, A., Obata, M., Takazawa, E. (1991) Compositional
1516 variations within the lower layered zone of the Horoman peridotite, Hokkaido,
1517 Japan: constraints on models for melt-solid segregation. In: *Orogenic lherzolites*
1518 *and mantle processes, Spec. Vol. J. Pet.* (Eds Menzies, M.A., Dupuy, C.,
1519 Nicholas, A.) Oxford University Press, Oxford, UK, pp 211-227.
1520
1521 Gaetani, G.A. and Grove, T.L. (1999) Wetting of mantle olivine by sulfide melt:
1522 Implications for Re/Os ratios in the mantle peridotite and late-stage core
1523 formation. *Earth Planet. Sci. Lett.* **169,** 147–163.
1524
1525 Galer, S.J.G., and O'Nions, R. K. (1988) Chemical and isotopic studies of ultramafic
1526 inclusions from the San Carlos Volcanic Field, Arizona: a bearing on their
1527 petrogenesis. *J. Petrol.* **30,** 1033-1064.
1528
1529 Gannoun, A., Burton, K.W., Thomas, L.E., Parkinson, I.J., van Calsteren, P., Schiano,
1530 P. (2004) Osmium isotope heterogeneity in the constituent phases of Mid-Ocean
1531 Ridge Basalts. *Science* **303,** 70-72.
1532
1533 Gannoun, A., Burton, K.W., Parkinson, I.J., Alard, O., Schiano, P., Thomas, L.E.
1534 (2007) The scale and origin of the osmium isotope variations in mid-ocean ridge
1535 basalts. *Earth Planet. Sci. Lett.* **259,** 541-556.
1536
1537 Gao, S., Rudnick, R.L., Carlson, R.W., McDonough, W.F., Liu, Y.-S. (2002) Re-Os
1538 evidence for replacement of ancient mantle lithosphere beneath the North China
1539 craton. *Earth Planet. Sci. Lett.* **198**, 307-322.

Granet, M., Wilson, M., Achauer, U. (1995) Imaging a mantle plume beneath the French Massif Central. *Earth Planet. Sci. Lett.* **136,** 281-296.

Griffin, W.L., Smith, D., Ryan, C.G., O'Reilly, S.Y., Win, T.T. (1996) Trace element zoning in mantle minerals: metasomatism and thermal events in the upper mantle. *Canad. Mineralogist* **34,** 1179-1193.

Griffin, W.L., Graham, W.S., O'Reilly, S.Y., Pearson, N.J. (2004) Lithosphere evolution beneath the Kaapvaal Craton: Re-Os systematics of sulfides in mantle derived peridotites. *Chem. Geol*. **208,** 89-118.

Gurney, J.J. and Harte, B. (1980) Chemical variations in upper mantle nodules from southern African kimberlites. *Philos. Trans. R. Soc. Lond.* **A297,** 273–293.

Handler, M.R., Bennett, V.C., Dreibus, G. (1999) Evidence from correlated Ir/Os and Cu/S for late stage Os mobility in peridotite xenoliths: implications for Re-Os systematics. *Geology* **27**, 75-78.

Hart, S.R. and Zindler, A. (1986) In search of a bulk Earth composition. *Chem. Geol.* **57**, 247-267.

Hart, S.R. and Ravizza, G. (1996) Os partitioning between phases in lherzolite and basalt. In: *Earth Processes: Reading the isotopic code.* (Eds Basu, A., Hart, S.R.) AGU, Washington *Geophys. Mon*. **95,** 123-134.

Hartmann, G. and Wedephol, K.H., (1993) The composition of peridotite tectonites from the Ivrea complex, northern Italy: residues from melt extraction. *Geochim. Cosmochim. Acta* **57**, 1761-1782.

Harvey, J., Gannoun, A., Burton, K.W., Rogers, N. W., Alard, O., Parkinson, I.J. (2006) Ancient melt extraction from the oceanic upper mantle revealed by Re-Os isotopes in abyssal peridotites from the Mid-Atlantic ridge. *Earth Planet. Sci. Lett.* **244**, 606-621.

Hauri, E.H. and Hart, S.R. (1997) Rhenium abundances and systematics in oceanic basalts. *Chem. Geol.* **139,** 185-205.

Herzberg, C. (2004) Geodynamic information in peridotite petrology. *J.Petrol.* **45**, 2507-2530.

Hoernle, K., Zang, Y.-S., Graham, D. (1995) Seismic and geochemical evidence for large-scale upwelling beneath the eastern Atlantic and western and central Europe. *Nature* **374**, 34-39.

Hirn, A. (1980) Le cadre structural profound d'après les profils sismiques, évolution structurale de France. 26° Congrés Géologique International Coll C-7 *Mémoires Bureau. Géologie et Mineralogie* **107,** 34-39.

1589 Hirschmann, M.M., Baker, M.B. with Stolper, E.M. (1998) The effect of alkalis on
1590 the silica content of mantle-derived melts. *Geochim. Cosmochim. Acta* **62,** 883-
1591 902
1592
1593 Hsieh, J.-C., Vkach, K. C., Chang, Y. A. (1987) The Fe-Ni-S system: I. A
1594 thermodynamic analysis of the phase equilibria and calculation of the phase
1595 diagram from 1173 to 1623 K. *High Temp. Sci.* **23,** 17–38.
1596
1597 Ionov, D.A., Dupuy, C., O'Reilly, S.Y., Kopylova, M.G., Genschaft, Y.S. (1993)
1598 Carbonated peridotite xenoliths from Spitzbergen: implications for the trace
1599 element signature of mantle carbonate metasomatism. *Earth Planet. Sci. Lett.* **119,**
1600 283-297.
1601
1602 Ionov., D. A., Shirey, S.B., Weiss, D., Brügmann, G. (2006) Os-Hf-Sr-Nd isotope and
1603 PGE systematics of spinel peridotite xenoliths from Tok, SE Siberian craton:
1604 Effects of pervasive metasomatism in shallow refractory mantle. *Earth Planet.*
1605 *Sci. Lett.* **241**, 47-64.
1606
1607 Ionov, D.A. and Hofmann, A.W. (2007) Depth of formation of subcontinental off-
1608 craton peridotites. *Earth Planet. Sci. Lett.* **261**, 620-634.
1609
1610 Irving, A.J. (1980) Petrology and geochemistry of composite ultramafic xenoliths in
1611 alkali basalts and implications for magmatic processes in the mantle. *Amer. J. Sci.*
1612 **280-A,** 389-426.
1613

1614 Irving, G.J, Pearson, D.G., Kjarsgaard, B.A., Carlson R.W., Kopylova, M.G.,
1615 Dreibus, G., (2003) A Re-Os isotope and PGE study of kimberlite-derived
1616 peridotite xenoliths from Somerset Island and a comparison to the Slave and
1617 Kaapvaal cratons. *Lithos* **71**, 461-488.
1618
1619 Jagoutz, E., Palme, H., Baddenhausen, H., Blum, K., Cendales, M., Dreibus, G.,
1620 Spettel, B., Lorenz, V., Waenke, H. (1979) The abundances of major, minor and
1621 trace elements in the Earth's mantle as derived from primitive ultramafic nodules.
1622 In: *Proceedings of the Lunar and Planetary Science Conference.* (Eds Merrill,
1623 R.B., Bogard, D.D., Hoerz, F., McKay, D.S. and Robertson, P.C.) Pergamon, New
1624 York. **2,** 2,031-2,050.
1625
1626 Kelemen, P.B., Dick, H.J.B, Quick, J.E. (1992). Formation of harzburgite by
1627 pervasive melt-rock reaction in the upper mantle. *Nature* **358**, 635-641.
1628
1629 Kopylova, M.G., Russell, J.K., Cookenboo, H. (1999) Petrology of peridotite and
1630 pyroxenite xenoliths from the Jericho kimberlite: implications for the thermal state
1631 of the mantle beneath the Slave craton, northern Canada. *Canad. J. Petrol.* **40,** 79–
1632 104.
1633
1634 Kuno, H. and Aoki, K. (1970) Chemistry of ultramafic nodules and their bearing on
1635 the origin of basaltic magmas. *Phys. Earth Planet. Interiors* **3,** 273–301.
1636

1637 Lardeau, J.M., Ledru, P., Daniel, I., Duchene, S. (2001) The Variscan French Massif
1638 Central – an new addition to the ultra-high pressure metamorphic "club":
1639 exhumation processes and geodynamic consequences. *Tectonophys.* **332**, 143-167.
1640
1641 Lenoir, X., Garrido, C.J., Bodinier, J.-L., Dautria, J.-M. (2000) Contrasting
1642 lithospheric domains beneath the Massif Central (France) revealed by the
1643 geochemistry of peridotite xenoliths. *Earth Planet. Sci. Lett.* **181,** 359-375.
1644
1645 Le Roux, V., Bodinier, J.-L., Tommasi, A., Alard, O., Dautria, J.-M., Vauchez, A.,
1646 Riches, A.J.V. (2007) The Lherz spinel lherzolite: refertilized rather than pristine
1647 mantle. *Earth Planet. Sci. Lett.* **259**, 599-612.
1648
1649 Le Roux, V., Tommasi, A., Vauchez, A., (2008) Feedback between melt percolation
1650 and deformation in an exhumed lithosphere-asthenosphere boundary. *Earth*
1651 *Planet. Sci. Lett.* **274**, 401-413.
1652
1653 Liu, C.-Z., Snow, J.E., Hellebrand, E., Brügmann, G., von der Handt, A., Büchl, A.,
1654 Hofmann, A.W. (2008) Ancient, highly heterogeneous mantle beneath Gakkel
1655 Ridge, Arctic Ocean. *Nature* **452**, 311-316.
1656
1657 Lorand, J.-P., and Alard, O. (2001) Platinum group element abundances in the upper
1658 mantle: New constraints from in situ and whole rock analyses of Massif Central
1659 xenoliths (France). *Geochim. Cosmochim. Acta* **65,** 2789-2806.
1660

1661 Lorand, J.-P., Alard, O., Luguet, A., Keays, R.R. (2003) Sulfur and selenium
1662 systematics of the subcontinental lithospheric mantle: Inferences from the Massif
1663 Central xenolith suite (France). *Geochim. Cosmochim. Acta* **67,** 4137-4151.
1664
1665 Lucazeau, F., and Bayer, R. (1982) Evolution geothermique et geodynamique du
1666 Massif Central Francais depuis l'Oligocene. *Annales Geophysicae* **38,** 405-429.
1667
1668 Luguet, A., Lorand, J.-P., Seyler, M. (2003) Sulfide petrology and highly siderophile
1669 element geochemistry of abyssal peridotites: a coupled study of samples from the
1670 Kane Fracture Zone (45^{o}W 23^{o}20'N, MARK area, Atlantic Ocean. *Geochim.*
1671 *Cosmochim. Acta* **67**, 1553-1570.
1672
1673 Marcantonio, F., Zindler, A., Elliott, T., Staudigel, H. (1995) Os isotope systematics
1674 of La Palma, Canary Islands: Evidence for recycled crust in the mantle source of
1675 HIMU ocean islands. *Earth Planet. Sci. Lett.* **133,** 397-410.
1676
1677 Mallman, G. and O'Neil, H.St.C. (2007) The effect of oxygen fugacity onthe
1678 partitioning of Re between crystals and silicate melt during mantle melting.
1679 *Geochim. Cosmochim. Acta* **71,** 2837-2857.
1680
1681 Mavrogenes, J.A. and O'Neill, H.St.C. (1999) The relative effects of pressure,
1682 temperature and oxygen fugacity on the solubility of sulfide in mafic magmas.
1683 *Geochim. Cosmochim. Acta* **63**, 1173-1180.
1684

1685 McDonough, W.F., (1990) Constraints on the composition of the continental
1686 lithospheric mantle. *Earth Planet. Sci. Lett.* **101**, 1-18.
1687
1688 McDonough, W.F. and Sun, S. S. (1995) The composition of the Earth. *Chem. Geol.*
1689 **120,** 223-253.
1690
1691 McDonough, W.F. (2004) Compositional model for the Earth's core. *Treatise*
1692 *Geochem.* **2,** (15) 547-568, Elsevier Publishing, Amsterdam.
1693
1694 McDonough, W.F. and Frey, F.A. (1989) Rare earth elements in upper mantle rocks.
1695 In: *Geochemistry and Mineralogy of Rare Earth Elements* (Eds Lipin, B.R.,
1696 McKay, G.A.) *Rev. Mineral.* **21,** 99-145.
1697
1698 McKenzie, D. and Bickle, M.J. (1988) The volume and composition of melt generated
1699 by extension of the lithosphere. *J. Petrol.* **29,** 625-679.
1700
1701 McKenzie, D. (1989) Some remarks on the movement of small melt fractions in the
1702 mantle. *Earth Planet. Sci. Lett.* **95,** 53–72.
1703
1704 Meen, J.K., Eggler, D.H., Ayres, J.C. (1989) Experimental evidence for very low
1705 solubility of rare earth elements in CO_2 rich fluids at mantle conditions. *Nature*
1706 **340,** 301-303.
1707
1708 Meisel, T., Walker, R.J., Morgan, J.W. (1996) The osmium isotopic composition of
1709 the Earth's upper mantle. *Nature* **383,** 517-520.

Meisel, T., Walker, R.J., Irving, A.J., Lorand, J.-P. (2001) Osmium isotopic composition of mantle xenoliths: a global perspective. *Geochim. Cosmochim. Acta* **65,** 1311-1323.

Meisel, T., Reisberg, L., Moser, J., Carignan, J., Melcher, F., Brugmann, G.E. (2003) Re-Os systematics of UB-N, a serpentinised peridotite reference material. *Chem. Geol.* **201,** 161-179.

Menzies, M. and Allen, C. (1974) Plagioclase lherzolite residual mantle relationships within two eastern Mediterranean ophiolites. *Contrib. Mineral. Petrol.* **45**, 197-213.

Menzies, M.A. and Wass, S.Y. (1983) CO_2 and LREE rich mantle below eastern Australia: a rare earth and isotope study of alkaline magmas and apatite rich mantle xenoliths from the Southern Highlands Province, Australia. *Earth Planet. Sci. Lett.* **65,** 287-302.

Menzies, M.A., Arculus, R.J., Best, M.G., Bergman, S.C., Ehrenberg, S.N., Irving, A.J., Roden, M.F., Schulze, D.J. (1987) A record of subduction process and within-plate volcanism in lithospheric xenoliths of the south-western USA. In: *Mantle xenoliths* (Ed Nixon, P.N.) John Wiley and Sons, Chichester 59-74.

Minarik, W.G., Ryerson, F.J., Watson, E.B. (1996) Textural entrapment of core-forming melts, *Science* **272**, 530-533.

Morgan, J.W. (1986) Ultramafic xenoliths: clues to Earths late accretionary history. *J. Geophys. Res.* **91,** 12375-12387.

Müntener, O., Pettke, T., Desmurs, L., Maier, M., Schaltegger, U. (2004) Refertilization of mantle peridotite in embryonic ocean basins: trace element and Nd isotopic evidence and implications for crust-mantle relationships. *Earth Planet. Sci. Lett.* **221**, 293-308.

Nicolas, A., Lucazeu, F., Bayer, R. (1987) Peridotite xenoliths in Massif Central basalts, France: textural and geophysical evidence for asthenospheric diapirism. In: *Mantle Xenoliths* (ed Nixon, P.H.) John Wiley and Sons Ltd, London, 563-574.

Nixon, P.H. and F.R. Boyd (1973) Petrogenesis of the granular and sheared ultrabasic nodule suite in kimberlite. In: *Lesotho Kimberlites* (ed Nixon P. H.). Cape and Transvaal, Maseru, 48–56.

O'Reilly, S.Y. and Griffin, W.L. (1988) Mantle metasomatism beneath western Victoria, Australia : (I) Metasomatic processes in Cr-diopside lherzolites. *Geochim. Cosmochim. Acta* **52,** 433-447.

Palme, H. and Nickel, K.G. (1985) Ca/Al ratio and composition of the Earth's upper mantle. *Geochim. Cosmochim. Acta* **49,** 2123-2132.

1760 Palme, H. and O'Neil, H. St. C. (2004) Cosmochemical estimates of mantle
1761 composition. *Treatise in Geochem.* **2** (01), 1-38. Elsevier Publishing, Amsterdam.
1762
1763 Pearson, D.G., Carlson, R.W., Shirey, S.B., Boyd, F.R., Nixon, P.H. (1995a)
1764 Stabilisation of Archean lithospheric mantle: A Re-Os isotope study of peridotite
1765 xenoliths from the Kaapvaal craton. *Earth Planet. Sci. Lett.* **134,** 341-357.
1766
1767 Pearson, D.G., Shirey, S.B., Carlson, R.W., Boyd, F.R., Pokhilenko, N.P., Shimizu,
1768 N. (1995b) Re-Os, Sm-Nd and Rb-Sr isotope evidence for thick Archean
1769 lithospheric beneath the Siberian craton modified by multistage metasomatism.
1770 *Geochim. Cosmochim. Acta* **59,** 959-977.
1771
1772 Pearson, D.G., Shirey, S.B., Harris, J.W., Carlson, R.W. (1998) Sulfide inclusions
1773 in diamonds from the Kofiefontein kimberlite, S. Africa: Constraints on diamond
1774 ages and mantle Re-Os systematics. *Earth Planet. Sci. Lett.* **160,** 311-326.
1775
1776 Pearson, D.G. (1999) The age of continental roots. *Lithos* **48,** 171-194.
1777
1778 Pearson, D.G., Canil, D., Shirey, S.B. (2003) Mantle samples included in volcanic
1779 rocks: xenoliths and diamonds. *Treatise Geochem.* **2,** (05) 171-275.
1780
1781 Pegram, B.J. and Allègre, C.J. (1992) Osmium isotopic compositions from oceanic
1782 basalts. *Earth Planet. Sci. Lett.* **111**, 59–68.
1783

1784 Pin, C. and Marini, F. (1993) Early Ordovician continental break-up in Variscan
1785 Europe: Nd-Sr isotope and trace element evidence for bimodal igneous
1786 associations of the Southern French Massif Central. *Lithos* **29**, 177-196.
1787
1788 Rampone, E., Bottazzi, P., Ottolini, L. (1991) Complementary Ti and Zr anomalies in
1789 orthopyroxene and clinopyroxene from mantle peridotites. *Nature* **354,** 518-520.
1790
1791 Rampone, E., Romairone, A., Abouchami, W., Piccardo, G.B., Hofmann, A.W.
1792 (2005) Chronology, petrology and isotope geochemistry of the Erro-Tobbio
1793 peridotites (Ligurian Alps, Italy): Records of late Palaeozoic lithospheric
1794 extension, *J. Pet.* **46**, 799-827.
1795
1796 Rampone, E. and Borghini, G. (2008) Melt migration and intrusion in the Erro-Tobbio
1797 peridotites (Ligurian Alps, Italy): Insights on lithospheric processes in extending
1798 lithospheric mantle. *Eur. J. Mineral.* **20**, 573-585.
1799
1800 Rehkämper, M., Halliday, A.N., Alt, J., Fitton, J.G., Zipfel, J., Takazawa, E. (1999)
1801 Non-chondritic platinum-group element ratios in oceanic mantle lithosphere:
1802 petrogenetic signature of melt percolation? *Earth Planet. Sci. Lett.* **172,** 65-81.
1803
1804 Reisberg, L., Zindler, A., Marcantonio, F., White, W., Wyman, D., Weaver, B. (1993)
1805 Os isotope systematics in ocean island basalts. *Earth Planet. Sci. Lett.* **120,** 149-
1806 167.
1807

1808 Reisberg, L. and Lorand, J.-P. (1995) Longevity of sub-continental mantle lithosphere
1809 from osmium isotope systematics in orogenic peridotite massifs. *Nature* **376,** 159-
1810 162.
1811
1812 Reisberg, L., Zhi, X., Lorand, J.-P., Wagner, C., Peng, Z., Zimmermann, C. (2005)
1813 Re-Os and S systematics of spinel peridotite xenoliths from east central China:
1814 Evidence for contrasting effects of melt percolation. *Earth Planet. Sci. Lett.* **239,**
1815 286-308.
1816
1817 Righter, K. and Hauri, E.H. (1998) Compatibility of rhenium in garnet during mantle
1818 melting and magma genesis. *Science* **280,** 1737-1741.
1819
1820 Righter, K., Campbell, A.J., Humayun, M., Hervig, M.R.L. (2004) Partitioning of Ru,
1821 Rh, Pd, Re, Ir and Au between Cr-bearing spinel, olivine, pyroxene and silicate
1822 melts. *Geochim. Cosmochim. Acta* **68**, 867-880.
1823
1824 Rivalentti, G., Vannucci, R., Rampone, E., Mezzucchelli, M., Piccardo, G.B. (1996)
1825 Peridotite clinopyroxene geochemistry reflects mantle processes rather than
1826 continental versus oceanic settings. *Earth Planet. Sci. Lett.* **139,** 423-437.
1827
1828 Robinson, J.A.C., Wood, B.J., Blundy, J.D. (1998) The beginning of melting of fertile
1829 and depleted peridotite at 1.5 GPa. *Earth Planet. Sci. Lett.* **155,** 97-111.
1830

1831 Roden, M.F., Frey, F.A., Francis, D. (1984) An example of consequent mantle
1832 metasomatism in peridotite inclusions from Nunivak Island, Alaska. *J. Petrol.* **25,**
1833 547-577.
1834
1835 Roden, M.F., Irving, A.J., Murthy, V.R. (1988) Isotopic and trace element
1836 composition of the upper mantle beneath a young continental rift: Results from
1837 Kilbourne Hole, New Mexico. *Geochim. Cosmochim. Acta* **52,** 461-476.
1838
1839 Rosenbaum, J.M., Wilson, M., Condliffe, E. (1997) Partial melts of phosphatic
1840 sediments in the mantle. *Geology* **25,** 77-80.
1841
1842 Ross, C.S., Foster, D.M., Myers, A.T. (1954) Origin of dunites and olivine rich
1843 inclusions in basaltic rocks. *Amer. Mineral.,* **39,** (9-10) 693-737.
1844
1845 Roy-Barman, M., Wasserburg, G. J., Papanastassiou, D.A., Chaussidon, M. (1998)
1846 Osmium isotopic compositions and Re-Os concentrations in sulfide globules from
1847 basaltic glasses. *Earth Planet. Sci. Lett.* **154,** 331-347.
1848
1849 Rudnick, R.L., McDonough, W.F., Chappell, B.W. (1993) Carbonatite metasomatism
1850 in the northern Tanzanian mantle: Petrographic and geochemical characteristics.
1851 *Earth Planet. Sci. Lett.* **114,** 463-475.
1852
1853 Rudnick, R.L., and Walker, R.J. (2009) Interpreting ages from Re-Os isotopes in
1854 peridotites. *Lithos*, in press.
1855

1856 Salters, V.J.M. and Stracke, A. (2004) Composition of the depleted mantle. *Geochem.*
1857 *Geophys. Geosys.* **5**(5), 1525-2027.
1858
1859 Sattari, P., Brenan, J.M., Horn, I., McDonough, W.F. (2002) Experimental constraints
1860 on the sulfide- and chromite-silicate melt partitioning behaviour of rhenium and
1861 platinum-group elements. *Econ. Geol.* **97,** 385-398.
1862
1863 Schiano, P. and Clocchiatti, R. (1994) Worldwide occurrence of silica-rich melts in
1864 sub-oceanic and sub-continental mantle minerals. *Nature* **368,** 621-624.
1865
1866 Schiano, P., Birck, J.-L., Allègre, C.J. (1997) Osmium – strontium – neodymium –
1867 lead isotopic covariations in mid-ocean ridge basalt glasses and the heterogeneity
1868 of the upper mantle. *Earth Planet. Sci. Lett.* **150,** 363-379.
1869
1870 Schiano, P., Bourdon, B., Clocchiatti, R., Massare, D., Varela, M. E. with Bottinga,
1871 Y. (1998) Low-degree partial melting trends recorded in upper mantle minerals.
1872 *Earth Planet. Sci. Lett.* **160**, 537-550
1873
1874 Schiano, P. and Bourdon, B. (1999) On the preservation of mantle information in
1875 ultramafic nodules: glass inclusions within minerals versus interstitial glass. *Earth*
1876 *Planet. Sci. Lett.* **169,** 173-188.
1877
1878 Schmidt, G. and Snow, J. (2002) Os isotopes in mantle xenoliths from the Eifel
1879 volcanic field and the Vogelsberg (Germany): age constraints on the lithospheric
1880 mantle. *Contrib. Mineral. Petrol.* **143**, 694-705.

Seyler, M., Lorand, J.-P., Dick, H.B.J., Drouin, M. (2007) Pervasive melt-percolation reactions in ultra-depleted refractory harzburgites at the Mid-Atlantic Ridge, 15°20N, ODP Hole 1274. *Contrib. Mineral. Petrol.* **153**, 303-319.

Shirey, S. B. and Walker, R. J. (1995) Carius tube digestion for low-blank rhenium-osmium analysis. *Anal. Chemistry* **34,** 2134-2141.

Shirey, S.B. and Walker, R.J. (1998) The Re-Os isotope system in cosmochemistry and high temperature geochemistry. *Ann. Rev. Earth Planet. Sci.* **26,** 423-500.

Sobolev. N.V. (1974) Deep-seated inclusions in kimberlites and the problem of the composition of the upper mantle. *Nauka,* Novosibirsk, 264pp (in Russian).

Sobolev, S.V., Zeyen, H., Stoll, G., Werling, F., Altherr, R., Fuchs, K. (1996) Upper mantle temperatures from teleseismic mantle tomography of French Massif Central including effects of composition, mineral reaction, anharmocity, anelasticity and partial melt. *Earth Planet. Sci. Lett.* **139,** 147-163.

Stosch, H.G. and Seck, H.A. (1980) Geochemistry and mineralogy of two spinel peridotite suites from Dreiser Weiher, West Germany. *Geochim. Cosmochim. Acta* **44,** 457-470.

1904 Sun, W., Bennett, V.C., Eggins, S.M., Arculus, R.J., Perfit, M.R. (2003) Rhenium
1905 systematics in submarine MORB and back-arc basin glasses: laser ablation ICP-
1906 MS results. *Chem. Geol.* **196**, 259-281.
1907
1908 Tarantola, A., and Valette, B. (1982) Generalized non-linear inverse problems solved
1909 using the least squares criterion. *Rev. Geophys. Space Phys.* **20,** 219-232.
1910
1911 Touron, S., Renac, C., O'Reilly, S.Y., Cottin, J.-Y., Griffin, W.L. (2008)
1912 Characterisation of the metasomatic agent in mantle xenoliths from Devès, Massif
1913 Central (France) using coupled trace-element and O, Sr and Nd isotopic
1914 compositions, In: *Metasomatism in oceanic and continental lithospheric mantle*
1915 (Eds: Coltorti, M., and Grégoire, M.), Geological Society, London, Special
1916 Publications **283**, 177-196.
1917
1918 van Acken, D., Becker, H., Walker, R.J. (2008) Refertilization of Jurassic oceanic
1919 peridotites from the Tethys ocean – Implications for the Re-Os systematics of the
1920 upper mantle. *Earth Planet. Sci. Lett.* **268**, 171-181.
1921
1922 Volkening, J., Walczyk, T., Heumann, K. (1991) Os isotope ratio determinations by
1923 negative thermal ionisation mass spectrometry. *Int. J. Mass Spectrom. Ion*
1924 *Processes* **105,** 147-159.
1925
1926 Walker, R.J., Echeverria, L.M., Shirey, S.B., Horan, M.F. (1991) Re-Os isotopic
1927 constraints on the origin of volcanic rocks, Gorgona Island, Colombia: Os isotopic

1928 evidence for ancient heterogeneities in the mantle. *Contrib. Mineral. Petrol.* **107,**
1929 150-162.
1930
1931 Walter, M.J., (2003) Melt extraction and compositional variability in mantle
1932 lithosphere. In: *Treatise on Geochemistry*. Eds. Holland, H.D., Turekian, K.K.
1933 Elsevier, Amsterdam, pp. 363–394.
1934
1935 Watson, E.B., Ben Othman, D., Luck, J.-M., Hofmann, A.W. (1987) Partitioning of
1936 U, Pb, Cs, Yb, Hf, Re and Os between chromian diopsidic pyroxene and
1937 haplobasaltic liquid. *Chem. Geol.* **62,** 191-208.
1938
1939 Wells, P.R.A. (1977) Pyroxene in simple and complex systems. *Contrib. Mineral.*
1940 *Petrol.* **62,** 62-129.
1941
1942 Wilshire, H.G. and Shervais, J.W. (1975) Al-augite and Cr-diopside ultramafic
1943 xenoliths in basaltic rocks from the Western United States. *Phys. Chem. Earth* **9,**
1944 257–272.
1945
1946 Wilshire, H.G. and Kirby, S.H. (1989) Dykes, joints and faults in the upper mantle.
1947 *Tectonophys.* **161**, 23-31.
1948
1949 Wilson M. and Downes H. (1991) Tertiary-Quaternary extension-related alkaline
1950 magmatism in western and central Europe. *J Petrol* **32**, 811-849.
1951

1952 Wilson M., Rosenbaum J.M., Dunworth, E.A. (1995) Melilitites: partial melts of the
1953 thermal boundary layer? *Contrib. Mineral. Petrol.* **119**, 181-196.
1954
1955 Witt-Eickschen, G. and Kramm, U. (1998) Evidence for the multiple stage evolution
1956 of the sub-continental lithospheric mantle beneath the Eifel (Germany) from
1957 pyroxenite and composite pyroxenite/peridotite xenoliths. *Contrib. Mineral.*
1958 *Petrol.* **131**, 258-272
1959
1960 Witt-Eickschen, G., Seck, H.A., Mezger, K., Eggins, S.M., Altherr, R. (2003)
1961 Lithospheric mantle evolution beneath the Eifel (Germany): constraints from Sr-
1962 Nd-Pb isotopes and trace element abundances in spine peridotite and pyroxenite
1963 xenoliths. *J.Petrol.* **44**, 1077-1095.
1964
1965 Wittig, N., Baker, J.A., Downes, H. (2006) Dating the mantle roots of young
1966 continental crust. *Geology* **34**, 237-240.
1967
1968 Wittig, N., Baker, J.A., Downes, H. (2007) U-Th-Pb and Lu-Hf isotope constraints on
1969 the evolution of sub-continental lithospheric mantle, French Massif Central,
1970 *Geochim. Cosmochim. Acta* **71**, 1290-1311.
1971
1972 Wittig, N., Pearson., D.G., Downes, H., Baker, J.A. (2009) The U, Th and Pb
1973 elemental and isotope compositions of mantle clinopyroxenes and their grain
1974 boundary contamination derived from leaching and digestion experiments.
1975 *Geochim. Cosmochim. Acta* **73**, 469-488.
1976

1977 Wu, F.-Y., Walker, R.J., Ren, X.-W., Sun, D.-Y., Zhou, X-H. (2003) Os isotope
1978 constraints on the age of lithospheric mantle beneath northeastern China.
1979 *Chem.Geol.* **196**, 107-129.
1980
1981 Xu, Y.-G., Menzies, M.A., Bodinier, J.-L., Bedini, R.M., Vroon, P., Mercier, J.-C.C.
1982 (1998) Melt percolation-reaction at the lithosphere-plume boundary: Evidence
1983 from the poikiloblastic peridotite xenoliths from Boreé (Massif Central, France).
1984 *Contrib. Mineral. Petrol.* **131,** 65-84.
1985
1986 Yaxley, G.M., Crawford, A.J., Green, D.H. (1991) Evidence for carbonatite
1987 metasomatism in spinel lherzolite xenoliths. *Earth Planet. Sci. Lett.* **107,** 305-317.
1988
1989 Yaxley, G.M. and Kamenetsky, V. (1999) In situ origin for glass in mantle xenoliths
1990 from south-eastern Australia: insights from the trace element compositions of
1991 glasses and metasomatic phases. *Earth Planet. Sci. Lett.* **172,** 97-109.
1992
1993 Yoshikawa, M., Kawamoto, T., Shibata, T., Yamamoto, J. (2009) Geochemical and
1994 Sr–Nd isotopic characteristics and P–T estimates of mantle xenoliths from the
1995 French Massif Central: evidence for melting and multiple metasomatism by
1996 silicate-rich carbonatite and asthenospheric melts. In: *Petrological Evolution of*
1997 *the European Lithospheric Mantle: From Archaean to Present Day,* Geological
1998 Society of London special publication, in press.
1999

2000 Yuan, H., Gao, S., Rudnick, R.L., Jin, Z., Liu, Y., Puchtel, I.S., Walker, R.J., Yu, R.
2001 (2007) Re-Os evidence for the age and origin of peridotites from the Dabie-Sulu
2002 ultra-high pressure metamorphic belt, China. *Chem. Geol.* **236**, 323-328.
2003
2004 Zangana, N.A., Downes, H., Thirlwall, M.F., Hegner, E. (1997) The relationship
2005 between deformation, equilibration temperatures, REE and radiogenic isotopes in
2006 mantle xenoliths (Ray Pic, Massif Central, France): an example of plume –
2007 lithosphere interaction? *Contrib. Mineral. Petrol.* **127,** 187-203.
2008
2009 Zangana, N.A., Downes, H., Thirlwall, M.F., Marriner, G.F., Bea, F. (1999)
2010 Geochemical variation in peridotite xenoliths and their constituent clinopyroxenes
2011 from Ray Pic (French Massif Central): implications for the composition of the
2012 shallow lithospheric mantle. *Chem. Geol.* **155**, 11-35.
2013
2014 Zindler, A. and Jagoutz, E. (1988) Mantle cryptology. *Geochim. Cosmochim. Acta* **52,**
2015 319-333.
2016
2017
2018
2019
2020
2021

TABLES.

Sample	MgO	SiO_2	Al_2O_3	CaO	[Ni]	[La]	[Ce]	[Sr]	[Yb]	[S]
MBr1	44.11	43.49	1.68	1.53	1941	0.094	0.274	7.31	0.289	8.3
MBr2	38.83	43.94	3.40	3.56	1733	0.612	1.799	24.3	0.498	4.1
MBr3	38.74	45.48	2.77	2.17	1831	0.600	1.624	14.3	0.286	0.0
MBr4	40.55	44.64	3.15	2.93	1796	0.137	0.343	8.02	0.363	14.6
MBr6	40.10	44.10	1.29	1.28	2040	3.150	1.626	36.0	0.106	0.0
MBr8	40.73	44.53	2.86	2.71	1818	0.241	0.490	11.2	0.320	0.0
MBr9	39.48	44.87	3.40	3.00	1797	0.413	1.027	12.5	0.330	2.1
MBr10	42.02	44.86	2.07	2.55	-	-	-	-	-	-
MBr11	40.06	45.12	3.14	3.19	-	-	-	-	-	-
MBr12	41.08	44.53	3.43	2.46	1818	0.624	1.430	13.1	0.267	-
MBr13	38.92	43.24	2.21	2.85	1695	0.661	2.055	15.0	0.219	6.2
MBr14	43.27	43.30	2.02	1.75	1995	0.484	1.050	11.3	0.222	6.2
MBr15	40.39	45.11	2.41	1.94	-	-	-	-	-	2.1
MBr16	46.11	42.83	1.19	0.85	2217	0.053	0.130	3.48	0.072	10.4
MBr18	41.60	45.10	2.40	2.15	-	-	-	-	-	-
MBr19	44.64	44.09	1.39	1.15	1946	0.462	0.895	8.04	0.109	29.2
MBr20	41.11	44.90	2.74	1.85	1841	0.138	0.322	5.39	0.201	10.4
MBr21	40.89	44.93	2.72	2.80	-	-	-	-	-	-
MBr22	39.31	44.22	3.58	3.16	-	-	-	-	-	-
MBr23	40.52	44.91	2.88	2.65	1791	0.233	0.611	11.7	0.308	10.4
MBr24	39.01	44.63	2.98	2.77	-	-	-	-	-	12.5
MBr25	38.58	44.61	3.42	3.04	-	-	-	-	-	-
MBr27	39.72	45.59	3.29	2.89	-	-	-	-	-	0.0
MBr28	41.40	45.12	2.67	2.49	1864	0.142	0.396	9.21	0.276	10.4

Table 1. Representative major and trace element data for peridotite xenoliths from Mont Briançon, Massif Central, France. SiO_2, Al_2O_3 and CaO abundances expressed in wt. %. Major element and Ni data quality assessed using two rock standards (WS-E and OUG-94). Reproducibility is within 2% of recommended values. All other abundances shown in ppm. Error on LREE measurements ranges from < 1 % for high concentration samples to >20% for the lowest concentration sample (MBr1). Errors on Sr measurements are all <3%. Errors on Yb measurements range are below 7% with the exception of the low concentration sample MBr16 (11%). All errors as 2 S.D. Complete major and trace element abundances for all of the samples are available in the online supplementary information.

Sample	[Os]	[Re]	$^{187}Os/^{188}Os$	error	$^{187}Re/^{188}Os$
Host basalt	0.214	0.223	0.15453	0.00055	4.820
MBr1	2.066	0.104	0.12897	0.00032	0.156
MBr2	1.551	0.063	0.12626	0.00007	0.119
MBr3	1.808	0.516	0.12347	0.00016	1.292
MBr4	2.189	0.091	0.11769	0.00011	0.115
MBr6	1.456	0.571	0.11541	0.00021	1.535
MBr8	1.172	0.479	0.12467	0.00014	1.836
MBr9	1.750	0.273	0.12544	0.00010	0.632
MBr9*	1.523	-	0.12529	0.00007	-
MBr12	2.147	0.083	0.12002	0.00007	0.112
MBr13	0.831	0.632	0.12452	0.00008	3.436
MBr14	1.605	0.146	0.11766	0.00020	0.324
MBr15	1.726	-	0.12032	0.00269	-
MBr16	1.513	0.147	0.12129	0.00032	0.345
MBr16*	2.194	-	0.12160	0.00007	-
MBr19	1.175	0.598	0.11754	0.00006	2.312
MBr20	1.665	0.516	0.11737	0.00006	1.382
MBr23	1.554	0.612	0.12419	0.00008	1.801
MBr28	1.024	0.634	0.12344	0.00007	2.825

Table 2. Re–Os isotope data for bulk-rock peridotite xenoliths from Mont Briançon, Massif Central, France. [Re] and [Os] expressed in parts per billion (ppb). Errors shown as 2σ mean. T_{RD} = (minimum) time of rhenium depletion calculated using a mean present-day chondritic value $^{187}Os/^{188}Os$ = 0.1278 from Walker et al. (2002) and assumes that $^{187}Re/^{188}Os_{sample}$ = 0. Given isotope ratios blank corrected. $^{187}Os/^{188}Os$ ratios normalised to $^{192}Os/^{188}Os$ = 3.08271 and corrected using measured $^{18}O/^{16}O$ and $^{17}O/^{16}O$ of 0.002047 and 0.00037 respectively. Johnson Matthey (n=26) 2.75ng Os standard $^{187}Os/^{188}Os$=0.17373±12 (2σ). "*" denotes duplicate measurement on separate powder split using the same digestion method.

2059

Sample	[Os]	[Re]	$^{187}Os/^{188}Os$	2 s.e.	$^{187}Re/^{188}Os$	T_{RD} (Gyr)
MBr2 olivine	16.87	21.8	0.1363	0.0018	2.05	-
MBr2 opx	76.50	218	0.1281	0.0008	20.5	-
MBr2 cpx	39.39	61.2	0.1369	0.0010	5.75	-
MBr2 spinel	117.6	80.2	0.1361	0.0014	7.53	-
MBr3 olivine	3.70	60.9	0.1300	0.0093	78.5	-
MBr3 opx	815	99.5	0.1233	0.0006	0.58	-
MBr3 cpx	84.38	103	0.1241	0.0008	5.80	-
MBr3 spinel	11.66	435	0.2909	0.0091	182	-
MBr sulfide 3_1	3.537	0.26	0.1224	0.0011	0.34	0.69
MBr sulfide 3_4	0.086	0.01	0.1298	0.0013	0.65	-
MBr sulfide 3_6	4.493	1.10	0.1240	0.0017	1.16	0.45
MBr6 olivine	29.32	94.3	0.1203	0.0008	8.86	-
MBr6 opx	37.46	239	0.1207	0.0009	22.5	-
MBr6 cpx	185.1	169	0.1195	0.0009	15.9	-
MBr6 spinel	47.79	924	0.1321	0.0009	86.9	-
MBr sulfide 6_1	0.047	-	0.1707	0.0055	-	-
MBr sulfide 6_2	2.638	0.76	0.1223	0.0008	1.36	0.70
MBr sulfide 6_3	0.514	5.01	0.1701	0.0041	46.8	-
MBr sulfide 6_5	0.686	0.11	0.1364	0.0020	0.74	-
MBr8 olivine	19.97	82.3	0.1255	0.0008	19.7	-
MBr8 opx	8.030	210	0.1417	0.0019	125.	-
MBr8 cpx	37.61	422	0.2031	0.0103	187	-
MBr8 spinel	50.07	584	0.1284	0.0005	55.7	-
MBr sulfide 8_3	40.84	112	0.1263	0.0003	13.1	0.11
MBr sulfide 8_4	2.518	15.9	0.1521	0.0022	30.1	-
MBr sulfide 8_5	4.758	1.31	0.1209	0.0025	1.31	0.90
MBr20 olivine	10.74	37.1	0.1265	0.0013	3.43	-
MBr20 opx	91.66	35.3	0.1260	0.0008	1.84	-
MBr20 cpx	28.27	167	0.1245	0.0013	28.1	-
MBr20 spinel	450.8	428	0.1401	0.0033	4.53	-
MBr sulfide 20_2	23.79	7.39	0.1257	0.0007	1.48	0.20
MBr sulfide 20_3	0.372	1.04	0.1220	0.0010	-	0.75
MBr sulfide 20_4	2.188	412	0.1149	0.0006	897	1.78
MBr sulfide 20_6	7.888	23.0	0.1204	0.0004	13.9	0.98

2060

2061

Table 3. Re–Os isotope data for mineral separates and sulfides from MBr2, 3, 6, 8 with 20. Errors shown are 2 σ mean. Re and Os concentrations expressed as parts per trillion (ppt) for silicates and spinel, and parts per million (ppm) for sulfides. Standards and corrections for $^{18}O/^{16}O$ and $^{17}O/^{16}O$ as in Table 2.

2085 **FIGURE CAPTIONS**

2086

2087 Figure 1. Simplified geological sketch map of the eastern French Massif Central
2088 (FMC) modified after Coisy and Nicholas (1978) and Lorand (2003) showing the
2089 location of Mont Briançon scoria cone, Devès area, last active during the Pliocene (c. 1 –
2090 4 Ma). Also shown is the boundary between the northern and southern FMC (dashed line
2091 at 45°30') (Lenoir et al., 2000; Downes et al., 2003)

2092

2093 Figure 2. The range of melt depletion experienced by Mont Briançon peridotite
2094 xenoliths. Polybaric melt extraction curves of Herzberg (2004) are also shown for 2 GPa
2095 melt depletion (solid line) and 1 GPa (dashed line) with indications of expected residual
2096 composition after 20 % melt extraction. Northern domain FMC xenoliths from Lenoir et
2097 al., (2000), southern domain FMC from Downes and Dupuy, (1987); Lenoir et al.,
2098 (2000) and Zangana et al., (1997).

2099

2100 Figure 3. Incompatible trace element abundances for 15 Mont Briançon peridotite
2101 xenoliths normalised to primitive mantle (Palme with O'Neil, 2004). (a) Seven
2102 peridotites with low primitive mantle-normalised Ce/Yb ratios i.e. $(Ce/Yb)_N$ = 0.24-0.51
2103 are inferred to have experienced the least cryptic metasomatism - their trace element
2104 abundances being due to varying degrees of melt depletion. (b) Seven peridotites with
2105 $(Ce/Yb)_N > 0.9 \leq 2.4$. Elevated light rare earth element ratios are unlikely to be
2106 attributable simply to melt depletion and suggest the influence of more intense cryptic
2107 metasomatism than in (a). (c) $(Ce/Yb)_N$ of MBr6 is the highest of all the samples in this
2108 study and is accompanied by a large Sr enrichment. This sample has experienced the
2109 most intense cryptic metasomatism.

Figure 4. Phase relations between silicate, CO_2 and sulfide melt and fluid inclusions. (a) Glassy silicate melt inclusions trapped within a re-annealed, formerly fractured olivine grain from MBr12. The trail of inclusions terminates in the intergranular glass to the left of the image. Plane polarized light (PPL). (b) Plane of melt inclusions trapped within an annealed olivine grain from MBr12 (PPL). (c) CO_2 fluid inclusion (top) with co-genetic, silicate melt inclusion beneath. The two phases are joined by a narrow neck approximately 1 μm wide (PPL). (d) Trail of silicate melt inclusions trapped within an olivine grain from MBr27. In reflected light the presence of co-genetic sulfide grains can be seen. (e) Co-genetic silicate and sulfide grains preserved as immiscible liquids within the same inclusion (PPL). (f) CO_2 fluid inclusion with co-genetic sulfide bleb within olivine from MBr12.

Figure 5. Sulfides from Mont Briançon peridotite xenoliths and their relationships with silicate phases and spinel. (a) Rounded sulfide included within olivine in MBr7. A trail of micron-scale sulfide blebs leads away from the main bleb (bottom right). Scale bar 100 μm. (b) Rounded sulfide blebs within olivine from MBr3. The three largest sulfides are joined by a network of micron sized blebs within the re-annealed olivine grain. Scale bar 100 μm. (c) Interstitial sulfide from MBr7. Scale bar 200 μm. Secondary sulfide has been precipitated and / or (re)mobilized along grain boundaries, or has exploited fracture in mineral grains as sulfide was precipitated / (re)mobilized during deformation (d) (Scale bar 100 μm). (e) Large weathered intergranular sulfide from MBr2. Small areas of fresh sulfide remain, however extensive oxidation has resulted in the formation of iron oxy-hydroxides. Scale bar 100 μm. (f) Small rounded sulfides preserved in metasomatic glass in MBr2. Despite the morphological similarity with

"enclosed" rounded sulfides,(a) above, these blebs are smaller and associated with interstitial glass in the vicinity of corroded spinel. Scale bar 50 µm.

Figure 6. Major element composition of 63 individual sulfide grains. Sulfides classification is based upon textural constraints, degree of weathering, and proximity to interstitial glass and corroded spinel. Only unweathered sulfides, unequivocally entirely enclosed within silicate grains, have a narrowly defined compositional range. All other sulfides, have much wider, and possibly disturbed, major element compositions.

Figure 7. (a) Scatter between $^{187}Re/^{188}Os$ and $^{187}Os/^{188}Os$ is particularly high amongst the xenoliths from Mont Briançon. No significant improvement is obtained in this study using previously utilised proxies such as (b) Al_2O_3, (c) S, or (d) Yb. Unless elements such as Al or Yb, conventionally considered to be immobile, have also been disturbed, the Os isotope ratio may also have been perturbed, either by the addition of radiogenic Os, or through Re addition and subsequent ingrowth of ^{187}Os.

Figure 8. Re-Os isotope systematics of silicate minerals, spinel and corresponding bulk-rocks for MBr 2, 3, 6, 8 with 20. Host basalt is shown for reference. Mineral $^{187}Os/^{188}Os$ ratios are consistently higher than their corresponding bulk-rock. Mean $^{187}Re/^{188}Os$ ratios for all of the separated phases are much greater than present day chondrite ($^{187}Re/^{188}Os = 0.406$) however no individual sample is systematically enriched in Re across all of its constituent phases.

Figure 9. [Os] and $^{187}Os/^{188}Os$ of individual sulfides from MBr3 (n=3), MBr6 (n=4), MBr8 (n=3), and MBr20 (n=4). As in cratonic mantle sulfides (e.g Griffin et al.,

2004), the most unradiogenic sulfides possess the greatest [Os]. With the exception of MBr3_1, all of the sulfides with subchondritic $^{187}Os/^{188}Os$ ratios have high Re/Os ratios. For these sulfides to retain subchondritic Os isotope ratios, Re must be added to the sulfide shortly before the host xenolith was brought to the surface. Moreover, not all of the sulfide grains with suprachondritic Os isotope ratios have a high Re abundance.

Figure 10. Re-Os isotope systematics of bulk-rock (open symbols) for MBr3, 6, 8 and 20 (circles, rectangles, triangles, diamonds respectively) and individual sulfide grains (n = 14, grey symbols) handpicked from the bulk-rock samples. Outlined white area denotes range of bulk-rock compositions of the entire Mont Briançon suite. Many of the sulfides (n=9) possess subchondritic Os isotope ratios that yield T_{RD} model ages of up to 1.8 Ga, i.e. similar to the oldest T_{RD} obtained from the most unradiogenic bulk-rock Os isotope analysis (1.7 Ga).

Figure 11. Incompatible trace element mass balance for MBr9. The most incompatible REEs and fluid mobile elements are the most deficient. The deficiency, in most cases, co-varies inversely with the partition coefficient of the elements in mantle silicates. Mass balance calculations performed using modal abundances of olivine, orthopyroxene, clinopyroxene and spinel (online supplementary information) and incompatible trace element compositions obtained by LA ICP MS (online supplementary information).

Figure 12. Os mass balance calculations for MBr3, MBr8 and MBr20. Silicates and spinel account for only < 3 % of Mont Briançon bulk-rock Os budgets, the remainder being accounted for by a balance between the two populations of sulphides. The

2184 difference in Os concentration between enclosed and interstitial sulphides is sufficiently
2185 large in MBr 3 that interstitial sulphide contributes no more than 1% to the whole rock
2186 budget whilst maintaining the measured whole rock isotopic ratio. Similarly, in MBr 8
2187 interstitial sulphide can contribute no more than 11 %, the remainder being accounted
2188 for by enclosed sulphide.
2189
2190 Figure 13. (a) OIB, MORB and PUM-derived magma have an order of magnitude
2191 more Re than lithospheric mantle. However, raising bulk xenolith [Re] to 2x PUM
2192 requires a melt/rock ratio of > 0.5, for which there is no textural evidence in this study.
2193 OIB (Reisberg et al., 1993; Marcantonio et al., 1995), MORB (Schiano et al., 1997;
2194 Gannoun et al., 2004, 2007; Escrig et al., 2005), PUM (Meisel et al., 2001). (b)
2195 Precipitation of 15–20 ppm metasomatic, i.e. secondary sulfide raises bulk xenolith [Re]
2196 to twice the value of fertile mantle and is consistent with textural observations (Figure 3
2197 with Figure 4). Wholesale removal of both primary sulfides (high [Os], low [Re],
2198 unradiogenic $^{187}Os/^{188}Os$) and pre-existing secondary sulfide (low [Os], high [Re] and
2199 radiogenic $^{187}Os/^{188}Os$; Alard et al., 2002) would systematically lower bulk-rock Re and
2200 Os abundances. Subsequent, or synchronous, addition of metasomatic sulfides with low
2201 Os and high Re abundance to some, but not all of the xenoliths, would raise Re
2202 abundances to those measured in the Re-enriched xenoliths.
2203

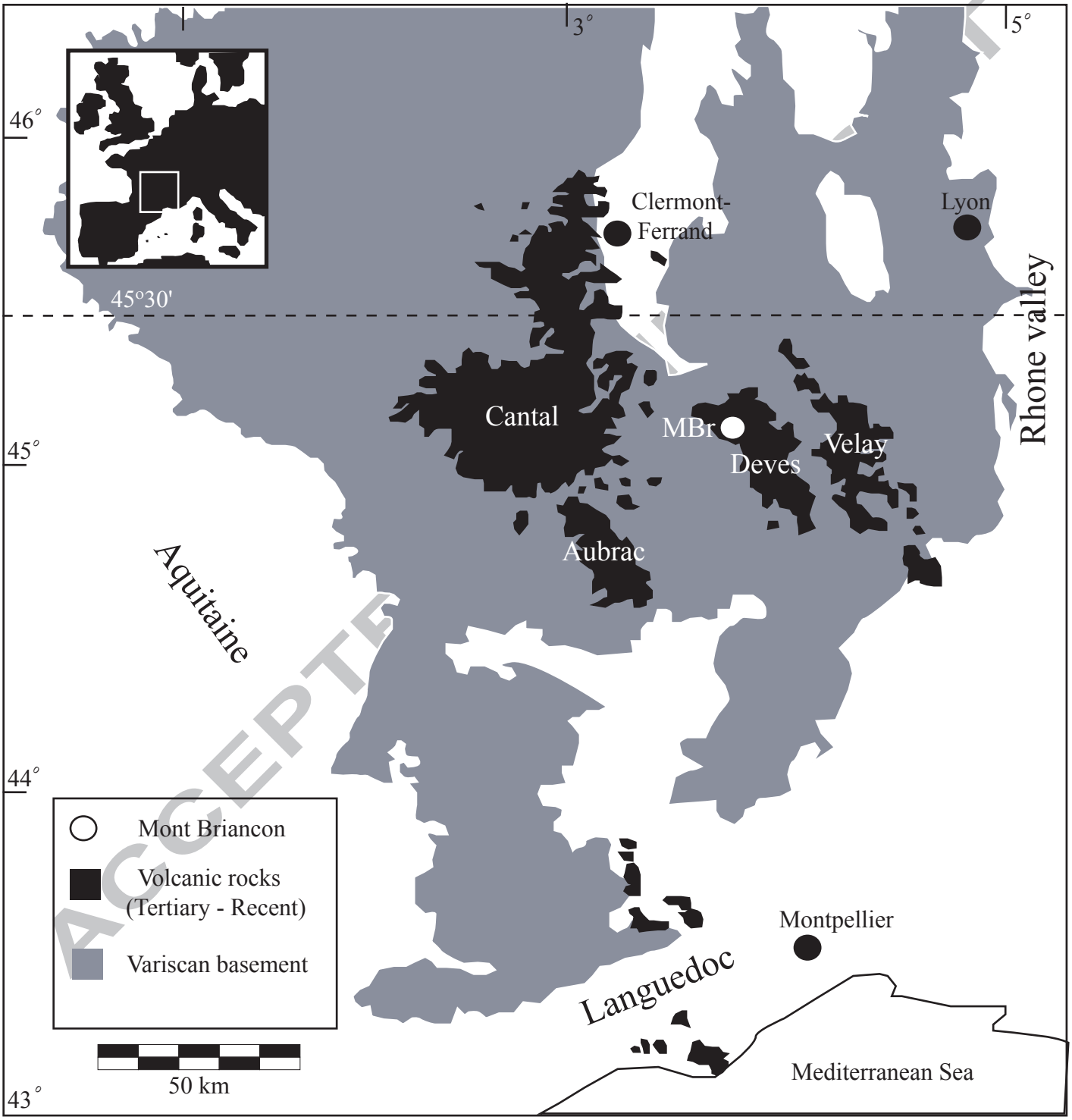

Figure 1

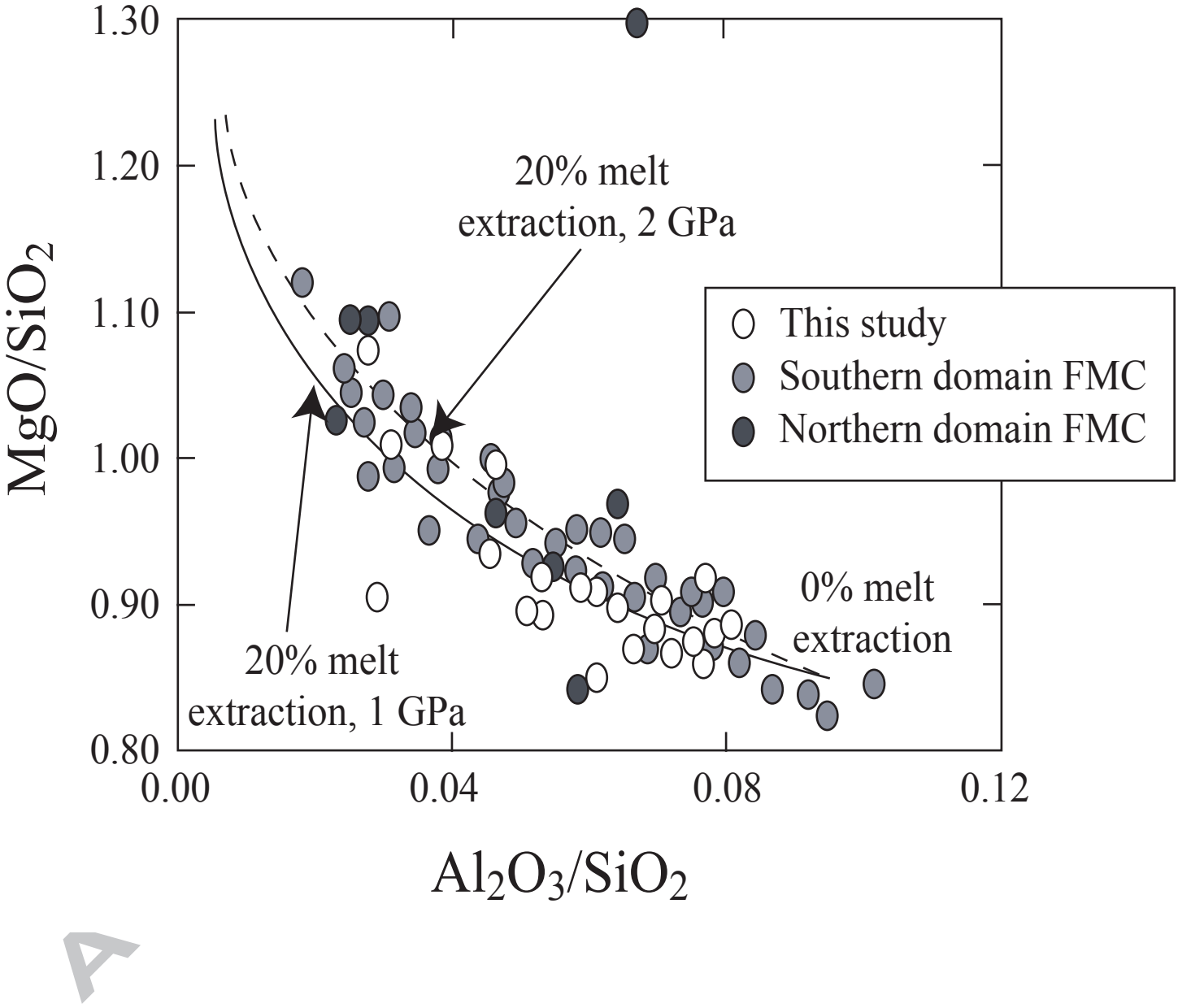

Figure 2

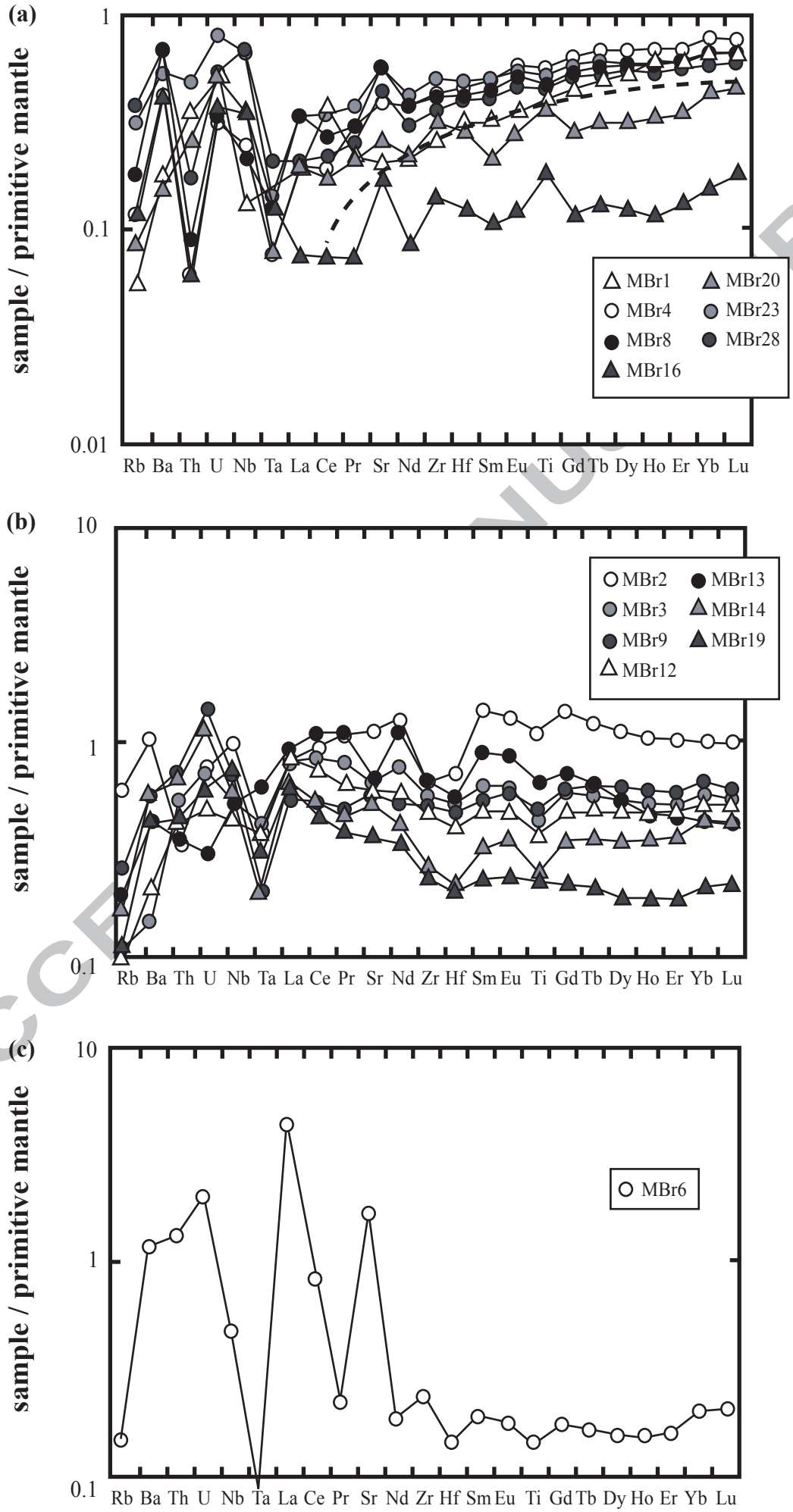

Figure 3.

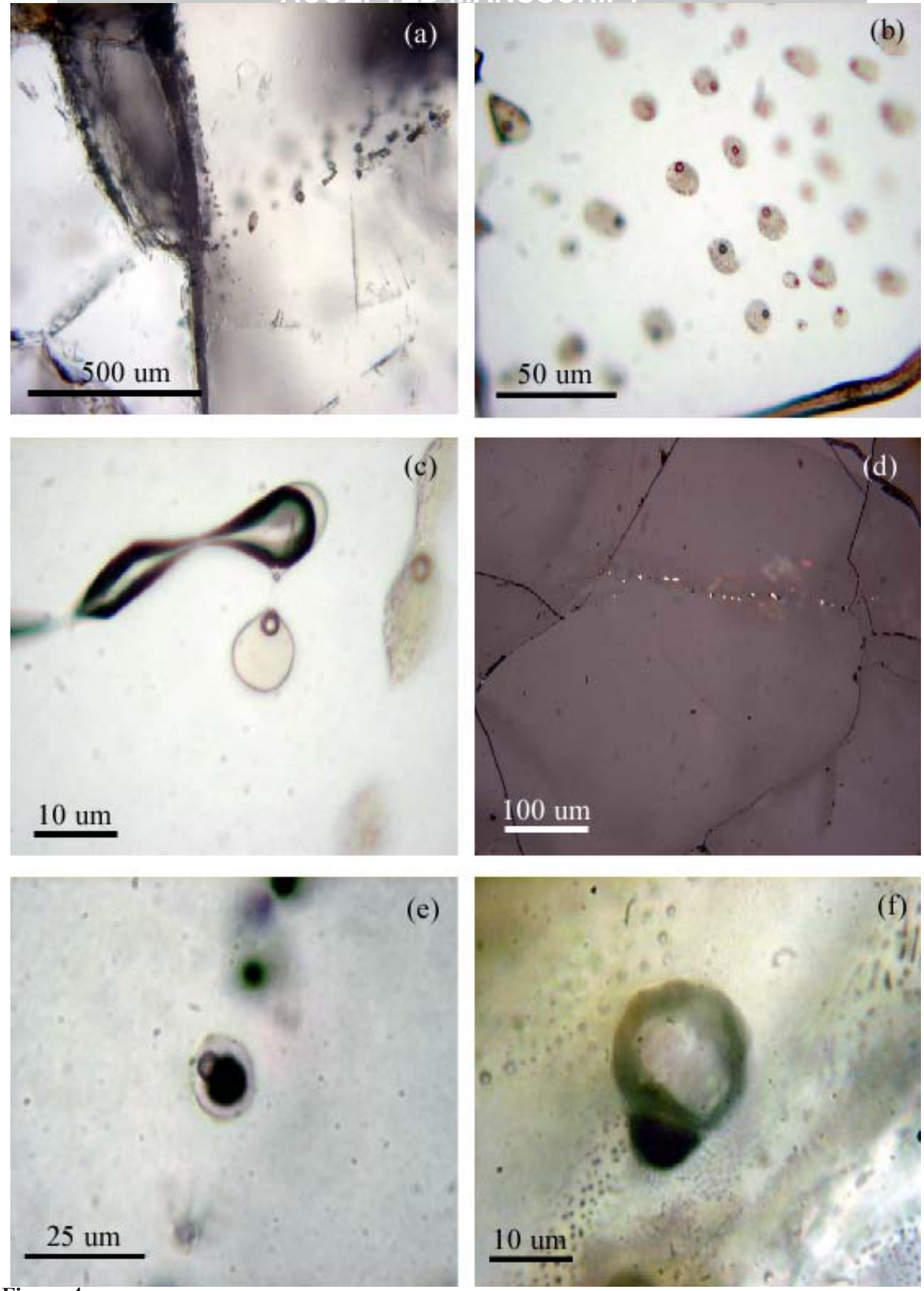

Figure 4

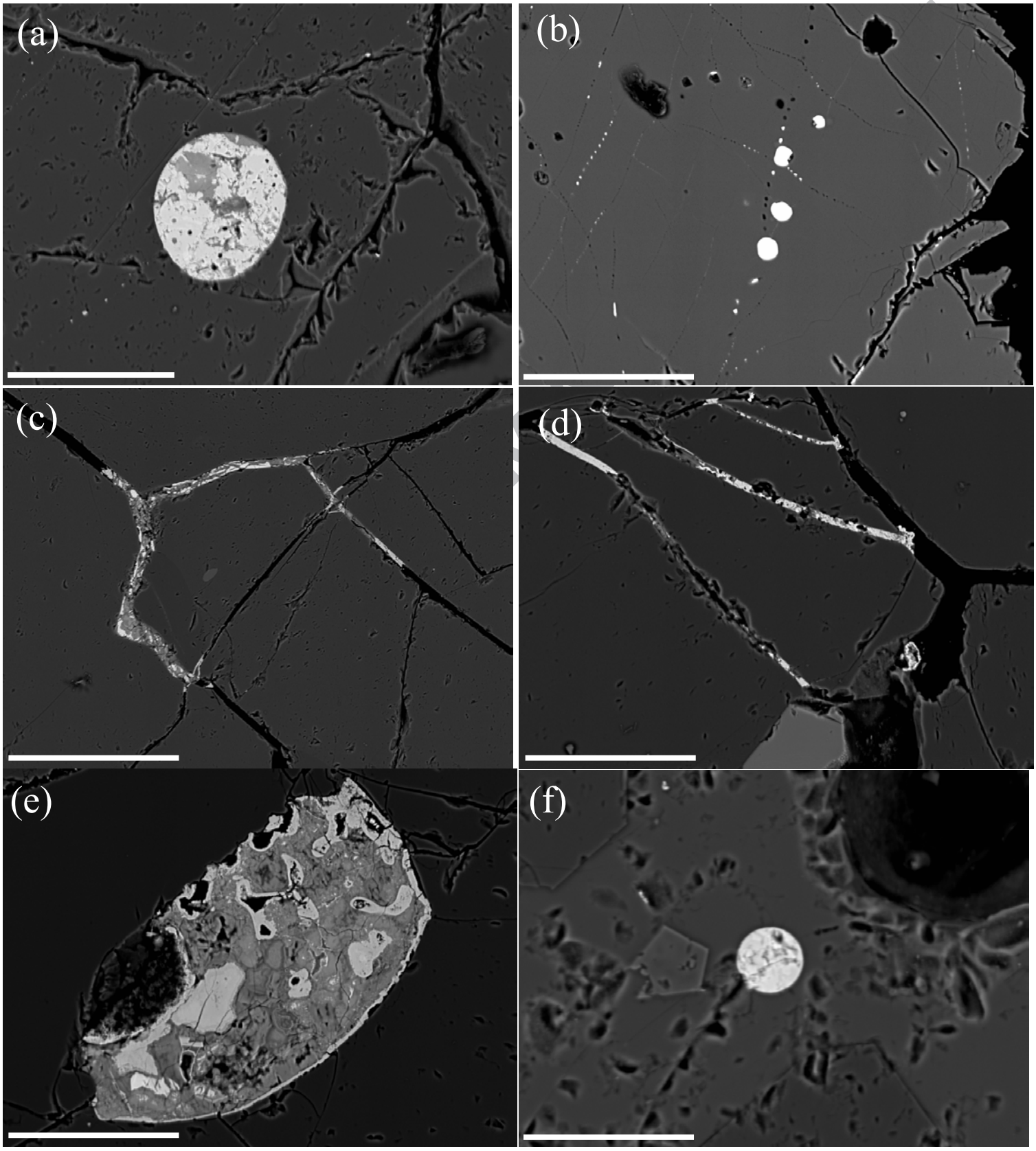

Figure 5

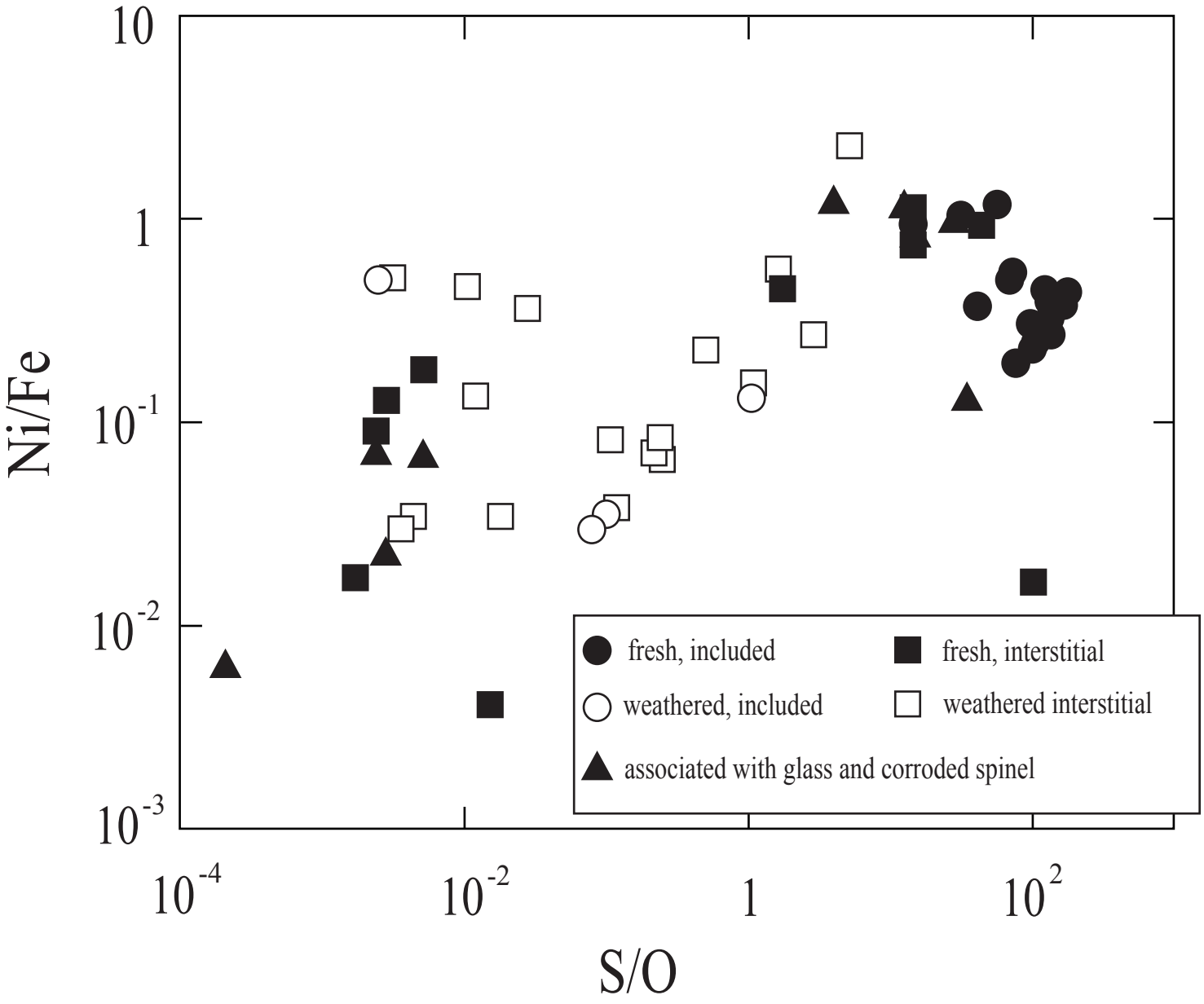

Figure 6

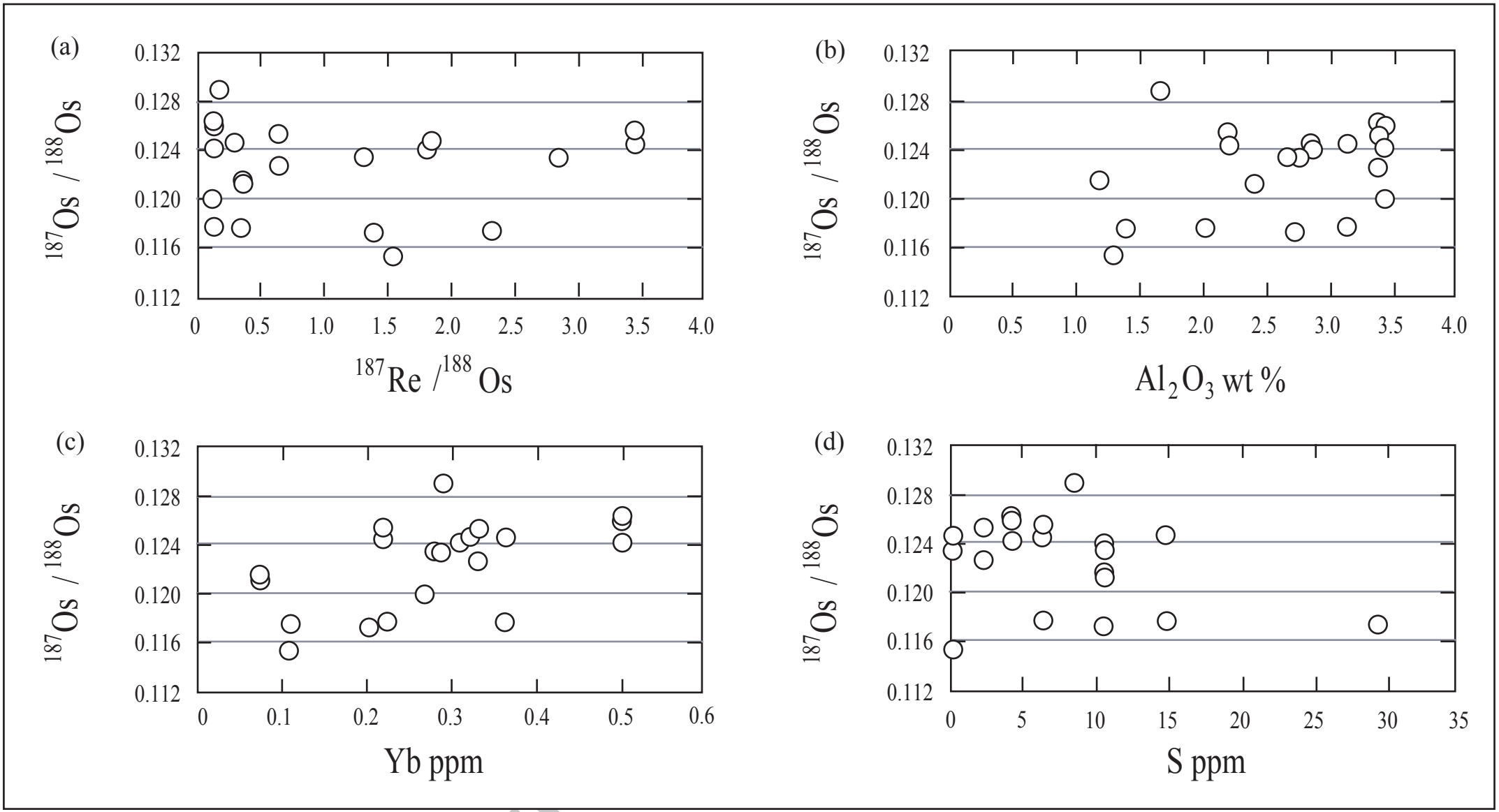

Figure 7

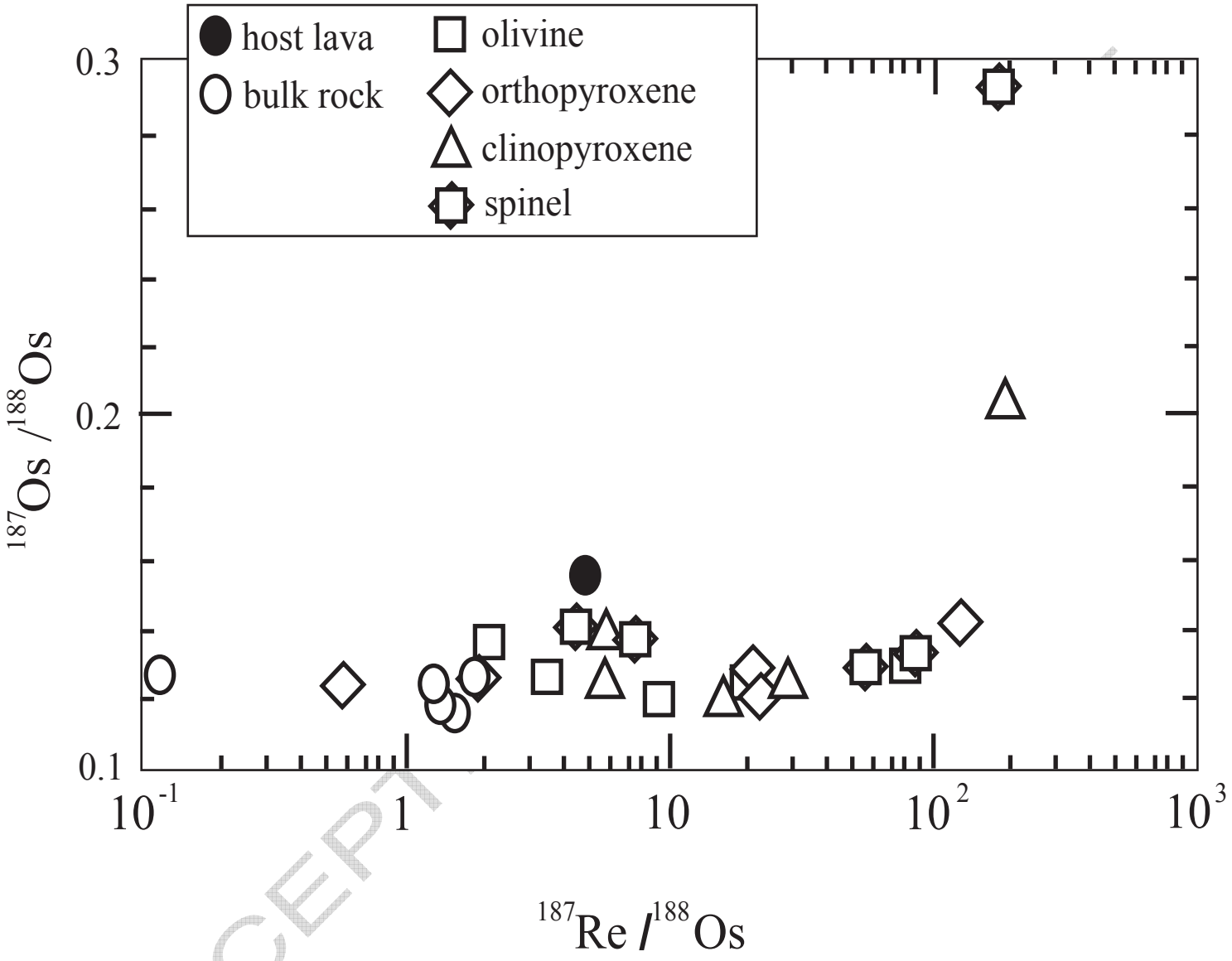

Figure 8

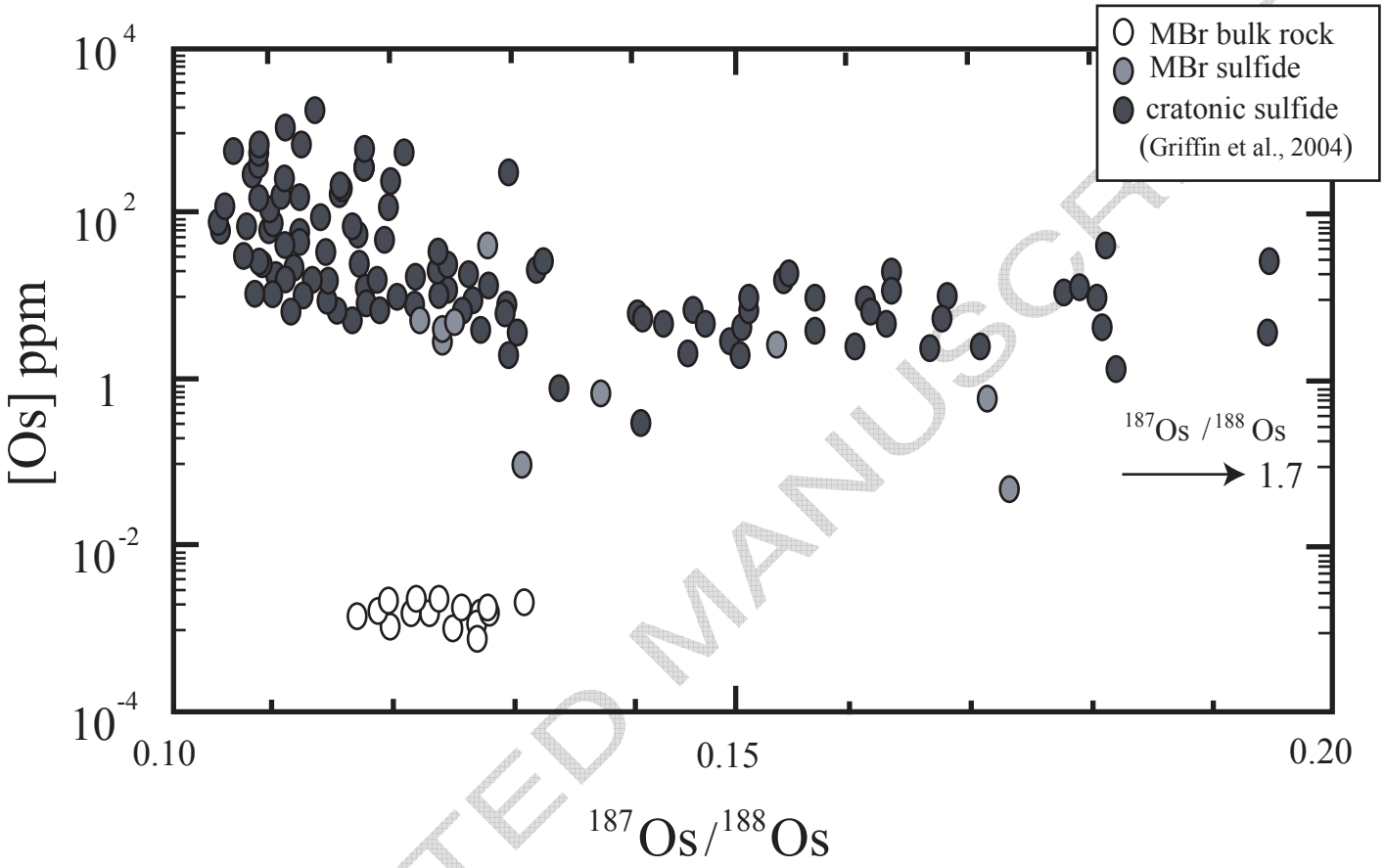

Figure 9

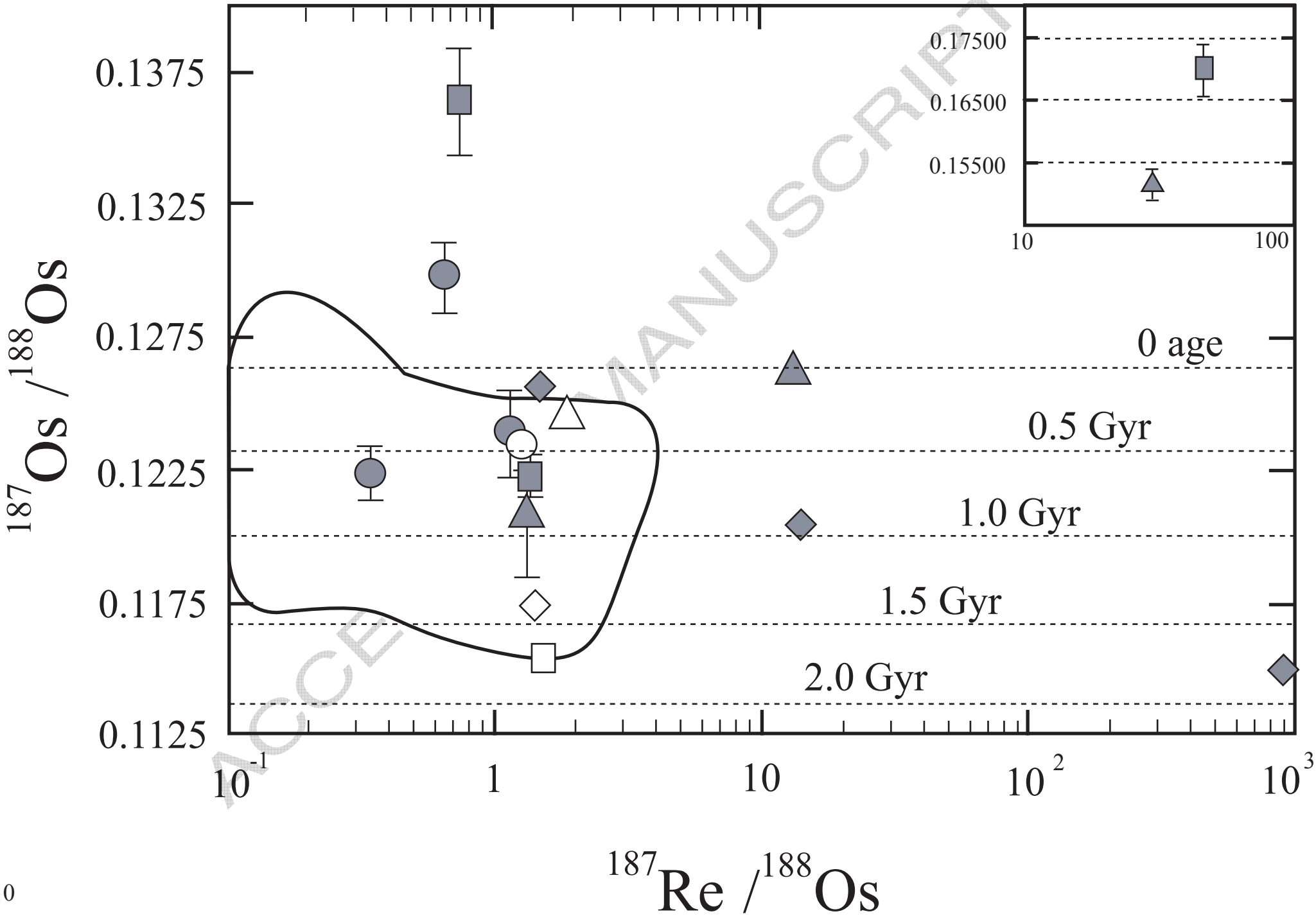
0.1375
0.1325
0.1275
0.1225
0.1175
0.1125
$^{187}Os / ^{188}Os$
0 age
0.5 Gyr
1.0 Gyr
1.5 Gyr
2.0 Gyr
10^{-1}
1
10
10^{2}
10^{3}
$^{187}Re / ^{188}Os$
0.17500
0.16500
0.15500
10
100

Figure 10

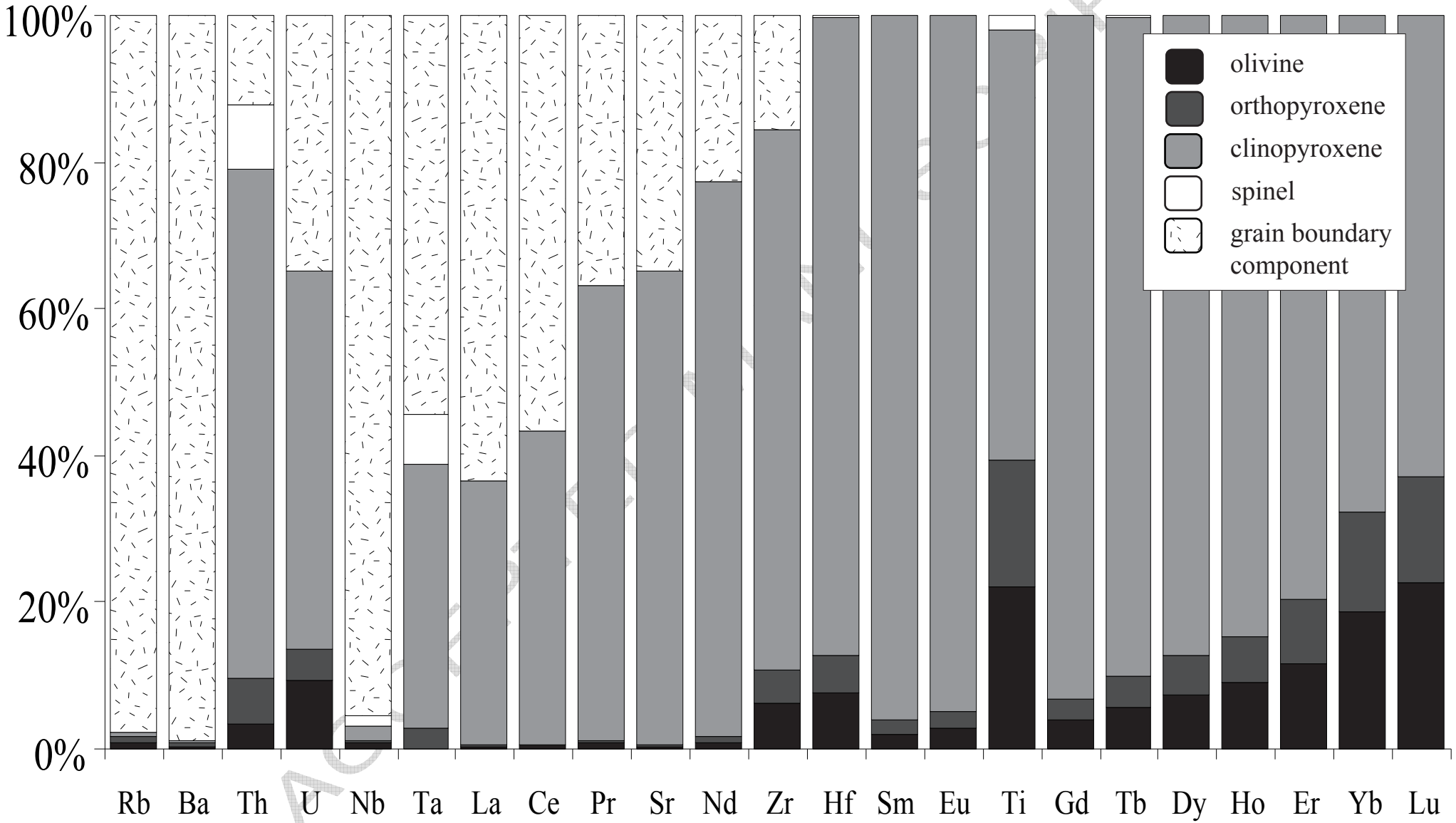
100%
80%
60%
40%
20%
0%
olivine
orthopyroxene
clinopyroxene
spinel
grain boundary component
Rb
Ba
Th
U
Nb
Ta
La
Ce
Pr
Sr
Nd
Zr
Hf
Sm
Eu
Ti
Gd
Tb
Dy
Ho
Er
Yb
Lu

Figure 11

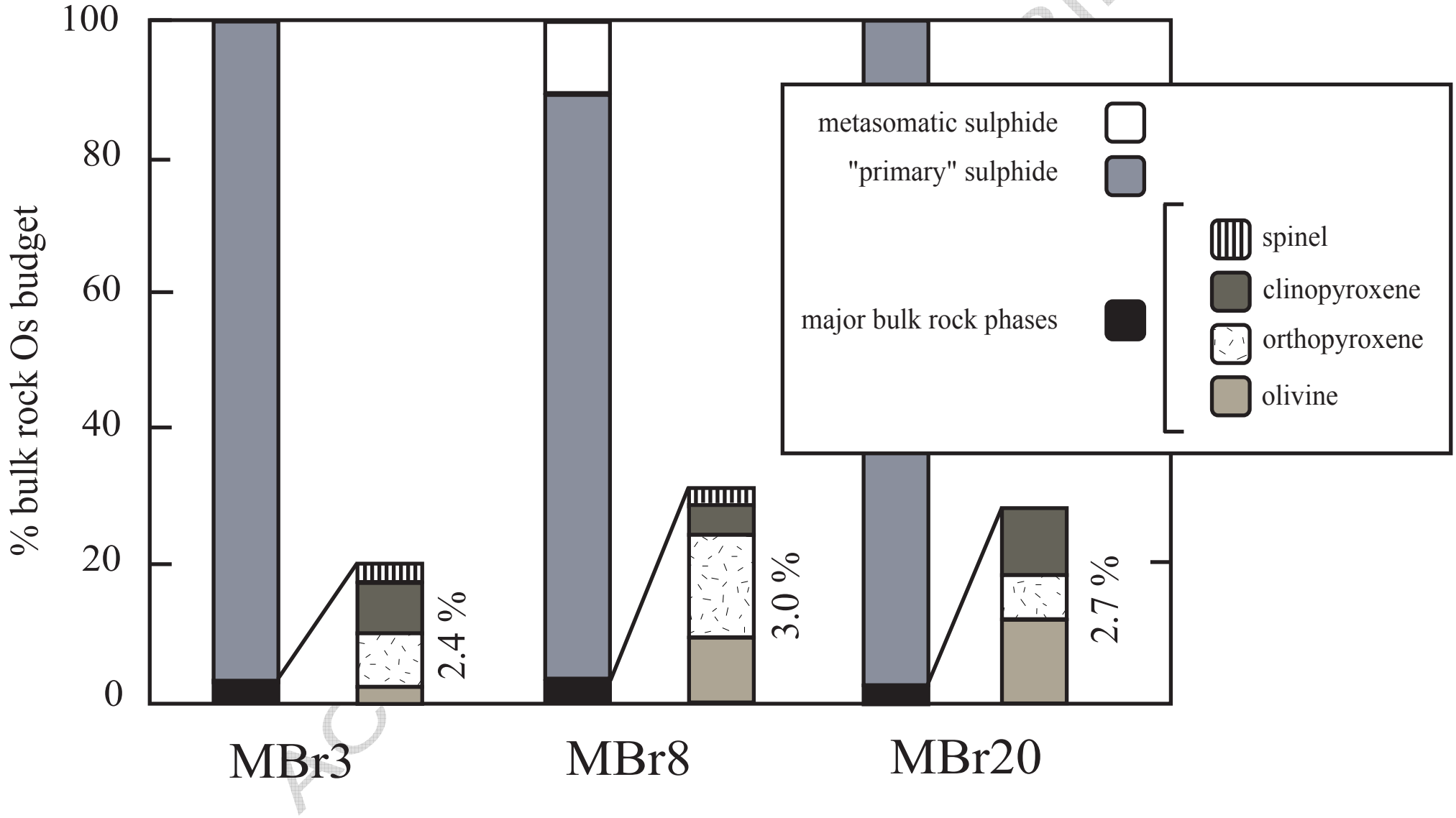
100
80
60
40
20
0
% bulk rock Os budget
metasomatic sulphide
"primary" sulphide
major bulk rock phases
spinel
clinopyroxene
orthopyroxene
olivine
2.4 %
3.0 %
2.7 %
MBr3
MBr8
MBr20

Figure 12

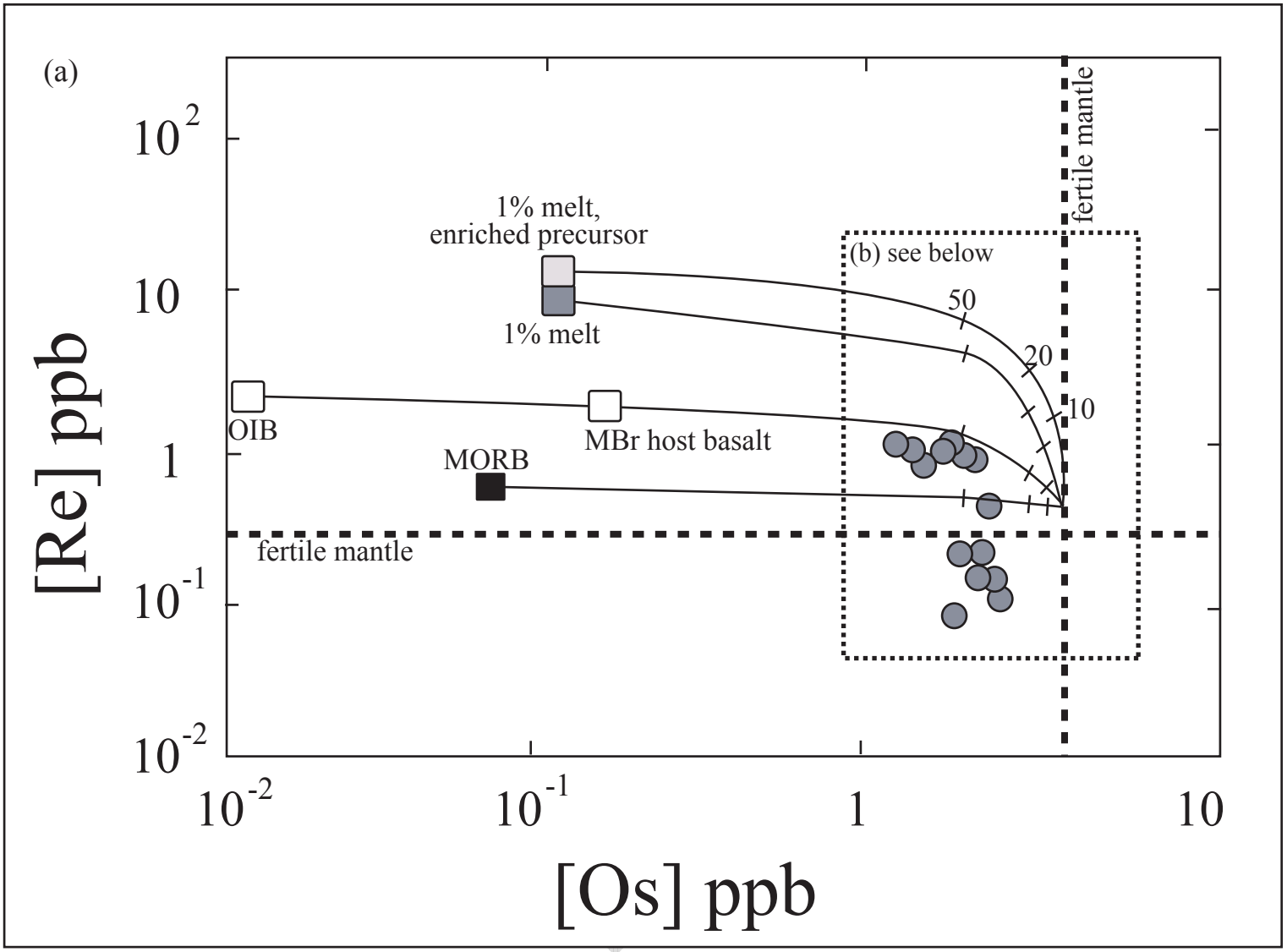
(a)
[Re] ppb
[Os] ppb
10^2
10
1
10^{-1}
10^{-2}
10^{-2}
10^{-1}
1
10
1% melt,
enriched precursor
1% melt
(b) see below
fertile mantle
fertile mantle
50
20
10
OIB
MBr host basalt
MORB

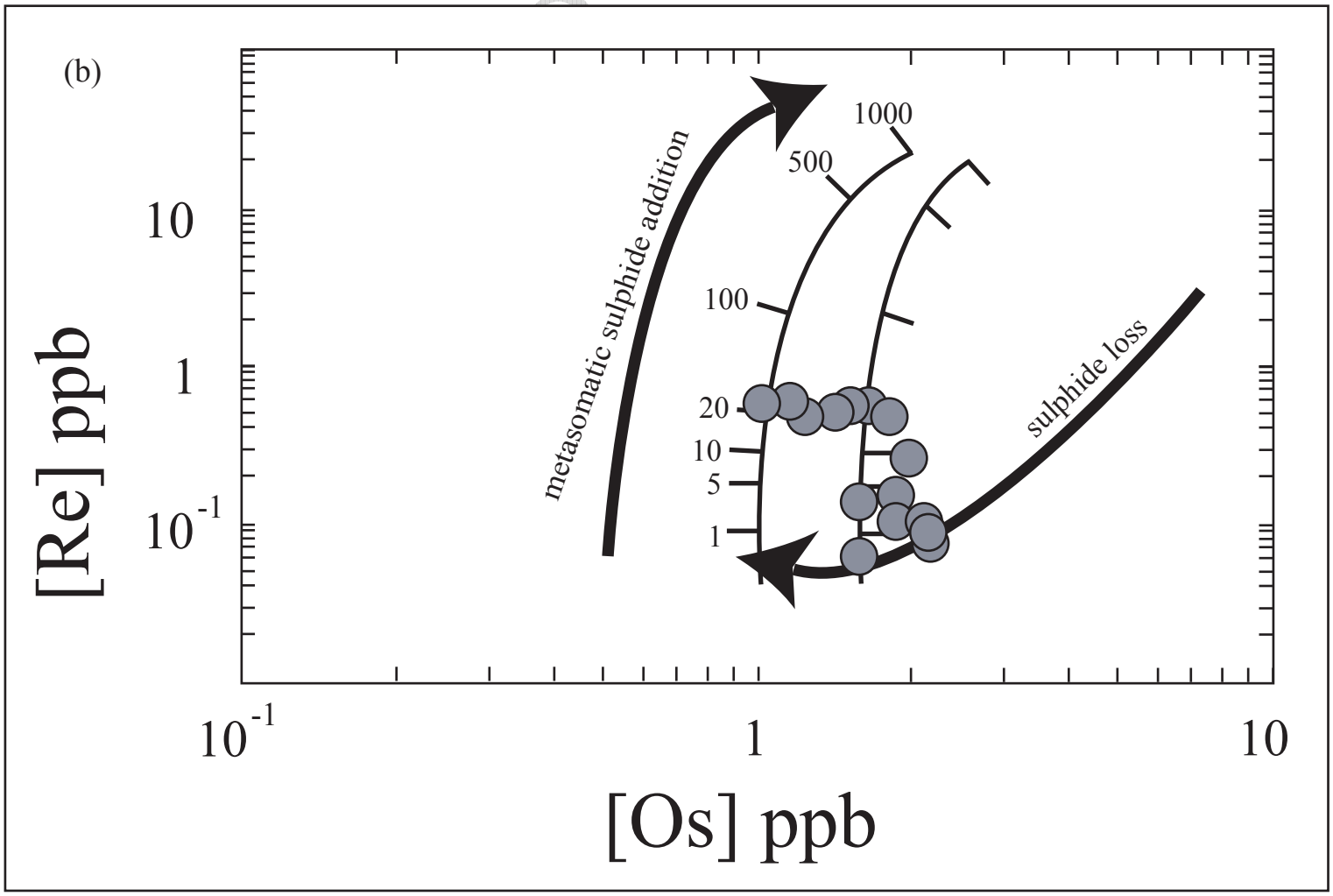
(b)
[Re] ppb
[Os] ppb
10
1
10^{-1}
10^{-1}
1
10
metasomatic sulphide addition
sulphide loss
1000
500
100
20
10
5
1

Figure 13